

Sparsity-promoting optimal control of power networks

A DISSERTATION
SUBMITTED TO THE FACULTY OF THE GRADUATE SCHOOL
OF THE UNIVERSITY OF MINNESOTA
BY

Xiaofan Wu

IN PARTIAL FULFILLMENT OF THE REQUIREMENTS
FOR THE DEGREE OF
Doctor of Philosophy

December 2016

Sparsity-promoting optimal control of
power networks

Copyright © 2016

by

Xiaofan Wu

ALL RIGHTS RESERVED

To Jingyi and my parents

Acknowledgements

I would like to express my sincere gratitude to my advisor Professor Mihailo R. Jovanović for his utmost support and guidance throughout the years of my graduate study. It is my greatest pleasure to have Mihailo as my academic teacher, research mentor, spiritual guide, soccer teammate and gym buddy. Those tremendous time that we spent together on brain storming, paper writing, problem solving, gym exercising, will be my most precious memories forever. His patience, motivation, enthusiasm, immense knowledge and commitment to excellence has always inspired me to be a better student and a better person.

I am extremely fortunate to have the opportunity to work with Professor Florian Dörfler for the past three years. His creativity and patience have made our collaboration possible. His insightful comments and suggestions have made our joint work successful. I am truly thankful to him for inviting me to Automatic Control Lab at ETH Zürich as a visiting scholar.

I owe sincere thankfulness to Professor Sairaj Dhople, Peter Seiler, Jarvis Haupt for serving on my defense committee. I have benefited from interacting with them and learned the knowledge that I need for completing my graduate study.

I am very grateful to have my labmates and friends: Dr. Fu Lin, Dr. Rashad Moarref, Dr. Binh Lieu, Dr. Armin Zare, Dr. Neil Dhingra, Dr. Yongxin Chen, Sepideh Hassan-Moghaddam, Wei Ran, Dongsheng Ding, Hamza Farooq, Karen Khatamifard, Dr. Sei Zhen Khong, Dr. Kaoru Yamamoto, Dr. Rohit Gupta, Dr. Marcello Colombino, and many other friends who have helped me. They have made my graduate study at UMN meaningful and colorful. I would like to thank Fu Lin for his generous help and guidance during my first years in Minnesota. I am very grateful to Binh Lieu for hosting all the warm and fun holiday events. I would like to express my special thanks to my

best buddies, Armin and Neil, for all the fun we had during these graduate school years.

It has been the greatest privilege to have my Chinese friends and buddies: Wei Zhang, Keping Song, Yinglong Feng, Yi Wang, Zisheng Zhang, Jie Kang, Yu Chen, Jun Fang, Cong Ma, Kejian Wu, Huanan Zhang, Peng Peng and many others. They have become an important part of my life in Minnesota. I will always remember the great times we have spent together.

I would like to sincerely thank my family. My parents have always been teaching me to study hard, work hard, party hard and enjoy life. They always encourage me and cheer me up when I am down. They always guide me through difficult time and help me pursue my dreams. Without their unconditional support, I would not be the person I am today.

Finally, I would like to extend my warmest thanks to the love of my life, my wife Jingyi Zhang. She has been my soul mate and my best friend. Throughout the years, she has been on my side, supporting me, helping me, trusting me and loving me. Her company and encouragement has made this dissertation possible.

Abstract

In this dissertation, we study the problems of structure design and optimal control of consensus and synchronization networks. Our objective is to design controller that utilize limited information exchange between subsystems in large-scale networks. To obtain controllers with low communication requirements, we seek solutions to regularized versions of the \mathcal{H}_2 optimal control problem. The proposed framework can be leveraged for control design in applications like wide-area control in bulk power systems, frequency regulation in power system/microgrids, synchronization of nonlinear oscillator networks, etc. The structure of the dissertation is organized as follows.

In Part I, we focus on the optimal control problems in systems with symmetries and consensus/synchronization networks. They are characterized by structural constraints that arise either from the underlying group structure or the lack of the absolute measurements for a part of the state vector. Our framework solves the regularized versions of the \mathcal{H}_2 optimal control problems that allow the state-space representations that are used to quantify the system's performance and sparsity of the controller to be expressed in different sets of coordinates. For systems with symmetric dynamic matrices, the problem of minimizing the \mathcal{H}_2 or \mathcal{H}_∞ performance of the closed-loop system can be cast as a convex optimization problem. Studying the symmetric component of a general system's dynamic matrices provides bounds on the \mathcal{H}_2 and \mathcal{H}_∞ performance of the original system.

Part II studies wide-area control of inter-area oscillations in power systems. Our input-output analysis examines power spectral density and variance amplification of stochastically forced systems and offers new insights relative to modal approaches. To improve upon the limitations of conventional wide-area control strategies, we also study the problem of signal selection and optimal design of sparse and block-sparse wide-area controllers. We show how different sparsity-promoting penalty functions can be used to achieve a desired balance between closed-loop performance and communication complexity. In particular, we demonstrate that the addition of certain long-range communication links and careful retuning of the local controllers represent an effective

means for improving system performance.

In Part III, we apply the sparsity-promoting optimal control framework to two problem encounters in distributed networks. First, we consider the optimal frequency regulation problem in power systems and propose a principled heuristic to identify the structure and gains of the distributed integral control layer. We define the proposed distributed PI-controller and formulate the resulting static output-feedback control problem. Second, we develop a structured optimal-control framework to design coupling gains for synchronization of weakly nonlinear oscillator circuits connected in resistive networks with arbitrary topologies. The structured optimal-control problem allows us to seek a decentralized control strategy that precludes communications between the weakly nonlinear Liénard-type oscillators.

Contents

Acknowledgements	ii
Abstract	iv
List of Tables	x
List of Figures	xi
1 Introduction	1
1.1 Motivation	1
1.2 Main topics of the dissertation	3
1.2.1 Optimal sparse feedback design	3
1.2.2 Sparsity-promoting optimal control of systems with invariances and symmetries	4
1.2.3 Wide-area control in power systems	5
1.2.4 Distributed-PI control in power systems	8
1.2.5 Design of optimal coupling gains for synchronization of nonlinear oscillators	10
1.3 Dissertation structure	11
1.4 Contributions of the dissertation	13
I Sparsity-promoting optimal control	16
2 Optimal Sparse Feedback Design	17
2.1 Motivation and background	17

2.1.1	Problem formulation	19
2.1.2	Examples	20
2.1.3	Sparsity-promoting penalty functions	23
2.2	Class of convex problems	24
2.3	Design of controller structure	26
2.3.1	Structure design via ADMM	26
2.3.2	Polishing step	31
2.4	Case study: synchronization network	31
2.5	Concluding remarks	34
3	Sparsity-promoting optimal control of systems with invariances and symmetries	36
3.1	Problem formulation	37
3.1.1	Applications	38
3.2	Symmetric system design	39
3.2.1	Convex optimal control for symmetric systems	40
3.2.2	Stability and performance guarantees	41
3.2.3	Approximation bounds	43
3.3	Computational advantages for structured problems	43
3.3.1	Spatially-invariant systems	45
3.4	Examples	46
3.4.1	Directed Consensus Network	46
3.4.2	Swift-Hohenberg Equation	46
3.5	Concluding remarks	50
II	Wide-area control of power systems	51
4	Decentralized optimal control of inter-area oscillations	52
4.1	Modeling and control preliminaries	52
4.1.1	Swing equations	53
4.1.2	Problem formulation	53
4.2	Input-output analysis	56

4.2.1	Power spectral density and variance amplification	56
4.3	Sparse and block-sparse optimal control	58
4.3.1	Elementwise sparsity	58
4.3.2	Block sparsity	59
4.4	Case study: IEEE 39 New England model	62
4.4.1	Analysis of the open-loop system	63
4.4.2	Sparsity-promoting optimal wide-area control	65
4.4.3	Comparison of open- and closed-loop systems	69
4.4.4	Robustness analysis	72
4.5	Concluding remarks	74
III	Optimal control in distributed networks	76
5	Design of distributed integral control action in power networks	77
5.1	Synchronous frequency and power sharing	78
5.2	Distributed integral control	79
5.2.1	Problem setup	79
5.2.2	Static output-feedback control problem	81
5.2.3	Optimal design of the centralized integral action	85
5.3	Sparsity-promoting optimal control	86
5.4	Case study: IEEE 39 New England model	89
5.5	Concluding remarks	91
6	Design of optimal coupling gains for synchronization of nonlinear oscillators	92
6.1	System of coupled weakly nonlinear oscillator circuits	93
6.1.1	Nonlinear oscillator model	93
6.1.2	Resistive electrical network	95
6.1.3	System dynamical model in polar coordinates	97
6.1.4	State-space representation of linearized system	97
6.2	Design of current gains	100
6.2.1	Linear quadratic control design	100

6.2.2	Sparsity-promoting optimal control	101
6.3	Case study	102
6.3.1	Optimal current-gain design	104
6.3.2	Time-domain simulations for original nonlinear and linearized models	105
6.4	Concluding remarks	105
References		106

List of Tables

4.1	Poorly-damped modes of New England model	63
-----	--	----

List of Figures

1.1	(a) Fishes utilize local relative distance measurements to form a fish school. (b) Computers achieve clock synchronization by exchanging local information in cyber networks. (c) Satellites measure relative distances between each other to maintain formations. (d) Generators exchange relative angle/frequency information to achieve synchronization.	2
1.2	A few typical inter-area oscillations in Europe.	6
1.3	(a) Fully-decentralized control strategies implemented locally, ineffective against inter-area oscillations. (b) Distributed wide-area control using remote signals, effective against inter-area oscillations.	7
2.1	Topology of a disconnected plant network with 3 clusters and 20 nodes.	32
2.2	Topology of controller network for different values of γ . Edges in the controller network are marked with red lines.	33
2.3	Sparsity pattern of K for $\gamma = 1$	33
2.4	Performance vs sparsity comparison with respect to the optimal centralized controller K_c for 50 logarithmically-spaced points $\gamma \in [10^{-3}, 1]$. . .	34
2.5	Performance degradation comparison of K resulting from our framework (dots) to the average of 100 feedback matrices of random sparsity patterns with same sparsity level for each γ	34
3.1	Directed network (black solid arrows) with added undirected edges (red dashed arrows). Both the \mathcal{H}_2 and \mathcal{H}_∞ optimal structured control problems yielded the same set of added edges. In addition to these edges, the controllers tuned the weights of the edges (1) – (3) and (1) – (5). . .	47
3.2	\mathcal{H}_2 and \mathcal{H}_∞ performance of the closed-loop symmetric system and the original system subject to a controller designed at various values of γ . .	48

3.3	Computation time for the general formulation (3.4) (blue \circ) and that which takes advantage of spatial invariance (3.6) (red $*$).	49
3.4	Feedback gain $v(x)$ for the node at position $x = 0$, computed with $N = 51$ and $\gamma = 0$ (black solid), $\gamma = 0.1$ (blue dashed), and $\gamma = 10$ (red dotted).	49
4.1	Block structure of the feedback matrix K . \bullet denote relative angle feedback gains, \bullet and \bullet represent local and inter-generator frequency and PSS gains, respectively.	60
4.2	Structural identity matrix I_s with \bullet representing locations of 1's.	62
4.3	The IEEE 39 New England Power Grid and its coherent groups identified using slow coherency theory.	62
4.4	Polar plots of the angle components of the six poorly-damped modes for the open-loop system.	64
4.5	(a) Power spectral density of the open-loop system; (b) zoomed version of the red square shown in (a). Red dots denote poorly-damped modes from Table 4.1.	64
4.6	Diagonal elements of the open-loop covariance matrix Z_1 determine contribution of each generator to the variance amplification.	65
4.7	(a) Eigenvalues; and (b)-(d) eigenvectors corresponding to the three largest eigenvalues λ_i of the open-loop output covariance matrix Z_1	66
4.8	Sparsity patterns of K resulting from (SP).	67
4.9	Performance vs sparsity comparison of sparse K and the optimal centralized controller K_c for 50 logarithmically-spaced points $\gamma \in [10^{-4}, 0.25]$	68
4.10	Sparsity patterns of K resulting from (4.8).	68
4.11	Performance vs sparsity comparison of block-sparse K and the optimal centralized controller K_c for 50 logarithmically-spaced points $\gamma = \gamma_\theta = \gamma_r \in [10^{-4}, 0.25]$	69

4.12	The eigenvalues of the open-loop system and the closed-loop systems with sparse/block-sparse/centralized controllers are represented by *, \circ , \diamond , and \square , respectively. The damping lines indicate lower bounds for damping ratios and they are represented by dashed lines using the same colors as for the respective eigenvalues. The 10% damping line is identified by cyan color. The numbered black asterisks correspond to the six poorly-damped modes given in Table 4.1.	70
4.13	Power spectral density comparison.	70
4.14	Eigenvalues of the output covariance matrix Z_1 . * represents the open-loop system, \circ , \diamond and \square represent the closed-loop systems with sparse, block-sparse, and optimal centralized controllers, respectively.	71
4.15	Time-domain simulations of the linearized model of the IEEE 39 New England power grid. The rotor angles and frequencies of all generators are shown. The closed-loop results are obtained using the fully-decentralized block-sparse controller. The initial conditions are given by the eigenvectors of the poorly-damped inter-area modes 2 (left) and 6 (right) from Table 4.1.	72
4.16	Performance histograms of open- and closed-loop linearized systems (with nominal controllers) for 10,000 uniformly distributed operating points. .	73
4.17	Multivariable phase margins as a function of γ	74
5.1	The IEEE 39 New England Power Grid.	90
5.2	Sparsity pattern of G resulting from (SP).	90
5.3	Performance vs sparsity comparison of sparse G and the optimal centralized controller G_c for 50 logarithmically-spaced points $\gamma \in [10^{-3}, 10]$. .	91
6.1	The Van der Pol oscillator circuit with a current gain κ admits the dynamics in (6.1). In this case, $\omega = 1/\sqrt{LC}$, $\varepsilon = \sqrt{L/C}$, and $h(v) = \int f(v)dv = \alpha\omega(v - \beta v^3/3)$ where α and β are positive real constants. . .	94
6.2	Kron reduction illustrated for a network of three oscillators. In this example, $\mathcal{A} = \{1, \dots, 5\}$, $\mathcal{N} = \{1, 2, 3\}$, and $\mathcal{I} = \{4, 5\}$	97

6.3	Sparsity-promoting optimal current gain design illustrated for a Kron-reduced network and two oscillators. As the sparsity emphasis γ increases, K becomes sparser and we eventually recover a diagonal matrix, K_d , which corresponds to local current gains. Dotted lines indicate communication links that correspond to dense feedback gain matrices. . . .	101
6.4	Schematic diagram of the electrical network. The topology is adopted from the IEEE 37-bus network.	102
6.5	Evolution of averaged amplitudes and phases with time for the nonlinear system in (6.11).	103
6.6	Performance versus sparsity comparison of sparse K and the optimal centralized controller K_c	103
6.7	Oscillator terminal-voltage magnitudes with designed current gains applied at time $t = 0.1$ s.	104

Chapter 1

Introduction

1.1 Motivation

This dissertation studies structure design and optimal control problems arise in distributed systems and consensus networks. In large networks of dynamical systems centralized information processing may impose heavy communication and computation burden on individual subsystems. This motivates the development of localized feedback control strategies that require limited information exchange between the subsystems in order to reach consensus or guarantee synchronization. These problems are encountered in a number of applications ranging from biology to computer science to power systems [1–11], see Fig. 1.1 for some examples. In each of these applications, it is of interest to reach an agreement or to achieve synchronization by exchanging relative information between the subsystems. The restriction on the absence of the absolute measurements imposes structural constraints for the analysis and design.

Conventional optimal control of distributed systems relies on centralized implementation of control policies [12]. In large networks of dynamical systems centralized information processing may impose heavy communication and computation burden on individual nodes. This motivates the development of localized feedback control strategies that require limited information exchange between the nodes in order to reach consensus or guarantee synchronization [2, 3, 5, 6, 10, 11, 13].

In this dissertation, our objective is to design controller structures and resulting



(a)



(b)



(c)



(d)

Figure 1.1: (a) Fishes utilize local relative distance measurements to form a fish school. (b) Computers achieve clock synchronization by exchanging local information in cyber networks. (c) Satellites measure relative distances between each other to maintain formations. (d) Generators exchange relative angle/frequency information to achieve synchronization.

control strategies that utilize limited information exchange between subsystems in large-scale networks. To design networks with low communication requirements, we seek solutions to the regularized version of the standard \mathcal{H}_2 optimal control problem. Such solutions trade off network performance and sparsity of the controller. For example, in the context of wide-area control of power systems [14–16], the optimal controller respects the structure of the original power network: in both open- and closed-loop systems, only relative rotor angle differences between different generators appear in the

state-space representation.

1.2 Main topics of the dissertation

In this section, we discuss the main topics of the dissertation.

1.2.1 Optimal sparse feedback design

In large networks of dynamical systems centralized information processing may impose prohibitively expensive communication and computation burden [17,18]. This motivates the development of theory and techniques for designing distributed controller architectures that lead to favorable performance of large-scale networks. Recently, regularized versions of standard optimal control problems were introduced as a means for achieving this goal [19–23]. For example, in consensus and synchronization networks, it is of interest to achieve desired objective using relative information exchange between limited subset of nodes [1–11].

The objective is to design controllers that provide a desired tradeoff between the network performance and the sparsity of the static output-feedback controller. This is accomplished by regularizing the \mathcal{H}_2 optimal control problem with a penalty on communication requirements in the distributed controller. In contrast to previous work [19–21], this regularization penalty reflects the fact that sparsity should be enforced in a specific set of coordinates. In [19–21], the elements of the state-feedback gain matrix were taken to represent communication links. Herein, we present a unified framework where a communication link is a linear function of the elements of the output-feedback gain matrix.

The proposed framework addresses challenges that arise in systems with invariances and symmetries, as well as consensus and synchronization networks. For example, the block diagonal structure of spatially-invariant systems in the spatial frequency domain facilitates efficient computation of the optimal centralized controllers [17]. However, since the sparsity requirements are typically expressed in the physical space, it is challenging to translate them into frequency domain specifications. Furthermore, in wide-area control of power networks [14–16], it is desired to design the controllers that respect

the structure of the original system: in both open- and closed-loop networks, only relative rotor angle differences between different generators are allowed to appear. To deal with these structural requirements, we introduce a coordinate transformation to eliminate the average mode and assure stabilizability and detectability of the remaining modes. Once again, it is desired to promote sparsity of the feedback gain in physical domain and it is challenging to translate these requirements in the transformed set of coordinates.

We leverage the alternating direction method of multipliers (ADMM) [24] to exploit the structure of the corresponding objective functions in the regularized optimal control problem. ADMM alternates between optimizing the closed-loop performance and promoting sparsity of the feedback gain matrix. The sparsity promoting step in ADMM has an explicit solution and the performance optimization step is solved using Anderson-Moore and proximal gradient methods. Our framework thus allows for performance and sparsity requirements to be expressed in different set of coordinates and facilitates efficient computation of sparse static output-feedback controllers.

For undirected consensus networks, the proposed approach admits a convex characterization. Furthermore, for systems with invariances and symmetries, transform techniques are utilized to gain additional computational advantage and improve efficiency. For example, by bringing matrices in a state-space representation of a spatially invariant systems into block-diagonal forms, the regularized optimal control problem amounts to easily parallelizable task of solving a sequence of smaller, fully-decoupled problems. While computational complexity of the algorithms that do not exploit spatially-invariant structure increases cubically with the number of subsystems, our algorithms exhibit a linear growth. After having identified a controller structure, the structured design step optimizes the network performance over the identified structure.

1.2.2 Sparsity-promoting optimal control of systems with invariances and symmetries

Structured control problems are, in general, challenging and nonconvex. Many recent works have identified classes of systems for which structured optimal control problems can be cast in convex forms. These include funnel causal and quadratically invariant systems [25,26], positive systems [27,28], structured and sparse consensus/synchronization

networks [2, 11, 29–32], optimal sensor/actuator selection [33, 34], and symmetric modifications to symmetric linear systems [35].

In many large-scale problems, controller structure is vitally important. As such, much effort has been devoted to developing scalable algorithms for nonconvex regularized \mathcal{H}_2 and \mathcal{H}_∞ design problems [19, 21–23, 33, 34, 36, 37]. Although many recent works have developed efficient algorithms for the nonconvex regularized \mathcal{H}_2 problems, in general, regularized \mathcal{H}_∞ problems are difficult because the \mathcal{H}_∞ norm is nonsmooth.

We propose a principled approach to general regularized \mathcal{H}_2 and \mathcal{H}_∞ optimal controller design. Our formulation treats control problems that minimize the \mathcal{H}_2 or \mathcal{H}_∞ norm by modifying the dynamical generator of a linear system, such as in linear state feedback. In this part, we use symmetries in system structure to form convex problems and gain computational advantage.

The contributions are twofold. First, in a similar vein as [35], we utilize the symmetric component of a general linear system to form a symmetric system for which the regularized \mathcal{H}_2 and \mathcal{H}_∞ optimal control problems are convex. We implement the controllers designed by this method on the original system. We show that this procedure guarantees stability and that the closed-loop \mathcal{H}_2 and \mathcal{H}_∞ performance of the symmetric system is an upper bound on the closed-loop \mathcal{H}_2 and \mathcal{H}_∞ performance of the original system.

Second, we provide a way to gain computational advantage by exploiting the block-diagonalizability of large scale systems. Such a structure arises, for example, in spatially-invariant systems [17]. In [38], the authors took advantage of this property to develop an efficient and scalable algorithm for sparsity-promoting feedback design. When a spatially-invariant system is subject to a spatially-invariant control law, the dynamics of the system can be represented as the sum of independent subsystems, making the problem amenable to distributed optimization.

1.2.3 Wide-area control in power systems

Inter-area oscillations in bulk power systems are associated with the dynamics of power transfers and involve groups of synchronous machines that oscillate relative to each other. Figure 1.2 These system-wide oscillations arise from modular network topologies, heterogeneous machine dynamics, adversely interacting controllers, and large inter-area

power transfers. With increased system loads and deployment of renewables in remote areas, long-distance power transfers will eventually outpace the addition of new transmission facilities. This induces severe stress and performance limitations on the transmission network and may even cause instability and outages [39].

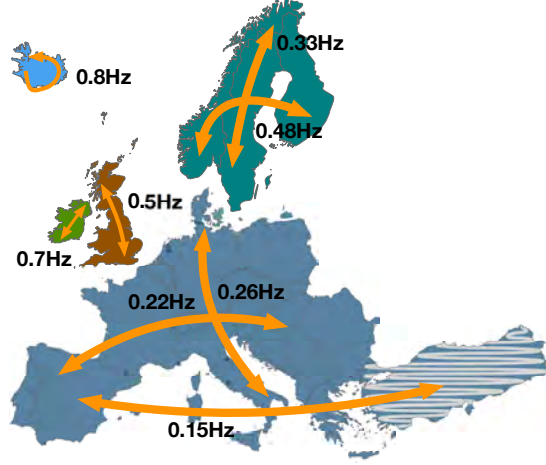


Figure 1.2: A few typical inter-area oscillations in Europe.

Traditional analysis and control of inter-area oscillations is based on modal approaches [40,41]. Typically, inter-area oscillations are identified from the spatial profiles of eigenvectors and participation factors of poorly damped modes [42,43], and they are damped via decentralized controllers, whose gains are carefully tuned using root locus [44,45], pole placement [46], adaptive [47], robust [48], and optimal [49] control strategies. To improve upon the limitations of decentralized control, recent research centers at distributed wide-area control strategies that involve the communication of remote signals [50,51]. See Fig. 1.3 for a comparison between conventional decentralized control and wide-area control strategies. The wide-area control signals are typically chosen to maximize modal observability metrics [52,53], and the control design methods range from root locus criteria to robust and optimal control approaches [54–56].

The spatial profiles of the inter-area modes together with modal controllability and observability metrics were previously used to indicate which wide-area links need to be added and how supplemental damping controllers have to be tuned. Here, we depart from the conventional modal approach and propose a novel methodology for analysis and

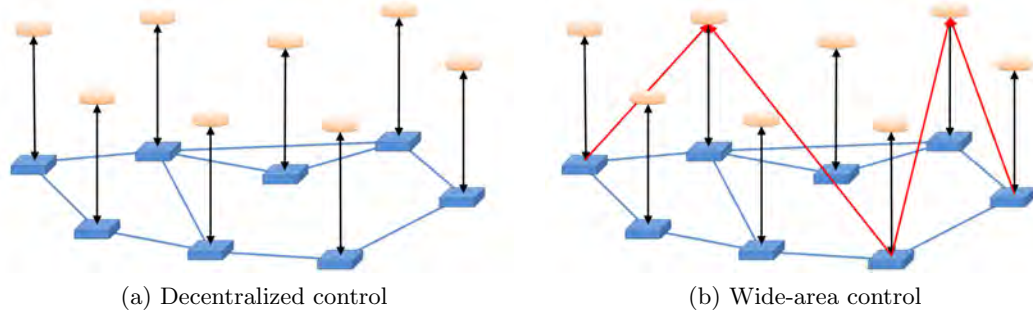


Figure 1.3: (a) Fully-decentralized control strategies implemented locally, ineffective against inter-area oscillations. (b) Distributed wide-area control using remote signals, effective against inter-area oscillations.

control of inter-area oscillations. In particular, we use input-output analysis to study oscillations in stochastically forced power systems. A similar approach was recently employed to quantify performance of consensus and synchronization networks [6, 11].

To identify wide-area control architectures and design optimal sparse controllers, we invoke the paradigm of sparsity-promoting optimal control [19–21, 30]. Recently, this framework was successfully employed for wide-area control of power systems [14, 15, 57, 58]. Here, we follow the formulation developed in [30] and find a linear state feedback that simultaneously optimizes a quadratic optimal control criterion (associated with incoherent and poorly damped oscillations) and induces a sparse control architecture. The main novel contributions of our control design approach are highlighted below. We improve the previous results [14, 15, 57, 58] at two levels: first, we preserve rotational symmetry of the original power system by allowing only relative angle measurements in the distributed controller, and, second, we allow identification of block-sparse control architectures, where local information associated with a subsystem is either entirely used (or discarded) for control.

We illustrate the utility of our approach using the IEEE 39 New England model [59]. We show how different sparsity-promoting penalty functions can be used to achieve a desired balance between closed-loop performance and communication complexity. In particular, we demonstrate that the addition of certain long-range communication links and careful retuning of the local controllers represent an effective means for improving system performance. For the New England model, it turns out that properly retuned

and *fully-decentralized* controllers can perform almost as well as the optimal centralized controllers. Our results thus provide a constructive answer to the much-debated question of whether locally observable oscillations in a power network are also locally controllable [60].

1.2.4 Distributed-PI control in power systems

The basic task of power system operation is to match load and generation. In an AC power grid, the synchronous frequency is a direct measure of the load-generation imbalance, which makes frequency control the fundamental power balancing mechanism. This task is traditionally accomplished by adjusting generation in a hierarchical three-layer structure: primary (droop control), secondary (automatic generation control) and tertiary (economic dispatch) layer, from fast to slow timescales, and from decentralized to centralized architectures [61, 62]. With the increasing penetration of distributed generation based on renewables, power systems are subject to larger and faster frequency fluctuations which have to be compensated by more and more small-scale and distributed generators. Thus, primary, secondary, and tertiary control tasks have to be handled in an increasing plug-and-play fashion, that is, using only local measurements, private model information, and without time-scale separations [63].

From a control-theoretic perspective, the three frequency control layers essentially correspond to proportional-integral (PI) control and set-point scheduling to solve a resource allocation problem. A broad range of research efforts have recently been put forward to decentralize these control tasks. While the primary layer is typically being implemented by means of proportional droop control, the secondary and tertiary integral and set-point controllers can be realized in a plug-and-play fashion through discrete-time averaging algorithms [64], continuous-time optimization approaches [65], or distributed averaging-based proportional-integral (DAPI) controllers [66]; see [67] for a recent literature review. Here, we focus on the simple yet effective DAPI controllers advocated, among others, in [66–70] to coordinate the action of multiple integral controllers through continuous averaging of the marginal injection costs to arrive at an optimal solution for a tertiary resource allocation problem.

More generally, PI control is a simple and effective method, it is well known for its ability to eliminate the influence of static control errors and constant disturbances, and it

is commonly used in many industrial applications [71,72]. For large-scale distributed systems DAPI-type control strategies have been used successfully for stabilization, disturbance rejection, and resource allocation, as summarized above for power systems [66–70] as well as for general network flow problems and other applications [73,74]. DAPI-type control strategies have also been studied from a pure theoretic perspective as natural extension to proportional consensus control; see [75,76] and the seminal paper [77].

A common theme of the above studies on various DAPI-type controllers is that the communication network among the integral controllers needs to be connected to achieve stable disturbance rejection and resource allocation. However, to the best of our knowledge, there are no studies addressing the question of how to optimally design the *cyber* integral control network relative to the *physical* dynamics and interactions. Here, we pursue this question for the special case of frequency regulation in a power system and using the DAPI controllers advocated in [66,67,69,70,78–80].

In this section, we identify topology of the integral control communication graph and design the corresponding edge weights for the DAPI controller. In previous studies, the common assumption on the controller graph being undirected appears overly restrictive and requires many communication resources. Our proposed approach allows us to identify stabilizing and optimal integral controllers with a sparse and directed communication architecture. As a preliminary pre-processing step, we introduce a coordinate transformation to enforce the structural constraints on the rotor angles and auxiliary integral states. In the new set of coordinates, the system dynamics are amenable to both standard linear quadratic regulator tools as well as a ℓ_1 regularized version of the standard \mathcal{H}_2 optimal control problem. We invoke the paradigm of sparsity-promoting optimal control developed in [19–21] and seek a balance between system performance and sparsity of the integral controller. An alternating direction method of multipliers (ADMM) algorithm is used to iteratively solve the static output-feedback control problem. Similar techniques have recently been successfully used to solve wide-area control problems in bulk power grids [14–16,81,82]. For the New England example, we show that distributed integral control can achieve reasonable performance compared to the optimal centralized controller. The optimal communication topology for the distributed integral controller is directed and related to the rotational inertia and cost coefficients of the synchronous generators.

1.2.5 Design of optimal coupling gains for synchronization of nonlinear oscillators

Synchronization of coupled Liénard-type oscillators is relevant to several engineering applications [83, 84]. This chapter outlines a structured control-synthesis method to regulate the voltage amplitudes of a class of weakly nonlinear Liénard-type oscillators coupled through connected resistive networks with arbitrary topologies. The feedback gain takes the connotation of a current gain (which scales the output current of the oscillator); and the structured optimal-control problem is of interest since we seek a decentralized control strategy that precludes communications between oscillators. The problem setup is motivated by the application of controlling power-electronic inverters in low-inertia microgrids in the absence of conventional synchronous generators. A compelling time-domain approach to achieve a stable power system in this setting is to regulate the inverters to emulate the dynamics of weakly nonlinear limit-cycle oscillators which achieves network-wide synchrony in the absence of external forcing or any communication [85, 86]. That said, this chapter offers several broad contributions to the topic of synchronization of nonlinear dynamical systems coupled over complex networks. First, we outline the control-synthesis approach with a broad level of generality to cover a wide array of circuit applications; in addition to power-systems and microgrids, these include solid-state circuit oscillators, semiconductor laser arrays, and microwave oscillator arrays [84, 87, 88]. Second, majority of the synchronization literature is primarily focused on phase- or pulse-coupled oscillator models [88, 89]. We depart from this line of work and focus on the complementary problem of optimally regulating the amplitude dynamics. (For the class of networks we study, phase synchrony can be guaranteed under fairly mild assumptions.)

Circuits with voltage dynamics governed by Liénard’s equation are common in several applications [90–92]. (The ubiquitous Van der Pol oscillator is a particular example.) We study the setting where the oscillators are connected to a resistive network with an arbitrary topology. The oscillator output currents are scaled by a gain which assumes the focus of the control design. Designing coupling gains with a view to synchronize the outputs of dynamical systems has been studied in a variety of applications [93–95]. The nonlinear dynamics complicate our problem setting, and the solution strategy we

propose draws from a variety of circuit- and system-theoretic tools including averaging methods for periodic nonlinear systems and structural reduction of electrical networks. Furthermore, conventional optimal control synthesis methods cannot guarantee decentralized control strategies (translating to local current gains). To address this, we leverage recent advances in structured control design.

Conventional optimal control design strategies typically return full feedback gain matrices. (A full feedback gain matrix in our setting would imply that extraneous communication links are required between the oscillators.) Since we seek a decentralized control strategy so that voltage regulation can be guaranteed only by tuning the local current gains, we leverage our expertise in structured feedback gain design for distributed systems that has demonstrated its effectiveness in the domain of power networks [14–16, 30, 81]. In particular, we present a sparsity-promoting optimal control design strategy [21] to design the current gains so that the differences between the oscillator terminal-voltage amplitudes can be minimized. The objective of the optimization problem is to tune the current gains to minimize the \mathcal{H}_2 norm of the system. In general, the optimization problem is non-convex and difficult to solve. We utilize the alternating direction method of multipliers (ADMM) algorithm to perform an iterative search for the optimal solution.

The control design strategy outlined above is tailored to linear system descriptions. The oscillator dynamics that derive from circuit laws are innately nonlinear and in Cartesian coordinates. As such, they pose a challenge for control synthesis. To facilitate control design, we leverage polar-coordinate transformations, tools from averaging theory, and linear systems theory [83, 96]. First, by transforming the system into the polar coordinates, we extract the amplitude and phase dynamics of the terminal voltages. We then average the periodic dynamics and linearize the system around the nominal operating point.

1.3 Dissertation structure

This dissertation consists of three parts. Each part focuses on a specific topic and includes individual chapters that studies relevant subjects. In each chapter, we provide background and motivation, problem formulation, design procedure, case study and

conclusion.

Part I considers optimal control problems in systems with symmetries and consensus/synchronization networks. These systems feature structural constraints that arise either from the underlying group structure or the lack of the absolute measurements for a part of the state vector. Chapter 2 propose a framework to solve the resulting sparsity-optimal control problem, which aims to design controller that utilize limited information exchange between subsystems in large-scale networks. Chapter 3 cast the problem of minimizing the \mathcal{H}_2 or \mathcal{H}_∞ performance of the closed-loop system with symmetric dynamic matrices as a convex optimization problem. Moreover, it provides bounds on the \mathcal{H}_2 and \mathcal{H}_∞ performance of the original system by studying the symmetric component of a general system's dynamic matrices.

Part II studies wide-area control of inter-area oscillation in bulk power systems. Non-modal tools are employed to analyze and control inter-area oscillations. Input-output analysis is used to examines power spectral density and variance amplification of stochastically forced systems and offers new insights relative to modal approaches. To improve upon the limitations of conventional wide-area control strategies, the problems of signal selection and optimal design of sparse and block-sparse wide-area controllers are studied. Case study on a bench mark example, the IEEE 39 New England model, is provided.

Part III focuses on two applications in sparse control design of distributed systems. Chapter 5 considers the optimal frequency regulation problem and propose a principled heuristic to identify the topology and gains of the distributed integral control layer. An ℓ_1 -regularized \mathcal{H}_2 -optimal control framework is employed for striking a balance between network performance and communication requirements. Illustrative example is shown to demonstrate that the identified sparse and distributed integral controller can achieve reasonable performance relative to the optimal centralized controller. Chapter 6 develops a structured optimal-control framework to design coupling gains for synchronization of weakly nonlinear oscillator circuits connected in resistive networks with arbitrary topologies. A sparsity-promoting optimal control algorithm is developed to tune the optimal diagonal feedback-gain matrix with minimal performance sacrifice.

1.4 Contributions of the dissertation

In this section, the structure of the dissertation is provided along with the main contributions of each part.

Part I

Optimal sparse feedback design. The objective is to design controllers that provide a desired tradeoff between the network performance and the sparsity of the static output-feedback controller. This is accomplished by regularizing the \mathcal{H}_2 optimal control problem with a penalty on communication requirements in the distributed controller. In contrast to previous work [19–21], this regularization penalty reflects the fact that sparsity should be enforced in a specific set of coordinates. In [19–21], the elements of the state-feedback gain matrix were taken to represent communication links. Herein, we present a unified framework where a communication link is a linear function of the elements of the output-feedback gain matrix. We show how alternating direction method of multipliers can be leveraged to exploit the underlying structure and compute sparsity-promoting controllers. In particular, for spatially-invariant systems, the computational complexity of our algorithms scales linearly with the number of subsystems. We also identify a class of optimal control problems that can be cast as semidefinite programs and provide an example to illustrate our developments.

Sparsity-promoting optimal control of systems with invariances and symmetries. A principled approach is proposed to general regularized \mathcal{H}_2 and \mathcal{H}_∞ optimal controller design. Our framework formulates optimal control problems that minimize the \mathcal{H}_2 or \mathcal{H}_∞ norm by modifying the dynamical generator of a linear system. We make use of the symmetries in system structure to cast the resulting optimal control design as convex problems and gain computational efficiency. We implement the controllers designed by our framework on the original system. This procedure guarantees stability and that the closed-loop \mathcal{H}_2 and \mathcal{H}_∞ performance of the symmetric system is an upper bound on the closed-loop \mathcal{H}_2 and \mathcal{H}_∞ performance of the original system. In addition, we provide a mean to gain computational efficiency by exploiting the block-diagonalizability of large scale systems. Such an example is provided for spatially-invariant systems.

Part II

Decentralized optimal control of inter-area oscillations. To improve upon the limitations of conventional decentralized controllers, we develop a distributed wide-area control strategy that involve the communication of remote signals and provide a potential approach for retuning of the existing decentralized control gains. We analyze inter-area oscillations by means of the Ht norm of this system, as in recent related approaches for interconnected oscillator networks and multi-machine power systems. We show that an analysis of power spectral density and variance amplification offers complementary insights that complement conventional modal approaches. The main novel contributions of our control design approach are as follows. We improve the previous results [14, 15, 57, 58] at two levels: first, we preserve rotational symmetry of the original power system by allowing only relative angle measurements in the distributed controller, and, second, we allow identification of block-sparse control architectures, where local information associated with a subsystem is either entirely used or discarded for control. We show how different sparsity-promoting penalty functions can be used to achieve a desired balance between closed-loop performance and communication complexity. In particular, we demonstrate that the addition of certain long-range communication links and careful retuning of the local controllers represent an effective means for improving system performance.

Part III

Design of distributed integral control action in power networks. We address the question of how to optimally design the cyber integral control network relative to the physical dynamics and interactions. Here, we pursue this problem for frequency regulation in a power system and using the DAPI controllers advocated in [66, 67, 69, 70, 78–80]. We identify optimal structure of the integral control communication graph and design the corresponding edge weights for the integral controller. We formulate the design of integral controller as a static output-feedback control problem. The sparsity-promoting optimal control algorithm is then used to solve the optimization problem.

Design of optimal coupling gains for synchronization of nonlinear oscillators.

This chapter outlines a structured control-synthesis method to regulate the voltage amplitudes of a class of weakly nonlinear Liénard-type oscillators coupled through connected resistive networks with arbitrary topologies. Our framework offers several broad contributions to the topic of synchronization of nonlinear dynamical systems coupled over complex networks. First, we outline the control-synthesis approach with a broad level of generality to cover a wide array of circuit applications; in addition to power-systems and microgrids, these include solid-state circuit oscillators, semiconductor laser arrays, and microwave oscillator arrays [84,87,88]. Second, majority of the synchronization literature is primarily focused on phase- or pulse-coupled oscillator models [88,89]. We depart from this line of work and focus on the complementary problem of optimally regulating the amplitude dynamics.

Part I

Sparsity-promoting optimal control

Chapter 2

Optimal Sparse Feedback Design

Optimal control problems in systems with symmetries and consensus/synchronization networks are characterized by structural constraints that arise either from the underlying group structure or the lack of the absolute measurements for a part of the state vector. Our objective is to design controller structures and resulting control strategies that utilize limited information exchange between subsystems in large-scale networks. To obtain controllers with low communication requirements, we seek solutions to regularized versions of the \mathcal{H}_2 optimal control problem [97].

2.1 Motivation and background

We consider a class of control problems

$$\begin{aligned}\dot{\hat{x}} &= \hat{A} \hat{x} + \hat{B}_1 \hat{d} + \hat{B}_2 \hat{u} \\ \hat{z} &= \hat{C}_1 \hat{x} + \hat{D} \hat{u} \\ \hat{y} &= \hat{C}_2 \hat{x} \\ \hat{u} &= -\hat{K} \hat{y}\end{aligned}\tag{2.1}$$

where \hat{x} is the state, \hat{d} and \hat{u} are the disturbance and control inputs, \hat{z} is the performance output, and \hat{y} is the measured output. The matrices \hat{C}_1 and \hat{D} are given by $[\hat{Q}^{1/2} \ 0]^*$ and $[0 \ \hat{R}^{1/2}]^*$ with standard assumptions on stabilizability and detectability of pairs (\hat{A}, \hat{B}_2) and $(\hat{A}, \hat{Q}^{1/2})$. Here, $(\cdot)^*$ denotes complex-conjugate transpose of a given matrix.

The matrices $\hat{Q} = \hat{Q}^* \succeq 0$ and $\hat{R} = \hat{R}^* \succ 0$ are the state and control performance weights, and the closed-loop system is given by

$$\begin{aligned}\dot{\hat{x}} &= (\hat{A} - \hat{B}_2 \hat{K} \hat{C}_2) \hat{x} + \hat{B}_1 \hat{d} \\ \hat{z} &= \begin{bmatrix} \hat{Q}^{1/2} \\ -\hat{R}^{1/2} \hat{K} \hat{C}_2 \end{bmatrix} \hat{x}.\end{aligned}\tag{2.2}$$

We assume that there is a stabilizing feedback gain matrix \hat{K} .

Our objective is to achieve a desired tradeoff between the \mathcal{H}_2 performance of system (2.2) and the sparsity of a matrix that is related to the feedback gain matrix \hat{K} through a linear transformation $\mathcal{T}(\hat{K})$. To address this challenge we consider a regularized optimal control problem

$$\underset{\hat{K}}{\text{minimize}} \quad J(\hat{K}) + \gamma g(\mathcal{T}(\hat{K}))\tag{2.3}$$

where $J(\hat{K})$ is the \mathcal{H}_2 norm of system (2.2), γ is a positive regularization parameter, and $g(\mathcal{T}(\hat{K}))$ is a sparsity-promoting regularization term (see Section 2.1.3 for details).

Linear transformation $\mathcal{T}(\hat{K})$ of the feedback gain \hat{K} in (2.3) reflects the fact that *sparsity should be enforced in a specific set of coordinates*. This characterization is more general than the one considered in [19–21] where the sparsity-promoting optimal control was originally introduced and algorithms were developed. In contrast to [19–21], where it was assumed that the state-space model is given in physically meaningful coordinates, herein we only require that the states in (2.2) are related to these coordinates via a linear transformation \mathcal{T} . One such example arises in spatially invariant systems where the “spatial frequency” domain is convenient for minimizing quadratic performance objective [17], whereas sparsity requirements are naturally expressed in the physical domain. Another class of problems is given by consensus and synchronization networks where the absence of absolute measurements confines standard control-theoretic requirements to a subspace of the original state-space.

2.1.1 Problem formulation

As mentioned earlier, while it is convenient to formulate minimization of the quadratic performance index in terms of the feedback gain \hat{K} , it may be desirable to promote sparsity in a different set of coordinates. By introducing an additional optimization variable K , we bring (2.3) into the following form,

$$\begin{aligned} & \underset{\hat{K}, K}{\text{minimize}} && J(\hat{K}) + \gamma g(K) \\ & \text{subject to} && \mathcal{T}(\hat{K}) - K = 0, \end{aligned} \quad (2.4a)$$

where $g(K)$ is a sparsity-promoting regularization term and \mathcal{T} is a linear operator. In the \mathcal{H}_2 setting, $J(\hat{K})$ is given by

$$J(\hat{K}) := \begin{cases} \text{trace} \left((\hat{Q} + \hat{C}_2^* \hat{K}^* \hat{R} \hat{K} \hat{C}_2) \hat{X} \right), & \hat{K} \text{ stabilizing} \\ \infty, & \text{otherwise} \end{cases} \quad (2.4b)$$

where the closed-loop controllability Gramian \hat{X} satisfies the Lyapunov equation

$$(\hat{A} - \hat{B}_2 \hat{K} \hat{C}_2) \hat{X} + \hat{X} (\hat{A} - \hat{B}_2 \hat{K} \hat{C}_2)^* + \hat{B}_1 \hat{B}_1^* = 0. \quad (2.4c)$$

Clearly, for any feasible \hat{K} and K , the optimal control problems (2.3) and (SP) are equivalent. We note that the linear constraint in (SP) is more general than the constraint considered in [19–21], where $\hat{K} - K = 0$. This introduces additional freedom in control design and broadens applicability of the developed tools.

In the set of coordinates where it is desired to promote sparsity, the closed-loop system takes the form

$$\begin{aligned} \dot{x} &= (A - B_2 K C_2) x + B_1 d \\ z &= \begin{bmatrix} Q^{1/2} \\ -R^{1/2} K C_2 \end{bmatrix} x, \end{aligned} \quad (2.5)$$

where $K = \mathcal{T}(\hat{K})$.

2.1.2 Examples

Consensus and synchronization networks

Consensus and synchronization problems are of increasing importance in applications ranging from biology to computer science to power systems [1–11, 14–16]. In each of these, it is of interest to reach an agreement or to achieve synchronization between the nodes in the network.

In consensus and synchronization networks with the state vector

$$x := \begin{bmatrix} p^* & q^* \end{bmatrix}^* \in \mathbb{R}^n$$

only relative differences between the components of the vector $p(t) \in \mathbb{R}^N$ are allowed to enter into (2.5). This requirement imposes structural constraints on the matrices in (2.5), which are partitioned conformably with the partition of the state vector x ,

$$\begin{aligned} A &= \begin{bmatrix} A_{11} & A_{12} \\ A_{21} & A_{22} \end{bmatrix}, \quad B_i = \begin{bmatrix} B_{ip} \\ B_{iq} \end{bmatrix}, \\ Q &= \begin{bmatrix} Q_p & 0 \\ 0 & Q_q \end{bmatrix}, \quad K = \begin{bmatrix} K_p & K_q \end{bmatrix}. \end{aligned} \tag{2.6}$$

For $C_2 = I$, the restriction on the absence of the access to the absolute measurements of the components of the vector p translates into the following requirements

$$A_{11} \mathbf{1} = 0, \quad A_{21} \mathbf{1} = 0, \quad Q_p \mathbf{1} = 0, \quad K_p \mathbf{1} = 0 \tag{2.7}$$

where $\mathbf{1}$ is the vector of all ones. Under these conditions, the closed-loop system (2.5) has an eigenvalue at zero and the corresponding eigenvector $\begin{bmatrix} \mathbf{1}^* & 0^* \end{bmatrix}^*$ is associated with the average of the vector p , $\bar{p} := (1/N) \mathbf{1}^* p$. If the pairs (A, B_2) and $(A, Q^{1/2})$ are stabilizable and detectable on the subspace \mathcal{S} ,

$$\mathcal{S} := \begin{bmatrix} \mathbf{1} \\ 0 \end{bmatrix}^\perp = \begin{bmatrix} \mathbf{1}^\perp \\ \mathbb{R}^{n-N} \end{bmatrix}$$

a coordinate transformation $\hat{x} := Tx$ can be introduced to eliminate the average mode

\bar{p} from (2.5).

To achieve the goal of eliminating the average mode, $\bar{p} := (1/N) \mathbf{1}^* p$, we introduce the following coordinate transformation

$$\underbrace{\begin{bmatrix} p \\ q \end{bmatrix}}_x = \underbrace{\begin{bmatrix} U & 0 \\ 0 & I \end{bmatrix}}_{T^+} \underbrace{\begin{bmatrix} \psi \\ q \end{bmatrix}}_{\hat{x}} + \begin{bmatrix} \mathbf{1} \\ 0 \end{bmatrix} \bar{p}$$

where the columns of the matrix $U \in \mathbb{R}^{N \times (N-1)}$ form an orthonormal basis for the subspace $\mathbf{1}^\perp$. For example, the columns of U can be obtained from the $(N-1)$ eigenvectors of the matrix Q_p corresponding to the non-zero eigenvalues. Using properties of the matrix U

$$U^* U = I, \quad U U^* = I - (1/N) \mathbf{1} \mathbf{1}^*, \quad U^* \mathbf{1} = 0,$$

we equivalently have

$$\underbrace{\begin{bmatrix} \psi \\ q \end{bmatrix}}_{\hat{x}} = \underbrace{\begin{bmatrix} U^* & 0 \\ 0 & I \end{bmatrix}}_T \underbrace{\begin{bmatrix} p \\ q \end{bmatrix}}_x.$$

This change of coordinates brings the closed-loop system (2.5) into the form (2.2) which does not contain the average mode \bar{p} . The matrices in (2.2) are given by

$$\begin{aligned} \hat{A} &:= T A T^+, & \hat{B}_i &:= T B_i, & \hat{C}_2 &:= C_2 T^+ \\ \hat{Q} &:= T^{+*} Q T^+, & \hat{R} &:= R \end{aligned}$$

with $\hat{u} = u$, $\hat{d} = d$, $\hat{z} = z$. Finally, we note that the feedback gain matrices \hat{K} and K are related by the transformation matrix T

$$K = \mathcal{T}(\hat{K}) = \hat{K} T \Leftrightarrow \hat{K} = K T^+,$$

which has the right inverse T^+ , $T T^+ = I$. In consensus and synchronization networks, the rows of the matrix T form an orthonormal basis and we thus have $T^+ = T^*$.

We next provide particular examples that can be described by (2.2) and (2.5) with structural constraints (4.4).

Swing equation. In power networks, swing equation is used to characterize energy exchange between generators [98]. After linearization around a stationary operating point, the swing equation reduces to

$$M \ddot{p} + D \dot{p} + L_p p = d + u \quad (2.8)$$

where p is the vector of rotor angles, M and D are diagonal matrices of inertia and damping coefficients, and L_p is the Laplacian matrix that describes the interaction topology. By setting $q := \dot{p}$, (5.1) is brought into the state-space form (2.5)-(2.6) with

$$A = \begin{bmatrix} 0 & I \\ -M^{-1} L_p & -M^{-1} D \end{bmatrix}, \quad B_i = \begin{bmatrix} 0 \\ M^{-1} \end{bmatrix}. \quad (2.9)$$

Since $L_p \mathbf{1} = 0$, the structural restrictions (4.4) are satisfied if $Q_p \mathbf{1} = 0$ and $K_p \mathbf{1} = 0$.

Single-integrator consensus networks. Networks in which each node updates a scalar variable p_i using relative information exchange with its neighbors can be obtained from (5.1) by setting the matrix M to zero; e.g., see [1]. In this case, the matrices in the state-space model (2.5)-(2.6) simplify to $A = -D^{-1} L_p$ and $B_1 = B_2 = D^{-1}$.

Power systems. Models of power networks account for the dynamics of generators, control devices, and algebraic equations that describe load flow, stators, and electronic circuits. Control actions are typically executed using generator excitation via power system stabilizers (PSS), governor control, or power electronics (FACTS). In addition to the rotor angles p and frequencies $v := \dot{p}$, additional states r that account for fast electrical devices are needed to describe the dynamics of the entire system. After linearization at a stationary operating point, the state-space model can be written in the form (2.5)-(2.6) by defining $q := \begin{bmatrix} v^* & r^* \end{bmatrix}^*$ with

$$\begin{aligned} A_{11} &:= 0, & A_{12} &:= \begin{bmatrix} I & 0 \end{bmatrix}, \\ A_{21} &:= \begin{bmatrix} -M^{-1} L_p \\ A_{rp} \end{bmatrix}, & A_{22} &:= \begin{bmatrix} -M^{-1} D & A_{qr} \\ A_{rq} & A_{rr} \end{bmatrix}. \end{aligned}$$

Since only differences between rotor angles of different generators enter into the original nonlinear differential equations, this property is shared by the linearized set of equations,

thereby implying $A_{21}\mathbf{1} = 0$. Furthermore, in the absence of the access to the absolute rotor angle measurements both the matrix A in (2.6) and its closed-loop equivalent in (2.5) have an eigenvalue at zero with the corresponding eigenvector $\begin{bmatrix} \mathbf{1}^* & 0^* \end{bmatrix}^*$. Such formulation has been recently utilized in [16].

Spatially-invariant systems

For systems with invariances and symmetries, transform techniques can be used to bring a large-scale analysis and design problems into a parametrized family of smaller problems. One such class is given by spatially invariant systems that evolve over a discrete spatially-periodic domain (e.g., a one-dimensional circle or a multi-dimensional torus). In this case, the matrices in (2.5) are block circulant matrices and the application of the discrete Fourier transform (DFT) in the spatially invariant directions brings them into a block-diagonal form (2.2). As shown in [17], the optimal centralized controllers for spatially invariant systems with quadratic performance indices are also spatially invariant; thus, in the transformed domain they also take the block-diagonal form. Consequently, determining the optimal centralized controller amounts to easily parallelizable task of solving a sequence of smaller, fully-decoupled optimal control problems.

For spatially-invariant systems (2.5) with block-circulant matrices, the application of DFT

$$\hat{x} = T x, \quad \hat{u} = T u, \quad \hat{d} = T d, \quad \hat{z} = T z,$$

brings the closed-loop system (2.5) to the form (2.2) with block-diagonal matrices \hat{A} , \hat{B}_1 , \hat{B}_2 , \hat{C}_2 , \hat{Q} , \hat{R} , and \hat{K} . Here, T is the discrete Fourier matrix and the feedback gain matrices are related via a linear transformation [38],

$$K = \mathcal{T}(\hat{K}) = T^* \hat{K} T.$$

2.1.3 Sparsity-promoting penalty functions

We briefly describe two classes of sparsity-promoting penalty functions. More sophisticated penalties can also be introduced; see [16] for examples in power networks.

Elementwise sparsity. The weighted ℓ_1 -norm,

$$g(K) := \sum_{i,j} W_{ij} |K_{ij}| \quad (2.10)$$

is a commonly used proxy for enhancing elementwise sparsity of the matrix K [99]. The non-negative weights W_{ij} provide additional flexibility relative to the standard ℓ_1 -regularization. An iterative reweighting method was introduced in [99] to provide better approximation of the non-convex cardinality function. In the m th iteration, the weights W_{ij} are set to be inversely proportional to the absolute value of K_{ij} in the previous iteration,

$$W_{ij}^m = 1 / (|K_{ij}^{m-1}| + \epsilon)$$

where $0 < \epsilon \ll 1$ guards against $K_{ij} = 0$.

Block sparsity. By selecting $g(K)$ to penalize the Frobenius norm of the ij th block of the matrix K ,

$$g(K) := \sum_{i,j} W_{ij} \|K_{ij}\|_F$$

sparsity can be enhanced at the level of submatrices [100]. In the iterative reweighting algorithm, the absolute value should be replaced by the Frobenius norm of K_{ij}

$$W_{ij}^m = 1 / (\|K_{ij}^{m-1}\|_F + \epsilon).$$

2.2 Class of convex problems

For an undirected consensus network in which each node updates a scalar value p_i , we next show that the sparsity-promoting optimal control problem can be formulated as an SDP. The closed-loop system (2.5) with

$$A := -L_p, \quad B_1 = B_2 := I, \quad C_2 = I, \quad K := L_k$$

can be written as

$$\begin{aligned}\dot{p} &= -(L_p + L_k)p + d \\ z &= \begin{bmatrix} Q^{1/2} \\ -R^{1/2} L_k \end{bmatrix} p\end{aligned}\tag{2.11}$$

where the symmetric positive semi-definite matrices L_p and L_k satisfy $L_p \mathbf{1} = 0$, $L_k \mathbf{1} = 0$. These two Laplacian matrices contain information about the interconnection structure of the open-loop system and the controller.

The ℓ_1 -regularized \mathcal{H}_2 optimal control problem can be formulated as

$$\underset{L_k}{\text{minimize}} \quad J(L_k) + \gamma \|W \circ L_k\|_{\ell_1}.\tag{2.12}$$

Here, \circ denotes elementwise matrix multiplication and the solution to the algebraic Lyapunov equation

$$(L_p + L_k)P + P(L_p + L_k) = Q + L_k R L_k$$

determines the \mathcal{H}_2 of the closed-loop system, $J(L_k) = \text{trace}(P)$. It is readily shown that the stability of (2.11) on the subspace $\mathbf{1}^\perp$ amounts to positive-definiteness of the matrix $(L_p + L_k)$ on $\mathbf{1}^\perp$. Under this condition, we can rewrite $J(L_k)$ as

$$\begin{aligned}J(L_k) &= \text{trace}((L_p + L_k)^\dagger (Q + L_k R L_k)) \\ &= \frac{1}{2} \text{trace}((L_p + L_k + \frac{1}{N} \mathbf{1}\mathbf{1}^T)^{-1} (Q + L_k R L_k))\end{aligned}$$

where $(L_p + L_k)^\dagger$ denotes the Moore-Penrose pseudoinverse of $(L_p + L_k)$, and cast the sparsity-promoting optimal control problem (2.12) to an SDP via the Schur complement,

$$\begin{aligned}&\underset{Y, Z, L_k}{\text{minimize}} \quad \frac{1}{2} \text{trace}(Y) + \gamma \mathbf{1}^T Z \mathbf{1} \\ &\text{subject to} \quad \begin{bmatrix} Y & \begin{bmatrix} Q^{1/2} \\ R^{1/2} L_k \end{bmatrix} \\ (\cdot)^* & L_p + L_k + \frac{1}{N} \mathbf{1}\mathbf{1}^T \end{bmatrix} \succeq 0 \\ &\quad L_k \mathbf{1} = 0 \\ &\quad -Z \leq W \circ L_k \leq Z.\end{aligned}\tag{2.13}$$

For small size problems, the resulting SDP formulation can be solved efficiently using available SDP solvers.

In addition to the optimal edge design in undirected consensus networks, several other classes of problems admit convex characterizations: a class of optimal synchronization problems [11], optimal actuator/sensor selection [33, 34], symmetric modifications of symmetric systems [19, 35], and diagonal modifications of positive systems [28].

2.3 Design of controller structure

We next develop an algorithm, based on the Alternating Direction Method of Multipliers (ADMM), to solve the sparsity-promoting optimal control problem (2.4),

$$\begin{aligned} & \underset{\hat{K}, K}{\text{minimize}} && J(\hat{K}) + \gamma g(K) \\ & \text{subject to} && \mathcal{T}(\hat{K}) - K = 0. \end{aligned}$$

As we describe next, the introduction of the linear constraint in (SP) in conjunction with utilization of the ADMM algorithm allows us to exploit the respective structures of the objective functions J and g in (2.4).

2.3.1 Structure design via ADMM

The structure of feedback gains that strike a balance between quadratic performance of the system and sparsity of the controller is designed via ADMM. The ADMM algorithm starts by introducing the augmented Lagrangian

$$\mathcal{L}_\rho(\hat{K}, K, \Lambda) = J(\hat{K}) + \gamma g(K) + \langle \Lambda, \mathcal{T}(\hat{K}) - K \rangle + \frac{\rho}{2} \langle \mathcal{T}(\hat{K}) - K, \mathcal{T}(\hat{K}) - K \rangle$$

where Λ is the Lagrange multiplier, ρ is a positive scalar, and $\langle \cdot, \cdot \rangle$ is the standard inner product between two matrices. Instead of minimizing the augmented Lagrangian jointly

with respect to \hat{K} and K , ADMM uses a sequence of iterations [24],

$$\begin{aligned}\hat{K}^{k+1} &= \underset{\hat{K}}{\operatorname{argmin}} \mathcal{L}_\rho(\hat{K}, K^k, \Lambda^k) \\ K^{k+1} &= \underset{K}{\operatorname{argmin}} \mathcal{L}_\rho(\hat{K}^{k+1}, K, \Lambda^k) \\ \Lambda^{k+1} &= \Lambda^k + \rho(\mathcal{T}(\hat{K}^{k+1}) - K^{k+1})\end{aligned}$$

until primal and dual residuals are smaller than specified thresholds,

$$\|\mathcal{T}(\hat{K}^{k+1}) - K^{k+1}\|_F \leq \epsilon_p, \quad \|K^{k+1} - K^k\|_F \leq \epsilon_d.$$

It is readily shown that \hat{K} -minimization step amounts to the quadratically-augmented minimization of $J(\hat{K})$,

$$\hat{K}^{k+1} := \underset{\hat{K}}{\operatorname{argmin}} \left(J(\hat{K}) + \frac{\rho}{2} \|\mathcal{T}(\hat{K}) - H^k\|_F^2 \right)$$

where $H^k := K^k - (1/\rho) \Lambda^k$. Similarly, using completion of squares, the K -minimization problem can be brought into the following form

$$K^{k+1} := \underset{K}{\operatorname{argmin}} \left(\gamma g(K) + \frac{\rho}{2} \|K - V^k\|_F^2 \right)$$

with $V^k := \mathcal{T}(\hat{K}^{k+1}) + (1/\rho) \Lambda^k$. Thus, updating K requires computation of the proximal operator of the function g .

K -minimization step

For elementwise sparsity, the objective function in the K -minimization step takes separable form,

$$\sum_{i,j} (\gamma W_{ij} |K_{ij}| + \frac{\rho}{2} (K_{ij} - V_{ij}^k)^2),$$

and the update of K is obtained via convenient use of the soft-thresholding operator,

$$K_{ij}^{k+1} = \begin{cases} (1 - a/|V_{ij}^k|) V_{ij}^k & |V_{ij}^k| > a \\ 0 & |V_{ij}^k| \leq a \end{cases}$$

where $a := (\gamma/\rho)W_{ij}$. This analytical update of K is independent of the quadratic performance index J . Similarly, for block sparsity, the minimizer is determined by

$$K_{ij}^{k+1} = \begin{cases} (1 - a/\|V_{ij}^k\|_F) V_{ij}^k & \|V_{ij}^k\|_F > a \\ 0 & \|V_{ij}^k\|_F \leq a \end{cases}$$

where K_{ij} and V_{ij} are the corresponding submatrices.

\hat{K} -minimization step

Finding the solution to the \hat{K} -minimization problem represents the biggest challenge to solving the sparsity-promoting optimal control problem (2.4) via ADMM. In what follows, we introduce two methods to solve the \hat{K} -minimization problem: the Anderson-Moore method and the proximal gradient method.

Anderson-Moore method. For the \mathcal{H}_2 optimal control problem (2.4), the optimality conditions in the \hat{K} -minimization step are given by

$$(\hat{A} - \hat{B}_2 \hat{K} \hat{C}_2) \hat{X} + \hat{X} (\hat{A} - \hat{B}_2 \hat{K} \hat{C}_2)^* = -\hat{B}_1 \hat{B}_1^* \quad (\text{NC-X})$$

$$(\hat{A} - \hat{B}_2 \hat{K} \hat{C}_2)^* \hat{P} + \hat{P} (\hat{A} - \hat{B}_2 \hat{K} \hat{C}_2) = -(\hat{Q} + \hat{C}_2^* \hat{K}^* \hat{R} \hat{K} \hat{C}_2) \quad (\text{NC-P})$$

$$2(\hat{R} \hat{K} \hat{C}_2 - \hat{B}_2^* \hat{P}) \hat{X} \hat{C}_2^* + \rho \mathcal{T}^\dagger(\mathcal{T}(\hat{K}) - H^k) = 0 \quad (\text{NC-K})$$

where \mathcal{T}^\dagger is the adjoint of the operator \mathcal{T} ,

$$\langle K, \mathcal{T}(\hat{K}) \rangle = \langle \mathcal{T}^\dagger(K), \hat{K} \rangle.$$

The unknowns in this system of nonlinear matrix-valued equations are the feedback gain \hat{K} as well as the controllability and observability Gramians \hat{X} and \hat{P} of the closed-loop system (2.2). These equations can have multiple solutions, each of which is a stationary point of the \hat{K} -minimization problem. In general, it is not known how many stationary points exist or how to find all of them.

The Anderson-Moore method solves the above system of equations in an iterative fashion. In each iteration, the algorithm starts with a stabilizing feedback matrix \hat{K} and solves two Lyapunov equations and one Sylvester equation. Specifically, it first

solves (NC-X) and (NC-P) for controllability and observability Gramians \hat{X} and \hat{P} with \hat{K} being fixed. Then the Sylvester equation (NC-K) is solved for \hat{K} with \hat{X} and \hat{P} being fixed.

For consensus and synchronization problems discussed in Section 2.1.2, we have

$$K = \mathcal{T}(\hat{K}) = \hat{K} T \Leftrightarrow \hat{K} = \mathcal{T}^\dagger(K) = K T^+$$

with $TT^+ = I$. If the control weight \hat{R} is given by a scaled version of the identity matrix

$$\hat{R} = r I, \quad r > 0$$

Sylvester equation (NC-K) can be explicitly solved for \hat{K} ,

$$\hat{K} = \left(2 \hat{B}_2^* \hat{P} \hat{X} \hat{C}_2^* + \rho H^k T^+ \right) \left(2 r \hat{C}_2 \hat{X} \hat{C}_2^* + \rho I \right)^{-1}.$$

Following [21], we can show that the difference between two consecutive updates of \hat{K} forms a descent direction for

$$L(\hat{K}) := J(\hat{K}) + \frac{\rho}{2} \|\mathcal{T}(\hat{K}) - H^k\|_F^2.$$

In conjunction with backtracking, this can be used to determine step-size to guarantee closed-loop stability and convergence to a stationary point of $L(\hat{K})$.

Proximal gradient method. Proximal gradient method provides an alternative approach to solving the \hat{K} -minimization step. It is based on a simple quadratic approximation of the quadratic objective function $J(\hat{K})$ around current inner iterate \hat{K}^m ,

$$J(\hat{K}) \approx J(\hat{K}^m) + \langle \nabla J(\hat{K}^m), \hat{K} - \hat{K}^m \rangle + \frac{1}{2\alpha_m} \|\hat{K} - \hat{K}^m\|_F^2$$

where α_m denotes the step-size and

$$\nabla J(\hat{K}^m) = 2(\hat{R} \hat{K}^m \hat{C}_2 - \hat{B}_2^* \hat{P}^m) \hat{X}^m \hat{C}_2^*.$$

Using completion of squares, the \hat{K} -minimization step can be written as

$$\hat{K}^{m+1} = \underset{\hat{K}}{\operatorname{argmin}} \left(\frac{1}{2\alpha_m} \left\| \hat{K} - \left(\hat{K}^m - \alpha_m \nabla J(\hat{K}^m) \right) \right\|_F^2 + \frac{\rho}{2} \left\| \mathcal{T}(\hat{K}) - H^k \right\|_F^2 \right)$$

and the optimality condition is given by

$$\frac{1}{\alpha_m} \left(\hat{K} - \left(\hat{K}^m - \alpha_m \nabla J(\hat{K}^m) \right) \right) + \rho \mathcal{T}^\dagger \left(\mathcal{T}(\hat{K}) - H^k \right) = 0 \quad (2.14)$$

For consensus and synchronization networks, $\mathcal{T}(\hat{K}) = \hat{K}T$, and we have an explicit update for \hat{K} ,

$$\hat{K}^{m+1} = \frac{1}{1 + \alpha_m \rho} \left(\hat{K}^m - \alpha_m \nabla J(\hat{K}^m) + \alpha_m \rho H^k T^+ \right)$$

The proximal gradient algorithm converge with rate $O(1/m)$ if α_m is smaller than the reciprocal of the Lipschitz constant of ∇J [101]. Since the Lipschitz constant is difficult to determine explicitly, we adjust α_m via backtracking procedure that we describe next. Furthermore, to enhance the speed of convergence, we initialize the step-size using the Barzilai-Borwein (BB) method [102],

$$\alpha_m^0 = \frac{\left\| \hat{K}^m - \hat{K}^{m-1} \right\|_F^2}{\left\langle \hat{K}^{m-1} - \hat{K}^m, \nabla J(\hat{K}^{m-1}) - \nabla J(\hat{K}^m) \right\rangle},$$

The BB method approximates the Hessian with a scaled version of the identity matrix and it represents an effective heuristics for improving convergence rate. The initial step-size α_m^0 is adjusted via backtracking to guarantee closed-loop stability and to make sure that,

$$J(\hat{K}^{m+1}) \leq J(\hat{K}^m) + \left\langle \nabla J(\hat{K}^m), \hat{K}^{m+1} - \hat{K}^m \right\rangle + \frac{1}{2\alpha_m} \left\| \hat{K}^{m+1} - \hat{K}^m \right\|_F^2.$$

The proximal gradient method terminates when

$$\left\| \nabla L(\hat{K}^m) \right\|_F \leq \epsilon_{\hat{K}}.$$

Remark 1. *For spatially-invariant systems, the computational complexity of each \hat{K} -minimization step is $O(Nn_s^3)$. Here, N denotes the number of subsystems and n_s is the number of states in each subsystem. This should be compared and contrasted to $O(n^3)$ complexity, with $n = Nn_s$, for systems without spatially-invariant structure.*

2.3.2 Polishing step

After having identified the sparsity pattern \mathcal{S}_p via ADMM, we optimize the network performance over the identified structure,

$$\begin{aligned} & \underset{\hat{K}}{\text{minimize}} && J(\hat{K}) \\ & \text{subject to} && \mathcal{T}(\hat{K}) \in \mathcal{S}_p. \end{aligned} \tag{2.15}$$

We fix the sparsity pattern of \hat{K} and solve the optimal control problem (2.15) via an ADMM algorithm, where the \hat{K} -minimization step is the same as in Section 2.3.1 while the K -minimization step is computed by projecting the new $K = \hat{K}T$ onto the convex set \mathcal{S}_p . This polishing step is used to further improve performance of sparse feedback gains resulting from the structure design step.

2.4 Case study: synchronization network

Twenty nodes in an undirected disconnected network shown in Fig. 2.1 are randomly distributed in a unit square. The nodes form three clusters and the network dynamics are described by the swing equation (5.1). The state-space model is given by (2.5) with $C_2 = I$ and the matrices A , B_1 , and B_2 determined by (2.9). The graph Laplacian L_p is obtained based on the proximity of the nodes: two nodes are connected if their distance is not greater than 0.25. The control objective is to minimize performance metric that penalizes angular kinetic energy and the mean square deviation from the angle average.

Information exchange links in the controller graph that result from elementwise sparsity-promoting regularizer with iterative re-weighting are illustrated in Fig. 2.2. Since local frequency measurements are readily available, the diagonal elements of the frequency feedback gains are not penalized in the function g . The red lines mark the

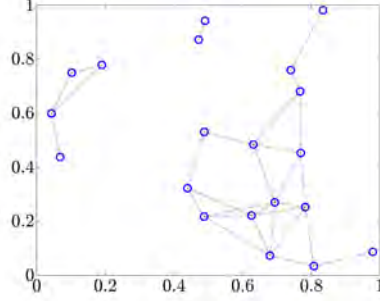


Figure 2.1: Topology of a disconnected plant network with 3 clusters and 20 nodes.

identified communication links (of either the rotational angles or the frequencies) between the nodes. As we increase γ , the controller graph becomes sparser. For $\gamma = 1$, there are only two long-range links that connect two small clusters to the large cluster of nodes. The controller makes the original disconnected graph connected by adding links between different clusters, thereby guaranteeing synchronization and optimizing the desired performance metric.

The structure of the feedback gain K for $\gamma = 1$ is shown in Fig. 2.3. The blue dots denote local feedback gains and the red dots identify information that needs to be communicated between different nodes. Since the frequency feedback gain matrix is diagonal, only local frequency measurements are required to form the control action. The two red dots correspond to the two red long-range links in Fig. 2.2d and they indicate that the controllers of the two furthest nodes require access to the angle measurements of the node in the center of the domain. Dropping any of these two links would yield a disconnected closed-loop network and synchronization would not be achieved.

Compared to the optimal centralized controller, the sparse controller with structure shown in Fig. 2.2d compromises performance by 8.81%; see Fig. 2.4. In contrast, the sparse controller in Fig. 2.2c has five additional long-range links and degrades performance by only 3.4%.

Finally, for each value of the regularization parameter γ we compare and contrast performance of the controller with the sparsity pattern shown in Fig. 2.3 with a heuristic strategy that has the same sparsity level. The diagonal elements of the frequency feedback gain are always non-zero and sparsity pattern for the rest of the elements is

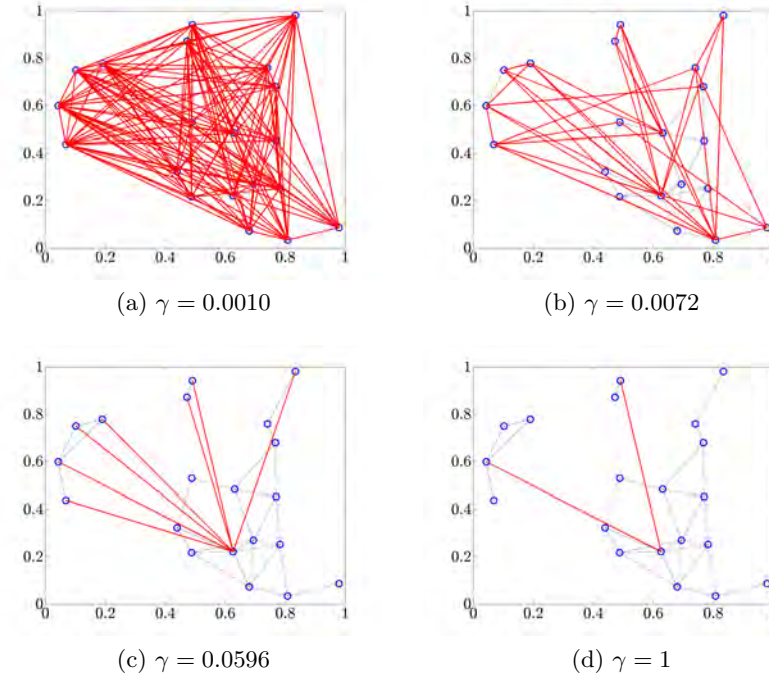


Figure 2.2: Topology of controller network for different values of γ . Edges in the controller network are marked with red lines.

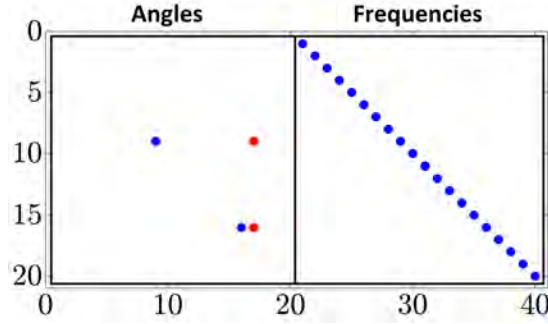


Figure 2.3: Sparsity pattern of K for $\gamma = 1$.

randomly selected. For each sparsity level, we randomly select 100 off-diagonal patterns and optimize feedback gains over the fixed structure. Figure 2.5 compares the average closed-loop performance degradation of this heuristic strategy to our method. For each sparsity level, our approach yields smaller performance loss and offers significant advantages for sparser control architectures (i.e., larger values of γ).

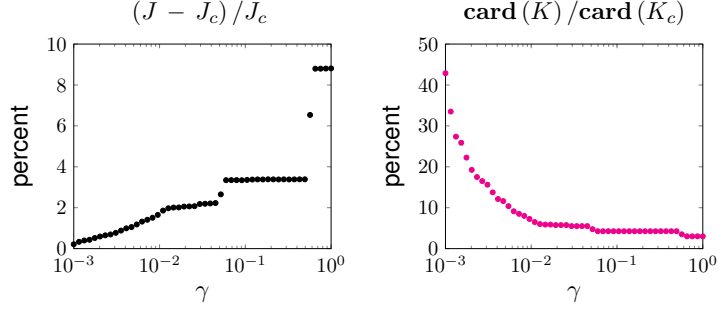


Figure 2.4: Performance vs sparsity comparison with respect to the optimal centralized controller K_c for 50 logarithmically-spaced points $\gamma \in [10^{-3}, 1]$.

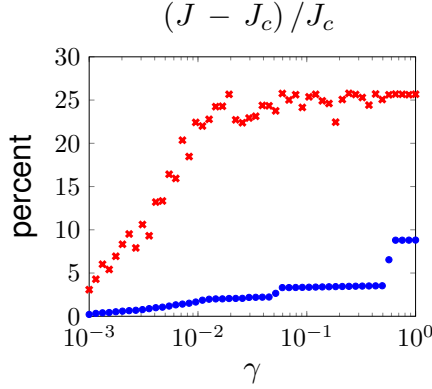


Figure 2.5: Performance degradation comparison of K resulting from our framework (dots) to the average of 100 feedback matrices of random sparsity patterns with same sparsity level for each γ .

2.5 Concluding remarks

In this section, we have considered a regularized version of the standard \mathcal{H}_2 optimal control problem where the regularization term serves as a proxy for inducing sparsity. We consider a class of systems in which state-space representation is not cast in the set of coordinates in which it is desired to enhance sparsity. This setup arises in systems with invariances and symmetries as well as in consensus and synchronization networks. We achieve desired performance with fewer communication links in the controller network by promoting sparsity of the feedback gain matrix. Alternating direction method of multipliers allows for performance and sparsity requirements to be expressed in different

set of coordinates and facilitates efficient computation. A synchronization network is provided as an illustrative example to demonstrate the value of our developments. Recently, our generalized sparsity-promoting optimal control framework was used to suppress inter-area oscillations in power networks [16].

Chapter 3

Sparsity-promoting optimal control of systems with invariances and symmetries

We take advantage of system invariances and symmetries to gain convexity and computational advantage in regularized \mathcal{H}_2 and \mathcal{H}_∞ optimal control problems. For systems with symmetric dynamic matrices, the problem of minimizing the \mathcal{H}_2 or \mathcal{H}_∞ performance of the closed-loop system can be cast as a convex optimization problem. Although the assumption of symmetry is restrictive, studying the symmetric component of a general system's dynamic matrices provides bounds on the \mathcal{H}_2 and \mathcal{H}_∞ performance of the original system. Furthermore, we show that for certain classes of systems, block-diagonalization of the system matrices can bring the regularized optimal control problems into forms amenable to efficient computation via distributed algorithms. One such class of systems is spatially-invariant systems, whose dynamic matrices are circulant and therefore block-diagonalizable by the discrete Fourier transform [103].

3.1 Problem formulation

We consider the class of systems,

$$\begin{aligned}\dot{x} &= (A - K(v))x + Bd \\ z &= \begin{bmatrix} C \\ R(v) \end{bmatrix} x\end{aligned}\tag{3.1}$$

where $v \in \mathbb{R}^m$ is a design parameter, $K(\cdot) : \mathbb{R}^m \rightarrow \mathbb{R}^{n \times n}$ is a linear operator, $x(t) \in \mathbb{R}^n$ is the state vector, C is mapping from the state to a regulated output, $R(v)$ is a mapping from the state to a measure of control effort, $d(t) \in \mathbb{R}^p$ is a white stochastic disturbance with $\mathbf{E}(d(t_1)d^T(t_2)) = I\delta(t_1 - t_2)$, and \mathbf{E} is the expectation operator. Taking $v = \text{vec}(F)$, $K(v) = B_2F$ and $R(v) = R^{1/2}F$ where $R \succeq 0 \in \mathbb{R}^{p \times p}$, $F \in \mathbb{R}^{p \times n}$, and $B_2 \in \mathbb{R}^{n \times p}$ yields the traditional state feedback control problem. We consider v to be constant in time.

Our objective is to design a stabilizing v that solves the regularized optimal control problem,

$$\begin{aligned}\underset{v}{\text{minimize}} \quad & J(v) + g(v) \\ \text{subject to} \quad & A - K(v) \text{ Hurwitz}\end{aligned}\tag{3.2}$$

where $J(v)$ is a performance metric, taken to be either the closed loop \mathcal{H}_2 or \mathcal{H}_∞ norm, and $g(v)$ can be any convex function of v . The \mathcal{H}_2 performance, which we denote by $J_2(v)$, is a measure of the variance amplification from the disturbances d to the regulated output z in system (3.1),

$$J_2(v) := \lim_{t \rightarrow \infty} \mathbf{E}(z^T(t)z(t))$$

which can be computed by

$$J_2(v) = \text{trace}(X(C^TC + R^T(v)R(v)))$$

where X is the controllability gramian

$$(A - K(v))X + X(A - K(v))^T + BB^T = 0.$$

The \mathcal{H}_∞ performance metric, which we denote by $J_\infty(v)$, is the maximum induced \mathcal{L}_2 gain from d to z in system (3.1),

$$J_\infty(v) := \sup_{\|d\|_{\mathcal{L}_2} \leq 1} \frac{\|z\|_{\mathcal{L}_2}}{\|d\|_{\mathcal{L}_2}},$$

where the \mathcal{L}_2 norm of a signal f is defined as,

$$\|f\|_{\mathcal{L}_2}^2 := \int_0^\infty f^2(t) dt.$$

This performance metric corresponds to the peak of the frequency response,

$$J_\infty(v) = \sup_{\omega} \sigma_{\max} \left(C (j\omega I - (A + K(v)))^{-1} B \right).$$

The unregularized \mathcal{H}_2 and \mathcal{H}_∞ -optimal linear state feedback problems can be cast in a convex form via a suitable change of coordinates; however, this change of coordinates does not preserve the structure of the design variable v .

For many applications, v has physical significance and penalizing it directly via $g(v)$ is desirable. For example, a quadratic penalty, $\|v\|_2^2$, would limit the magnitude of v , and an ℓ_1 penalty, $\|v\|_1 := \sum_i |v_i|$, would promote sparsity.

Many structured optimal control problems can be cast in the form of (3.2). For example, structured state feedback problems have been extensively studied with particular applications to consensus networks and power systems [16, 21, 30, 81, 82, 104, 105]. Two other applications are given below.

3.1.1 Applications

Design of edges in networks

The problem of adding undirected edges to an existing network can be cast in this problem form. The dynamics are,

$$\dot{x} = - (L + E \operatorname{diag}(v) E^T) x + d$$

where L is a directed graph Laplacian which contains information about how the nodes are connected, E contains information about the locations of potential added edges, and $K(v) := E \text{diag}(v) E^T$ is a diagonal matrix of added edge weights [106]. Taking the regularizer to be the ℓ_1 norm $g(v) = \sum_i |x_i|$ would limit the number of edges added to the network.

Combination drug therapy design for HIV treatment

The problem of designing drug dosages for treating HIV [107, 108] can be cast as,

$$\dot{x} = \left(A - \sum_{k=1}^m v_k D_k \right) x + d.$$

Here, the elements of x represent populations of HIV mutants. The diagonal elements of A represent each mutant's replication rate and the off diagonal elements of A represent the probability of mutation from one mutant to another. The components of the vector v are dosages of different drugs, where D_k is a diagonal matrix containing information about how efficiently drug k kills each HIV mutant. Here, quadratic regularization $g(v) = \|v\|_2^2$ would limit the dose of the drugs prescribed and ℓ_1 regularization $g(v) = \sum_i |x_i|$ would limit the amount of drugs prescribed.

3.2 Symmetric system design

One class of system for which $J_2(v)$ and $J_\infty(v)$ are convex arises when $B = C = I$, and A and $K(v)$ are symmetric matrices. Although this assumption seems restrictive, studying such systems can inform the design of structured controllers for more general classes of systems.

Any matrix A can be decomposed into its symmetric $A_s = \frac{1}{2}(A + A^T)$ and antisymmetric $A_a = \frac{1}{2}(A - A^T)$ components. The system which corresponds to the symmetric components of the general system (3.1),

$$\dot{x} = (A_s - K_s(v)) x + d \tag{3.3}$$

where $K_s(v) = \frac{1}{2}(K(v) + K^T(v))$ reveals interesting characteristics of the original system.

In this section, we first show the convex formulations that correspond to the optimal \mathcal{H}_2 and \mathcal{H}_∞ design of symmetric systems. We then establish stability guarantees and performance bounds for applying controllers designed by solving the convex problem of regularized optimal control on the symmetric system (3.3) to the original system (3.1). Finally, we use perturbation analysis to show that the symmetric system is a high fidelity approximation for systems which are dominated by the symmetric component.

3.2.1 Convex optimal control for symmetric systems

Although more general symmetric systems can be cast as convex problems, here we assume $B = C = I$ and $R(v) = 0$ to facilitate the transition to the discussion of spectral properties and performance bounds.

\mathcal{H}_2 -optimal control

When $A_s = A_s^T$ is symmetric, the controllability Gramian of system (3.3) can be explicitly expressed as,

$$X_s = -\frac{1}{2} (A_s - K_s(v))^{-1}$$

and, by taking a Schur complement, the regularized optimal \mathcal{H}_2 control problem can be cast in a convex function of v and an auxiliary variable Θ ,

$$\begin{aligned} & \underset{v, \Theta}{\text{minimize}} && \frac{1}{2} \text{trace}(\Theta) + g(v) \\ & \text{subject to} && \begin{bmatrix} \Theta & I \\ I & -A_s + K_s(v) \end{bmatrix} \succ 0. \end{aligned} \tag{3.4}$$

The matrix $A_s - K_s(v)$ is always invertible when it is Hurwitz. We note the structured LQR problem (i.e., $R(v) = R^{1/2}K_s(v)$) for symmetric systems can also be expressed as an SDP by taking the Schur complement of $K_s(v)RK_s(v)$.

\mathcal{H}_∞ -optimal control

The peak of the frequency response of a symmetric system occurs at $\omega = 0$.

Proposition 1. *For a system (3.3) with symmetric dynamics, the disturbance that achieves the maximum induced \mathcal{L}_2 amplification corresponds to the constant signal $d(t) = v$ where v is the right principal singular vector of A^{-1} .*

Proof. A symmetric matrix can be diagonalized as, $A_s = U\Lambda U^T$ where Λ is a diagonal matrix with the eigenvalues of A_s on the main diagonal and the columns of U contain the corresponding eigenvectors. For such a matrix,

$$(j\omega I - A_s)^{-1} = U \operatorname{diag} \left\{ \frac{1}{j\omega - \lambda_i} \right\} U^T.$$

It is clear that $\omega = 0$ maximizes the singular values of the above matrix. Thus, the \mathcal{H}_∞ norm of (3.3) can be characterized by $\sigma_{\max}(-(A_s - K(v))^{-1})$. \square

The \mathcal{H}_∞ -optimal control problem for symmetric systems can therefore be expressed as,

$$\begin{aligned} & \underset{v, \Theta}{\text{minimize}} && \sigma_{\max}(\Theta) + g(v) \\ & \text{subject to} && \begin{bmatrix} \Theta & I \\ I & -A_s + K_s(v) \end{bmatrix} \succeq 0. \end{aligned} \tag{3.5}$$

As we show in the next subsection, this convex problem can be used for structured \mathcal{H}_∞ control design. This is particularly advantageous because many of the existing algorithms for general structured \mathcal{H}_2 control cannot be extended to the structured \mathcal{H}_∞ problem.

3.2.2 Stability and performance guarantees

Stability of the symmetric system (3.3) implies stability of the corresponding original system (3.1).

Lemma 2. *[35, Lemma 1] Let the symmetric part of A , $A_s := (A + A^T)/2$, be Hurwitz. Then, A is Hurwitz.*

Remark 2. *This is not a necessary condition; A may be Hurwitz even if A_s is not.*

Performance guarantees

The \mathcal{H}_2 and \mathcal{H}_∞ norms of the symmetric system are upper bounds on the \mathcal{H}_2 and \mathcal{H}_∞ norms of the original system.

Proposition 3. *[35, Cor. 3] When the systems (3.1) and (3.3) are stable, the \mathcal{H}_2 norm of the general system (3.1) is bounded from above by the \mathcal{H}_2 norm of the symmetric system (3.3).*

We show that an analagous bound holds for the \mathcal{H}_∞ .

Proposition 4. *When the systems (3.1) and (3.3) are stable, the \mathcal{H}_∞ norm of the general system (3.1) is bounded from above by the \mathcal{H}_∞ norm of the symmetric system (3.3).*

Proof. From the bounded real lemma [109], the \mathcal{H}_∞ norm of the general system (3.1) is less than γ if there exists a $P \succ 0$ such that,

$$A^T P + P A + I + \gamma^{-2} P^2 \prec 0.$$

From Proposition 1, for the symmetric system (3.3), $\gamma > \sigma_{\max}(A_s^{-1})$. Taking $P = \gamma I$ for any $\gamma > \sigma_{\max}(A_s^{-1})$ and substituting it into the above linear matrix inequality (LMI) applied to the symmetric system (3.3) yields,

$$2\gamma A_s + 2I \prec 0.$$

Since A_s is Hurwitz, $A_s \prec 0$. Since $\gamma > -\lambda_{\max}(A_s^{-1})$, $\gamma^{-1} < -\lambda_{\min}(A_s)$, so $A_s \prec -\gamma^{-1}I$. Therefore the LMI is satisfied. Since $A_a = -A_a^T$, setting $P = \gamma I$ implies,

$$A^T P + P A = 2\gamma A_s$$

therefore substituting P into the bounded real lemma LMI for the general system (3.1), where $A = A_s + A_a$, yields,

$$A^T P + P A + I + \gamma^{-2} P^2 = 2\gamma A_s + 2I \prec 0.$$

□

3.2.3 Approximation bounds

In addition to being an upper bound, the \mathcal{H}_2 and \mathcal{H}_∞ norms of the symmetric (3.3) and full (3.1) systems are close when A is dominated by the symmetric component.

Proposition 5. *[35, Prop. 4] Let A_n be a normal matrix. The $O(\epsilon)$ correction to the \mathcal{H}_2 norm of the system*

$$\dot{x} = A_n x + d$$

from an $O(\epsilon)$ antisymmetric perturbation A_a is zero.

We show that a similar property holds for the \mathcal{H}_∞ norm.

Proposition 6. *Let A_s be a symmetric matrix. The $O(\epsilon)$ correction to the \mathcal{H}_∞ norm of the system*

$$\dot{x} = A_s x + d$$

from an $O(\epsilon)$ antisymmetric perturbation A_a is zero.

Proof. From Proposition 1, the \mathcal{H}_∞ norm of the symmetric system is given by $\sigma_{\max}(-A_s^{-1})$. The maximum singular value of a matrix is equivalent to,

$$\sigma_{\max}(X) = \sup_{\|v\|_2 \leq 1, \|w\|_2 \leq 1} v^T X w.$$

Since A_s is symmetric, $w = v$. Taking an $O(\epsilon)$ antisymmetric perturbation A_a to the above expression,

$$\sigma_{\max}(-(A_s + \epsilon A_a)^{-1}) \approx -v^T A_s^{-1} v + \epsilon v^T A_s^{-1} A_a A_s^{-1} v.$$

Since A_a is antisymmetric, $\langle A_s^{-1} v v^T A_s^{-1}, A_a \rangle = 0$. □

3.3 Computational advantages for structured problems

Structured control is often of interest for large-scale systems. As such, the computational scaling of algorithms used to compute optimal controllers is very important. In this section, we identify a class of systems which are amenable to scalable distributed algorithms.

When A and $K(v)$ are always simultaneously block-diagonalizable, the dynamics of the system can be expressed as the sum of independent subsystems. Define $\hat{x} := Px$ and let P be a unitary matrix such that,

$$\dot{\hat{x}} = (\hat{A} + \hat{K}(v))\hat{x}$$

where

$$\hat{A} := P A P^T, \quad \hat{K}(v) := P K(v) P^T,$$

and, for any choice of v , $\hat{A} + \hat{K}(v) = \text{blkdiag}\{\hat{A}_{11} + \hat{K}_{11}, \dots, \hat{A}_{NN} + \hat{K}_{NN}\}$ is block-diagonal with N blocks of size $n \times n$ each.

For problems of this form, computing optimal control strategies is much more efficient in the \hat{x} coordinates because the majority of the computational burden in solving problems (3.4) and (3.5) comes from the $nN \times nN$ LMI constraint involved in minimizing the performance metrics $J_2(v)$ or $J_\infty(v)$.

For this class of system, the \mathcal{H}_2 -optimal control problem (3.4) can be expressed as,

$$\begin{aligned} & \underset{v, \Theta_i}{\text{minimize}} \quad \frac{1}{2} \sum_i \text{trace}(\Theta_i) + g(v) \\ & \text{subject to} \quad \begin{bmatrix} \Theta_i & I \\ I & -(\hat{A}_s)_{ii} + (\hat{K}_s(v))_{ii} \end{bmatrix} \succeq 0. \end{aligned} \tag{3.6}$$

which is an SDP with N separate $n \times n$ LMI blocks. Since SDPs scale with the sixth power of the LMI blocks, solving this reformulation scales with n^6 as opposed to $n^6 N^6$.

Analogously, the structured \mathcal{H}_∞ -optimal control problem (3.5) can be cast as,

$$\begin{aligned} & \underset{v, \Theta_i}{\text{minimize}} \quad \max_i (\sigma_{\max}(\Theta_i)) + g(v) \\ & \text{subject to} \quad \begin{bmatrix} \Theta_i & I \\ I & (\hat{A}_s)_{ii} - (\hat{K}_s(v))_{ii} \end{bmatrix} \succeq 0. \end{aligned} \tag{3.7}$$

One important class of system which satisfies these assumptions is spatially-invariant systems. This structure was used in [38] to develop efficient techniques for sparse feedback synthesis.

3.3.1 Spatially-invariant systems

Spatially-invariant systems have a block-circulant structure which is block-diagonalizable by a Discrete Fourier Transform (DFT). A spatially-invariant system can be represented by N subsystems with n states each. The state vector $x \in \mathbb{R}^{nN}$ is composed of N subvectors $x_i \in \mathbb{R}^n$ which denotes the state of the subsystem. The matrix $A \in \mathbb{R}^{nN \times nN}$ is block-circulant with blocks of the size $n \times n$. For example, when $N = 3$,

$$A = \begin{bmatrix} A_0 & A_1 & A_{-1} \\ A_{-1} & A_0 & A_1 \\ A_1 & A_{-1} & A_0 \end{bmatrix}$$

where the blocks $\{A_0, A_{-1}, A_1\} \in \mathbb{R}^{n \times n}$.

It was shown in [17] that the optimal feedback controller for a spatially-invariant system is itself spatially-invariant. Assuming that the optimal *sparse* feedback controller is also spatially-invariant is equivalent to assuming that $K(v)$ is block-circulant. Block circulant matrices are block-diagonalizable by the appropriate DFT. Let the block Fourier matrix be

$$\Phi := \Phi_N \otimes I_n,$$

where I_n is the $n \times n$ identity matrix, Φ_N is the $N \times N$ discrete Fourier transform matrix, and \otimes represents the Kronecker product. By introducing the change of variables $\hat{x} := \Phi x$, where

$$\hat{x} = \begin{bmatrix} \hat{x}_1^T & \cdots & \hat{x}_N^T \end{bmatrix}^T,$$

and $\hat{x}_i \in \mathbb{R}^n$, the original system's dynamics can be expressed as N independent $n \times n$ subsystems,

$$\hat{A} = \begin{bmatrix} \hat{A}_{11} & & \\ & \hat{A}_{22} & \\ & & \hat{A}_{33} \end{bmatrix}$$

Consequently, the optimal structured control problems (3.4) and (3.5) can be cast as (3.6) and (3.7), which are more amenable to efficient computations.

3.4 Examples

3.4.1 Directed Consensus Network

In this example, we illustrate the utility of the approach described in Section 3.2. Consider the network dynamics given by a directed network as described in Section 3.1.1,

$$\dot{x} = -(L + E \operatorname{diag}(v) E^T) x$$

where L is a directed graph Laplacian, $K(v) = E \operatorname{diag}(v) E^T$ represents the addition of undirected links, v is a vector that contains weights of these added links, and the incidence matrix E describes which edges may be added or altered. The regularization on v is given by,

$$g(v) = \|v\|_2^2 + \gamma \sum_i |v_i|$$

where the quadratic term limits the size of the edge weights, the ℓ_1 norm promotes sparsity of added links, and $\gamma > 0$ parametrizes the importance of sparsity.

For this concrete example, the network topology is given by Figure 3.1. The potential added edges can connect the following pairs of nodes: (1) – (2), (1) – (3), (1) – (5), (1) – (6), (2) – (5), (2) – (6), (3) – (6), and (4) – (5).

Controllers were designed by solving problems (3.4) and (3.5) for the symmetric version of the network over 50 log-distributed values of $\gamma \in [10^{-4}, 1]$. The closed-loop \mathcal{H}_2 and \mathcal{H}_∞ norms obtained by applying these controllers to the symmetric and original systems are shown in Fig. 3.2. Figure 3.1 also shows which edges were added for $\gamma = 1$.

3.4.2 Swift-Hohenberg Equation

Here we illustrate the utility of the block-diagonalization we describe in Section 3.3. Consider a particular realization of the Swift-Hohenberg equation [110],

$$\partial_t \psi(t, x) = \beta \psi(t, x) - (1 + \partial_{xx})^2 \psi(t, x) + v(x) \psi(t, x)$$

where $\beta \in \mathbb{R}$, and $\psi(t, \cdot), v(\cdot) \in L_2(-\infty, \infty)$, and $v(x)$ is a spatially-invariant feedback controller which is to be designed. A finite dimensional approximation of this system can be obtained by using the differentiation suite from [111] to discretize the problem

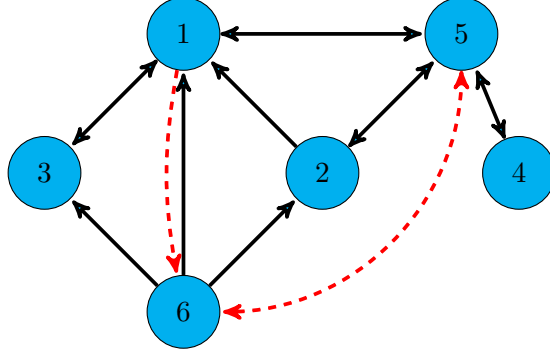


Figure 3.1: Directed network (**black** solid arrows) with added undirected edges (**red** dashed arrows). Both the \mathcal{H}_2 and \mathcal{H}_∞ optimal structured control problems yielded the same set of added edges. In addition to these edges, the controllers tuned the weights of the edges (1) – (3) and (1) – (5).

into N points and approximating the infinite domain with periodic boundary conditions over the domain $L_2[0, 2\pi]$. A sparse \mathcal{H}_2 feedback controller $v(x)$ can then be identified by solving problem (3.4).

We contrast this method with the approach we advocate in Section 3.3, where we use the DFT to decompose the system into N first-order systems corresponding to eigenfunctions of the Swift-Hohenberg equation and solve problem (3.6).

The state vector takes the form of $\psi(x)$ evaluated at grid points in x where the dynamics are given by,

$$\dot{\psi} = (A - V)\psi$$

where, $A = \beta I - (I + D^2)^2$. Here D is a discrete differentiation matrix from [111], and V is the circulant state feedback matrix.

Using the DFT over x , the Swift-Hohenberg equation can be expressed as a set of independent first-order systems,

$$\dot{\hat{\psi}}_x = (a_x - \hat{v}_x)\hat{\psi}_x$$

where $a_x := \beta - (1 - \kappa_x^2)^2$, and the new coordinates are $\hat{\psi} := P\psi$, P is the DFT matrix, κ_x is the wavenumber (spatial frequency), and \hat{v} represents V in the Fourier space; i.e., $V = P^T \text{diag}(\hat{v})P$.

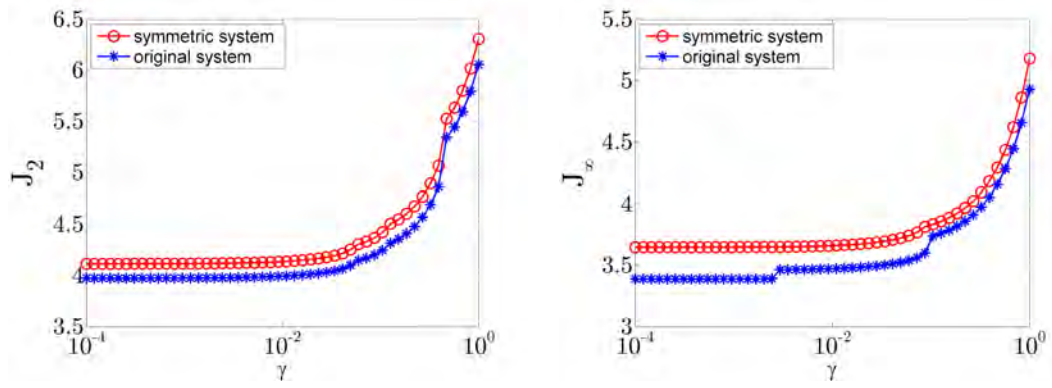


Figure 3.2: \mathcal{H}_2 and \mathcal{H}_∞ performance of the closed-loop symmetric system and the original system subject to a controller designed at various values of γ .

We take the regularization term to be

$$g(v) = \|V\|_F^2 + \gamma \|V\|_1$$

where $\|X\|_1 := \sum_{ij} |X_{ij}|$ is the elementwise ℓ_1 norm and γ is a parameter which specifies the emphasis on sparsity relative to performance.

For the \mathcal{H}_2 problem, the regularized optimal control problem is of the form of (3.4) with $K_s(v) = V$ and V is circulant. In that formulation, the problem is an SDP with one $N \times N$ LMI block. In the Fourier space, the problem can be expressed as (3.6), which takes the particular form,

$$\begin{aligned} & \underset{\hat{v}}{\text{minimize}} && \frac{1}{2} \sum \frac{1}{-a_x + \hat{v}_x} + g(P^T \text{diag}(\hat{v})P) \\ & \text{subject to} && -a_x + \hat{v}_x \geq 0 \end{aligned}$$

which does not require the large SDP constraints in (3.4).

We solved the regularized \mathcal{H}_2 optimal control problem by solving the general formulation (3.4) and the more efficient formulation (3.6) for $\beta = 0.1$, $\gamma = 1$ and N varying from 5 to 51 using CVX, a general purpose convex optimization solver [112].

Taking advantage of spatial invariance yields a significant computational advantage, as can be seen in Figure 3.3. Although both expressions of the problem yield the same

solution, solving the realization in (3.6) is much faster and allows us to examine much larger problem dimensions. In Figure 3.4, we show the spatially-invariant feedback controller for one point in the domain, i.e., one row of V , computed for $N = 101$ at $\gamma = 0$, $\gamma = 0.1$, and $\gamma = 10$.

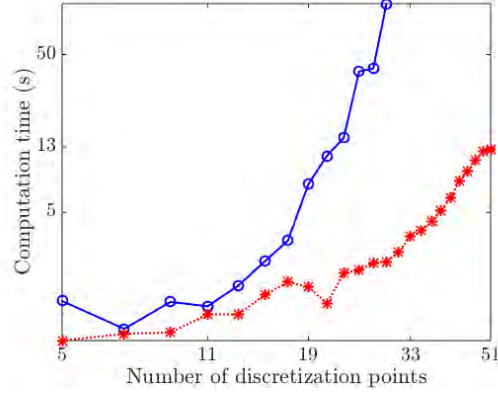


Figure 3.3: Computation time for the general formulation (3.4) (blue \circ) and that which takes advantage of spatial invariance (3.6) (red $*$).

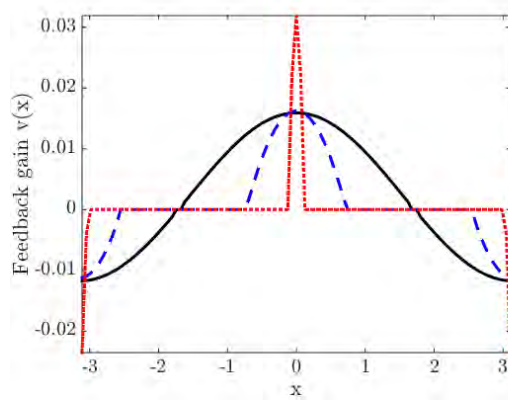


Figure 3.4: Feedback gain $v(x)$ for the node at position $x = 0$, computed with $N = 51$ and $\gamma = 0$ (black solid), $\gamma = 0.1$ (blue dashed), and $\gamma = 10$ (red dotted).

3.5 Concluding remarks

We have provided a convex methodology for structured \mathcal{H}_2 and \mathcal{H}_∞ controller design and a procedure to gain computational efficiency for spatially invariant systems and problems with similar forms. Ongoing work will focus on deriving a bound on the error between a general linear system and the system corresponding to its symmetric component.

Part II

Wide-area control of power systems

Chapter 4

Decentralized optimal control of inter-area oscillations

Local and inter-area oscillations in bulk power systems are typically identified using spatial profiles of poorly damped modes, and they are mitigated via carefully tuned decentralized controllers. In this chapter, we employ non-modal tools to analyze and control inter-area oscillations. Our input-output analysis examines power spectral density and variance amplification of stochastically forced systems and offers new insights relative to modal approaches. To improve upon the limitations of conventional wide-area control strategies, we also study the problem of signal selection and optimal design of sparse and block-sparse wide-area controllers. In our design, we preserve rotational symmetry of the power system by allowing only relative angle measurements in the distributed controllers. For the IEEE 39 New England model, we examine performance tradeoffs and robustness of different control architectures and show that optimal re-tuning of fully-decentralized control strategies can effectively guard against local and inter-area oscillations.

4.1 Modeling and control preliminaries

A power network is described by a nonlinear system of differential-algebraic equations. Differential equations govern the dynamics of generators and their controllers, and the algebraic equations describe quasi-stationary load flow and circuitry of generators and

power electronics [98]. A linearization around a stationary operating point and elimination of the algebraic equations yield a linearized state-space model

$$\dot{x} = Ax + B_1 d + B_2 u. \quad (4.1)$$

Here, $x(t) \in \mathbb{R}^n$ is the state, $u(t) \in \mathbb{R}^m$ is the generator excitation control input, and $d(t) \in \mathbb{R}^p$ is the stochastic disturbance which may arise from power imbalance and uncertain load demands [98]. For example, the choice $B_1 = B_2$ can be used to quantify and mitigate the impact of noisy or lossy communication among spatially distributed controllers [15].

4.1.1 Swing equations

The dominant electro-mechanical dynamics of a power system are given by the linearized *swing equations* [98],

$$M_i \ddot{\theta}_i + D_i \dot{\theta}_i + \sum_j L_{ij} (\theta_i - \theta_j) = 0.$$

These equations are obtained by neglecting fast electrical dynamics and eliminating the algebraic load flow. Here, θ_i and $\dot{\theta}_i$ are the rotor angle and frequency of generator i , M_i and D_i are the generator inertia and damping coefficients, and L_{ij} is the (i, j) element of the network susceptance matrix indicating the interactions between generators i and j [15]. Even though the swing equations do not fully capture complexity of power systems, they nicely illustrate the causes of inter-area oscillations: Inter-area oscillations originate from sparse links between densely connected groups of generators (so-called areas). These areas can be aggregated into coherent groups of machines which swing relative to each other using the slow coherency theory [113, 114]. Our goal is to design wide-area controllers to suppress inter-area oscillations.

4.1.2 Problem formulation

Under a linear state-feedback,

$$u = -Kx$$

the closed-loop system takes the form

$$\begin{aligned}\dot{x} &= (A - B_2 K) x + B_1 d \\ z &= \begin{bmatrix} z_1 \\ z_2 \end{bmatrix} = \begin{bmatrix} Q^{1/2} \\ -R^{1/2} K \end{bmatrix} x\end{aligned}\tag{4.2}$$

where z is a performance output with state and control weights Q and R . We choose R to be the identity matrix and a state objective that quantifies a desired potential energy and the kinetic energy stored in the electro-mechanical dynamics,

$$x^T Q x = \theta^T Q_\theta \theta + \frac{1}{2} \dot{\theta}^T M \dot{\theta}.$$

Here, $M = \text{diag}(M_i)$ is the inertia matrix and the matrix Q_θ penalizes the deviation of angles from their average $\bar{\theta}(t) := (1/N) \mathbf{1}^T \theta(t)$,

$$Q_\theta = I - (1/N) \mathbf{1} \mathbf{1}^T\tag{4.3}$$

where N is the number of generators and $\mathbf{1}$ is the vector of all ones. In a power system without a slack bus, the generator rotor angles are only defined in a relative frame of reference, as can be observed in the swing equations. Thus, they can be rotated by a uniform amount without changing the fundamental dynamics (4.1). We preserve this rotational symmetry and study problems in which only differences between the components of the vector $\theta(t) \in \mathbb{R}^N$ enter into (4.2). As a result of the rotational symmetry, both the open-loop A -matrix and the performance weight Q_θ have an eigenvalue at zero which characterizes the mean of all rotor angles.

By expressing the state vector as

$$x(t) := \begin{bmatrix} \theta(t) \\ r(t) \end{bmatrix} \in \mathbb{R}^n$$

where $r(t) \in \mathbb{R}^{n-N}$ represents the rotor frequencies and additional states that account for fast electrical dynamics, we arrive at the structural constraints on the matrices

in (4.2),

$$A \begin{bmatrix} \mathbf{1} \\ 0 \end{bmatrix} = 0, \quad Q_\theta \mathbf{1} = 0, \quad K \begin{bmatrix} \mathbf{1} \\ 0 \end{bmatrix} = 0.$$

In earlier work [14,15], we have removed this rotational symmetry by adding a small *regularization* term to the diagonal elements of the matrix Q_θ . This has resulted in a controller that requires the use of absolute angle measurements to stabilize the average rotor angle. Such a regularization induces a slack bus (a reference generator with a fixed angle) and thereby alters the structure of the original power system.

We preserve the natural rotational symmetry by restricting our attention to relative angle measurements. This requirement implies that the average rotor angle has to remain invariant under the state feedback $u = -Kx$. To cope with these additional structural constraints, the sparsity-promoting approach of [21] has been recently augmented in [30].

To eliminate the average-mode $\bar{\theta}$ from (4.2) we introduce the following coordinate transformation [30],

$$x = \begin{bmatrix} \theta \\ r \end{bmatrix} = \underbrace{\begin{bmatrix} U & 0 \\ 0 & I \end{bmatrix}}_T \xi + \begin{bmatrix} \mathbf{1} \\ 0 \end{bmatrix} \bar{\theta} \quad (4.4)$$

where the columns of the matrix $U \in \mathbb{R}^{N \times (N-1)}$ form an orthonormal basis that is orthogonal to $\text{span}(\mathbf{1})$. For example, these columns can be obtained from the $(N-1)$ eigenvectors of the matrix Q_θ in (4.3) that correspond to the non-zero eigenvalues. In the new set of coordinates, $\xi(t) = T^T x(t) \in \mathbb{R}^{n-1}$, the closed-loop system takes the form

$$\begin{aligned} \dot{\xi} &= (\bar{A} - \bar{B}_2 F) \xi + \bar{B}_1 d \\ z &= \begin{bmatrix} z_1 \\ z_2 \end{bmatrix} = \begin{bmatrix} \bar{Q}^{1/2} \\ -R^{1/2} F \end{bmatrix} \xi \end{aligned} \quad (4.5)$$

where

$$\bar{A} := T^T A T, \quad \bar{B}_i := T^T B_i, \quad \bar{Q}^{1/2} := Q^{1/2} T.$$

The feedback matrices K and F (in the original x and new ξ coordinates, respectively)

are related by

$$F = K T \Leftrightarrow K = F T^T.$$

Because of a marginally stable average mode, the matrix A in (4.2) is not Hurwitz. The coordinate transformation (4.4) eliminates the average angle $\bar{\theta}$ from (4.2), thereby leading to (5.15) with Hurwitz \bar{A} . In the presence of stochastic disturbances, $\bar{\theta}(t)$ drifts in a random walk. Since $\bar{\theta}$ is not observable from the performance output z (which quantifies the mean-square deviation from angle average, kinetic energy, and control effort), z has a finite steady-state variance. This variance is determined by the square of the \mathcal{H}_2 norm of system (5.15).

4.2 Input-output analysis

The conventional analysis of inter-area oscillations in power systems is based on spatial profiles of eigenvectors and participation factors of poorly damped modes. Similarly, traditional control design builds on a modal perspective [42, 43]. In systems with non-normal A -matrices, modal analysis may lead to misleading conclusions about transient responses, amplification of disturbances, and robustness margins [115–117]. Non-normal matrices are common in power systems; such matrices do not have orthogonal eigenvectors and they cannot be diagonalized via unitary coordinate transformations.

In what follows, we utilize an approach that offers additional and complementary insights to modal analysis. This approach is based on the input-output analysis, where the input d is the source of excitation and the output z is the quantity that we care about. In stochastically forced systems, input-output analysis amounts to the study of power spectral density and variance amplification. Our approach builds on the \mathcal{H}_2 paradigm [12], which analyzes and mitigates amplification of white stochastic disturbances.

4.2.1 Power spectral density and variance amplification

We next provide a brief overview of the power spectral density and variance amplification analyses of linear dynamical systems. Let $H(j\omega)$ denote the frequency response

of (5.15),

$$z(j\omega) = H(j\omega) d(j\omega).$$

The Hilbert-Schmidt norm determines the power spectral density of $H(j\omega)$,

$$\|H(j\omega)\|_{\text{HS}}^2 = \text{trace}(H(j\omega) H^*(j\omega)) = \sum \sigma_i^2(H(j\omega))$$

where σ_i 's are the singular values of the matrix $H(j\omega)$. The \mathcal{H}_2 norm quantifies the steady-state variance (energy) of the output z of stochastically forced system (5.15). It is obtained by integrating the power spectral density over all frequencies [12],

$$\|H\|_2^2 := \lim_{t \rightarrow \infty} \mathbf{E}(z^T(t) z(t)) = \frac{1}{2\pi} \int_{-\infty}^{\infty} \|H(j\omega)\|_{\text{HS}}^2 d\omega$$

where \mathbf{E} is the expectation operator. Equivalently, the matrix solution X to the Lyapunov equation,

$$(\bar{A} - \bar{B}_2 F) X + X (\bar{A} - \bar{B}_2 F)^T = -\bar{B}_1 \bar{B}_1^T$$

can be used to compute the \mathcal{H}_2 norm [12],

$$\begin{aligned} J(F) &:= \|H\|_2^2 = \text{trace}(X(\bar{Q} + F^T R F)) \\ &= \text{trace}(Z_1) + \text{trace}(Z_2). \end{aligned} \tag{4.6}$$

Here, X is the steady-state covariance matrix of the state ξ in (5.15), $X := \lim_{t \rightarrow \infty} \mathbf{E}(\xi(t) \xi^T(t))$, and the covariance matrices of the outputs z_1 and z_2 are determined by

$$\begin{aligned} Z_1 &:= \lim_{t \rightarrow \infty} \mathbf{E}(z_1(t) z_1^T(t)) = \bar{Q}^{1/2} X \bar{Q}^{1/2} \\ Z_2 &:= \lim_{t \rightarrow \infty} \mathbf{E}(z_2(t) z_2^T(t)) = R^{1/2} F X F^T R^{1/2}. \end{aligned}$$

Note that $\text{trace}(Z_1)$ and $\text{trace}(Z_2)$ quantify the system's kinetic and potential energy and the control effort, respectively. In particular, the eigenvalue decomposition of the matrix Z_1 ,

$$Z_1 = \sum \lambda_i y_i y_i^T$$

determines contribution of different *orthogonal* modes y_i to the kinetic and potential energy in statistical steady-state. The total energy is given by $\text{trace}(Z_1)$, i.e., the sum of the eigenvalues λ_i of the covariance matrix Z_1 . Each mode y_i contributes λ_i to the variance amplification and the spatial structure of the most energetic mode is determined by the principal eigenvector y_1 of the matrix Z_1 .

4.3 Sparse and block-sparse optimal control

In this section, we study the problem of optimal signal selection and optimal design of wide-area controllers. We approach this problem by invoking sparsity-promoting versions of the standard \mathcal{H}_2 optimal control formulation. We build on the framework developed in [19–21, 30] which is aimed at finding a state feedback that simultaneously optimizes the closed-loop variance and induces a sparse control architecture. This is accomplished by introducing additional regularization terms to the optimal control problem. These serve as proxies for penalizing the number of communication links in the wide-area controller, thereby inducing a sparse control architecture.

4.3.1 Elementwise sparsity

As shown in Section 4.2, the \mathcal{H}_2 norm of system (5.15) is determined by (4.6). While the \mathcal{H}_2 performance is expressed in terms of the feedback matrix F in the new set of coordinates, it is necessary to enhance sparsity of the feedback matrix K in the physical domain. A desired tradeoff between the system's performance and the sparsity of K is achieved by solving the regularized optimal control problem [30],

$$\begin{aligned} & \underset{F, K}{\text{minimize}} && J(F) + \gamma g(K) \\ & \text{subject to} && F T^T - K = 0. \end{aligned} \tag{4.7}$$

The regularization term in (SP) is given by the weighted ℓ_1 -norm of K ,

$$g(K) := \sum_{i,j} W_{ij} |K_{ij}|$$

which is an effective proxy for inducing elementwise sparsity [99]. The weights W_{ij} 's are updated iteratively using the solution to (SP) from the previous iteration; see [99] for details. In (SP), γ is a fixed positive scalar that characterizes the emphasis on the sparsity level of the feedback matrix K . A larger value of γ introduces a sparser feedback gain K at the expense of degrading the closed-loop performance.

We solve the optimal control problem (SP) for different values of the positive regularization parameter γ via the alternating direction method of multipliers; see [21, 30] for algorithmic details. This allows us to identify a parameterized family of distributed control architectures that strikes an optimal balance between competing performance and sparsity requirements.

4.3.2 Block sparsity

In power systems, only rotor angle differences enter into the dynamics and information about absolute angles is not available. It is thus advantageous to treat rotor angles separately from the remaining states in the control design. We partition K conformably with the partition of the state vector x ,

$$K = \begin{bmatrix} K_\theta & K_r \end{bmatrix}$$

where K_θ and K_r are the feedback gains acting on the rotor angles and the remaining states, respectively.

The actuators in wide-area control range from Power System Stabilizers (PSSs) to power electronics devices (FACTS) to HVDC links. While our design methodology is general, in the sequel we restrict our presentation to PSSs. For PSSs the control action is usually formed in a fully-decentralized fashion using local measurements of frequencies and power injections. We represent the vector r as

$$r = \begin{bmatrix} r_1^T & \cdots & r_N^T \end{bmatrix}^T$$

where r_i is the vector of states of the controlled generator i (modulo angles). If K_r is partitioned conformably with the partition of the vector r , then the block-diagonal elements of K_r provide a means for retuning the local control action. Since r_i is readily

available to the controller of generator i , in what follows we do not introduce sparsity-promoting penalty on the block-diagonal elements of K_r . On the other hand, there are many options for treating the components of K_r associated with the states of other generators. We next illustrate three possible options.

Consider a system of four generators with controllers. The states of each controlled generator are given by angle, frequency, fluxes, and excitation control system; see Fig. 4.1. Sparsity of the inter-generator control gains can be enhanced either via elementwise or group penalties. Inter-generator information exchange can be treated with an elementwise penalty in the same way as in Section 4.3.1; see Fig. 4.1a for an illustration. On the other hand, group penalties [100] can be imposed either on the states of individual generators or on the states of all other generators; cf. Figs. 4.1b and 4.1c.

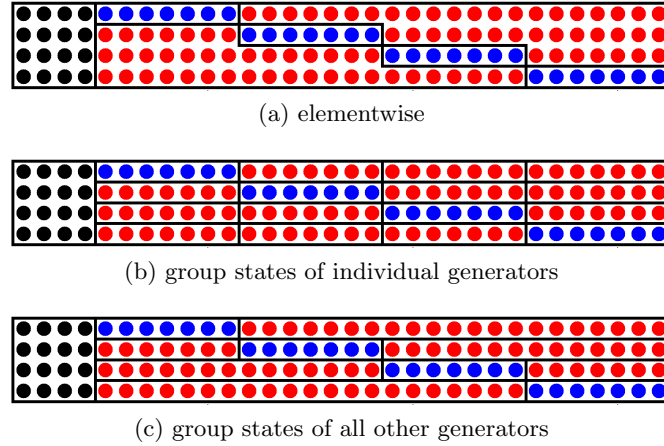


Figure 4.1: Block structure of the feedback matrix K . ● denote relative angle feedback gains, ● and ● represent local and inter-generator frequency and PSS gains, respectively.

The above objectives can be accomplished by solving the sparsity-promoting optimal control problem

$$\begin{aligned}
 & \text{minimize} && J(F) + \gamma_\theta g_\theta(K_\theta) + \gamma_r g_r(K_r) \\
 & \text{subject to} && F T^T - \begin{bmatrix} K_\theta & K_r \end{bmatrix} = 0
 \end{aligned} \tag{4.8}$$

where

$$g_\theta(K_\theta) := \sum_{i,j} W_{ij} |K_{\theta ij}|. \quad (4.9a)$$

On the other hand, for the three cases discussed and illustrated in Fig. 4.1 the corresponding regularization functions are

$$g_{r1}(K_r) := \sum_{i,j} W_{ij} |(I_s \circ K_r)_{ij}| \quad (4.9b)$$

$$g_{r2}(K_r) := \sum_{i \neq k} \beta_{ik} W_{ik} \|e_i^T (I_s \circ K_r) \circ v_k^T\|_2 \quad (4.9c)$$

$$g_{r3}(K_r) := \sum_i \beta_i W_i \|e_i^T (I_s \circ K_r)\|_2 \quad (4.9d)$$

where $i = \{1, \dots, m\}$, $j = \{1, \dots, n - N\}$, $k = \{1, \dots, N\}$, and

$$\begin{aligned} \beta_{ik} &= \mathbf{card} (e_i^T (I_s \circ K_r) \circ v_k^T) \\ \beta_i &= \mathbf{card} (e_i^T (I_s \circ K_r)). \end{aligned} \quad (4.9e)$$

The elementwise penalty (4.9b) eliminates individual components of the feedback gain. In contrast, the group penalties (4.9c) and (4.9d) simultaneously eliminate feedback gains associated with a particular generator or feedback gains associated with all other generators, respectively. The *cardinality* function $\mathbf{card}(\cdot)$ in (4.9e) counts the number of nonzero elements of a matrix, \circ is elementwise matrix multiplication, $I_s \in \mathbb{R}^{m \times (n-N)}$ is the structural identity matrix (see Fig. 4.2 for the structure of I_s), $e_i \in \mathbb{R}^m$ is the i th unit vector, and $v_k \in \mathbb{R}^{n-N}$ is the structural identity vector. This vector is partitioned conformably with the partition of the vector r ,

$$v_k := \begin{bmatrix} \vartheta_1^T & \dots & \vartheta_N^T \end{bmatrix}^T$$

where $\vartheta_l = \mathbf{1}$ for $l = k$ and $\vartheta_l = 0$ for $l \neq k$.

We note that the Euclidean norm ($\|\cdot\|_2$, not its square) is a widely used regularizer for enhancing group sparsity [100]. The group weights W_{ik} 's and W_i 's are updated iteratively using the solution to (4.8) from the previous iteration [99]. The scaling factors β_{ik} and β_i account for variations in the group sizes.

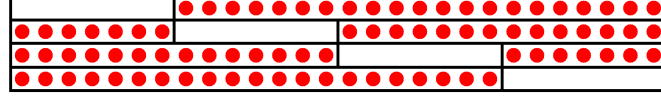


Figure 4.2: Structural identity matrix I_s with \bullet representing locations of 1's.

4.4 Case study: IEEE 39 New England model

The IEEE 39 New England Power Grid model consists of 39 buses and 10 detailed two-axis generator models; see Fig. 5.1. All loads are modeled as constant power loads. Generators 1 to 9 are equipped with PSSs, and generator 10 is an equivalent aggregated model representing the transmission network of a neighboring area. This generator has an inertia which is an order of magnitude larger than the inertia of other generators.

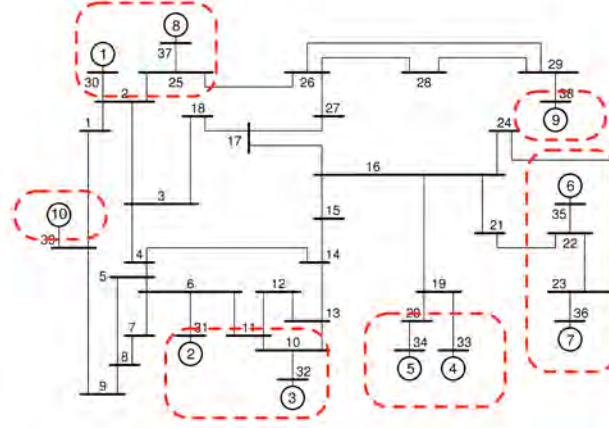


Figure 4.3: The IEEE 39 New England Power Grid and its coherent groups identified using slow coherency theory.

The uncontrolled open-loop system is unstable, and PSSs are used for stabilization and to suppress local oscillations. For the subsequent analysis and the wide-area control design, we assume that *the PSS inputs are embedded in the open-loop matrix* $A \in \mathbb{R}^{75 \times 75}$ in (4.2). The transfer function of the local PSS controller on the i th generator is given by

$$u_i(s) = k_i \cdot \frac{T_{w,i}s}{1 + T_{w,i}s} \cdot \frac{1 + T_{n1,i}s}{1 + T_{d1,i}s} \cdot \frac{1 + T_{n2,i}s}{1 + T_{d2,i}s} \cdot \dot{\theta}_i(s)$$

with controller gains $T_{w,i} = 5$, $T_{n1,i} = T_{n2,i} = 0.1$, $T_{d1,i} = T_{d2,i} = 0.01$, $k_i = 3$ for $i \in \{1, \dots, 9\}$. This set of PSS control gains stabilizes the unstable open-loop system, but it still features several poorly-damped modes. Our objective is to augment the local PSS control strategy with an optimal wide-area controller in order to simultaneously guard against inter-area oscillations and weakly dampened local oscillations.

Our computational experiments can be reproduced using the code available at:

www.umn.edu/~mihailo/software/lqrsp/matlab-files/lqrsp-wac.zip

4.4.1 Analysis of the open-loop system

Despite the action of the local PSS controllers, modal and participation factor analyses reveal the presence of six poorly-damped modes in the New England power grid model; see Table 4.1 and Fig. 4.4. Mode 4 is a local mode because it only involves oscillations between generators 2 and 3, which belong to the same coherent group. All other modes are inter-area modes where groups of generators oscillate against each other. Since these inter-area modes are poorly damped with damping ratios as low as 1.20% and 2.61%, the local PSS controllers need to be complemented by supplementary wide-area controllers to improve the damping of the inter-area oscillations.

We depart from the modal perspective and examine the power spectral density and variance amplification of the open-loop system. This type of analysis allows us to identify (i) the temporal frequencies for which large amplification occurs; and (ii) the spatial structure of strongly amplified responses.

Table 4.1: Poorly-damped modes of New England model

mode no.	eigenvalue pair	damping ratio	freq. [Hz]	coherent groups
1	$-0.0882 \pm j 7.3695$	0.0120	1.1618	1,6,7,8 vs. 2,3,9
2	$-0.1788 \pm j 6.8611$	0.0261	1.0918	2,3,6,7 vs. 1,4,5,8,9
3	$-0.2404 \pm j 6.5202$	0.0368	1.0377	1,2,3,8,9 vs. 4-7
4	$-0.4933 \pm j 7.7294$	0.0637	1.2335	2 vs. 3
5	$-0.4773 \pm j 6.9858$	0.0682	1.1141	6,7 vs. 1-5,8,9
6	$-0.3189 \pm j 4.0906$	0.0777	0.6525	10 vs. all others

Figure 4.5 illustrates the power spectral density of the open-loop system. The largest peak occurs at $\omega_1 = 7.2925$ rad/s ($f_1 = \omega_1/2\pi = 1.1606$ Hz) and it corresponds to mode

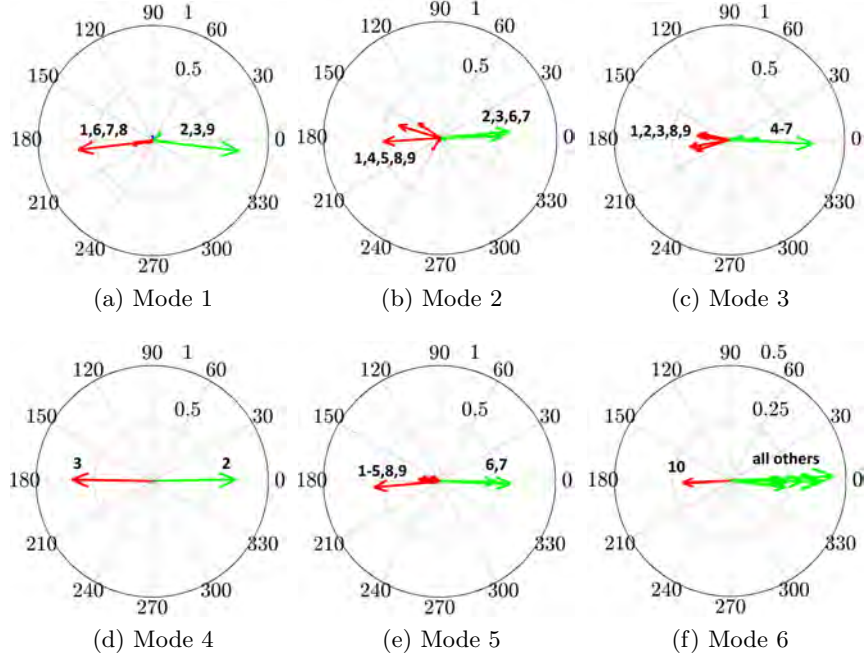


Figure 4.4: Polar plots of the angle components of the six poorly-damped modes for the open-loop system.

1 in Table 4.1 and Fig. 4.4. Another resonant peak at $\omega_2 = 4.0930$ rad/s ($f_2 = 0.6514$ Hz) corresponds to mode 6 in Table 4.1 and Fig. 4.4. The red dots in Fig. 4.5b indicate all six poorly-damped modes.

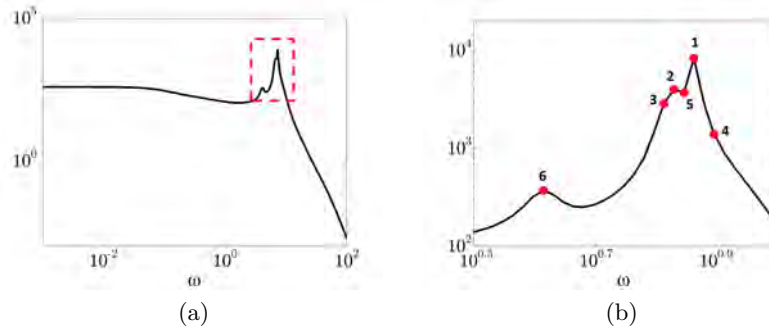


Figure 4.5: (a) Power spectral density of the open-loop system; (b) zoomed version of the red square shown in (a). Red dots denote poorly-damped modes from Table 4.1.

The contribution of each generator to the steady-state variance is shown in Fig. 4.6. The diagonal elements of the output covariance matrix Z_1 contain information about mean-square deviation from angle average and variance amplification of frequencies of the individual generators. From Fig. 4.6, we see that the largest contribution to the variance amplification arises from the misalignment of angles of generators 1, 5, and 9, and misalignment of frequencies of generators 1 and 9.

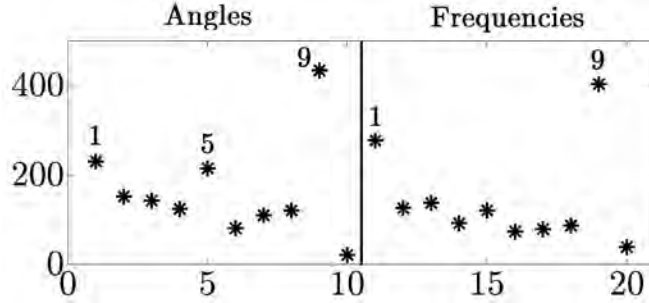


Figure 4.6: Diagonal elements of the open-loop covariance matrix Z_1 determine contribution of each generator to the variance amplification.

Similar observations can be made from Fig. 4.7. In Fig. 4.7a, we observe two dominant eigenvalues of the output covariance matrix Z_1 . We also show the spatial structure of the three principal eigenvectors (modes) of Z_1 , which contain 47.5% of the total variance. Although the angle and frequency fluctuations in experiments and nonlinear simulations are expected to be more complex than the structures presented in Fig. 4.7, the spatial profiles identified here are likely to play significant role in amplification of disturbances in power systems.

4.4.2 Sparsity-promoting optimal wide-area control

Elementwise sparsity

We first consider an optimal sparse controller whose structure is identified using the solution to (SP). Sparsity patterns of the feedback matrix $K \in \mathbb{R}^{9 \times 75}$ for different values of γ are illustrated in Fig. 4.8. The blue dots denote information coming from the generators on which the particular controller acts, and the red dots identify information that needs to be communicated from other generators. For $\gamma = 0.0818$, the identified

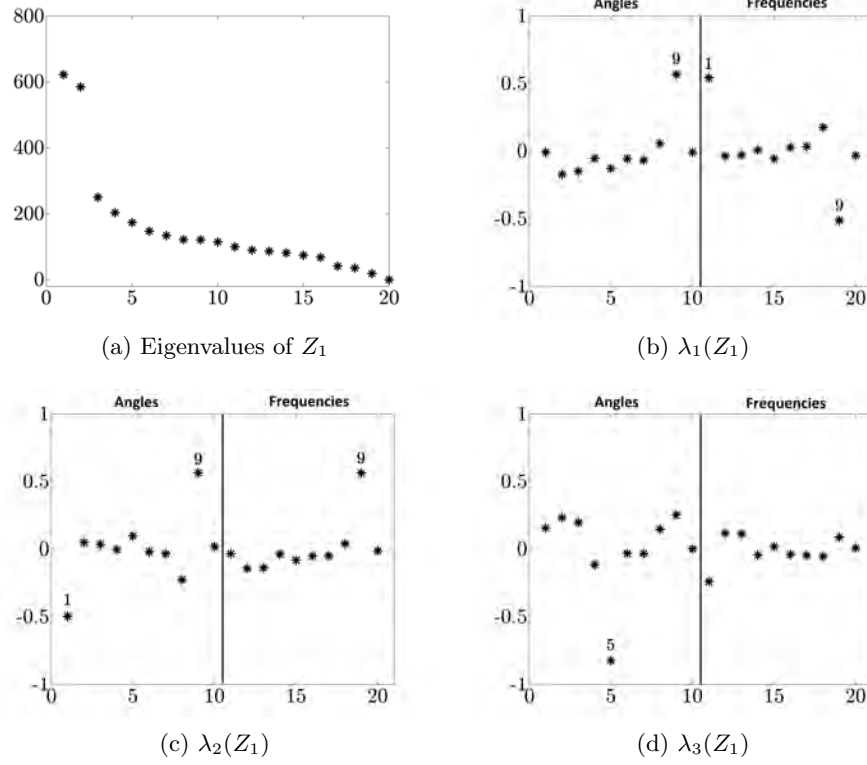


Figure 4.7: (a) Eigenvalues; and (b)-(d) eigenvectors corresponding to the three largest eigenvalues λ_i of the open-loop output covariance matrix Z_1 .

wide-area control architecture imposes the following requirements: (i) the controller of generator 9, which contributes most to the variance amplification of both angles and frequencies, requires angle and field voltage measurements of the aggregate generator 10; (ii) the controller of generator 5 requires the difference between its angle and the angle of the equivalenced model 10; and (iii) the controllers of generators 1, 4, and 7 utilize the field voltage information of generators 10, 5, and 6, respectively.

When γ is increased to 0.1548, only one long-range link remains. This link is identified by the red dot in Fig. 4.8b, indicating that the controller of generator 9 requires access to the angle mismatch relative to generator 10. By further increasing γ to 0.25, we obtain a fully-decentralized controller. Compared to the optimal centralized controller, our fully-decentralized controller degrades the closed-loop performance by about 3.02%; see Fig. 4.9. This fully-decentralized controller can be embedded into the local generator

excitation system by directly feeding the local measurements to the automatic voltage regulator, thereby effectively retuning the PSS controller.

In earlier work [14, 15], a small regularization term was added to the diagonal elements of the matrix Q_θ in order to provide detectability of the average mode. This has resulted in a controller that requires access to the absolute angle measurements to stabilize the average rotor angle. Our results indicate that long-range links identified in [14, 15] do not have significant influence on the system performance.

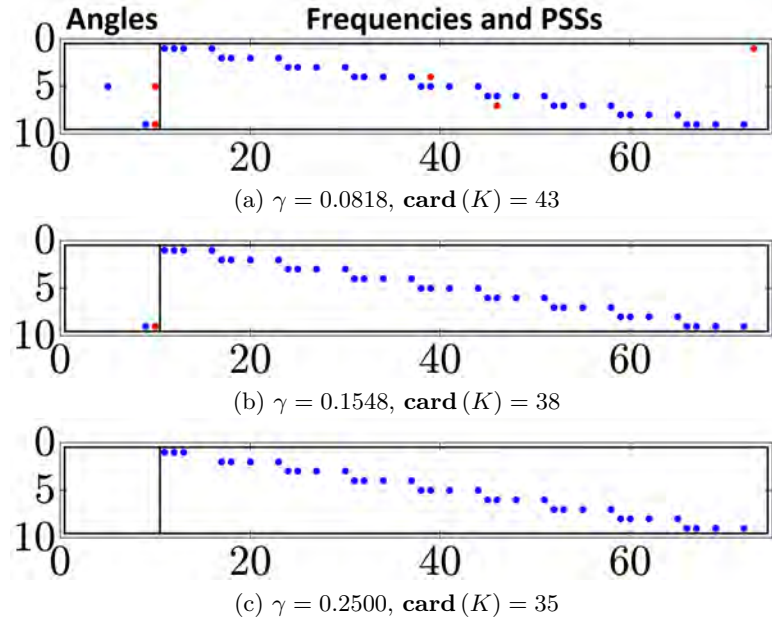


Figure 4.8: Sparsity patterns of K resulting from (SP).

Block sparsity

Three identified sparsity patterns of the feedback matrix resulting from the solution to (4.8), with g_θ and g_r given by (4.9a) and (4.9d), are shown in Fig. 4.10. In all three cases, structures of the angle feedback gains agree with the elementwise sparse controllers; cf. Fig. 4.8. On the other hand, the group penalty (4.9d) yields block-diagonal feedback gains that act on the remaining states of generators 1-9. Since no information exchange with aggregate generator 10 is required, this part of the controller can be implemented in a fully-decentralized fashion in all three cases.

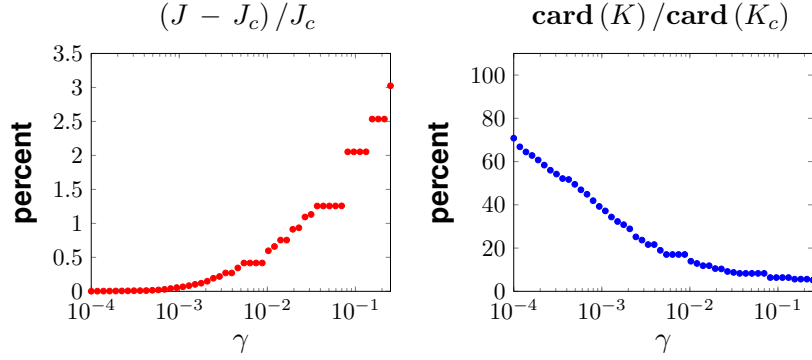


Figure 4.9: Performance vs sparsity comparison of sparse K and the optimal centralized controller K_c for 50 logarithmically-spaced points $\gamma \in [10^{-4}, 0.25]$.

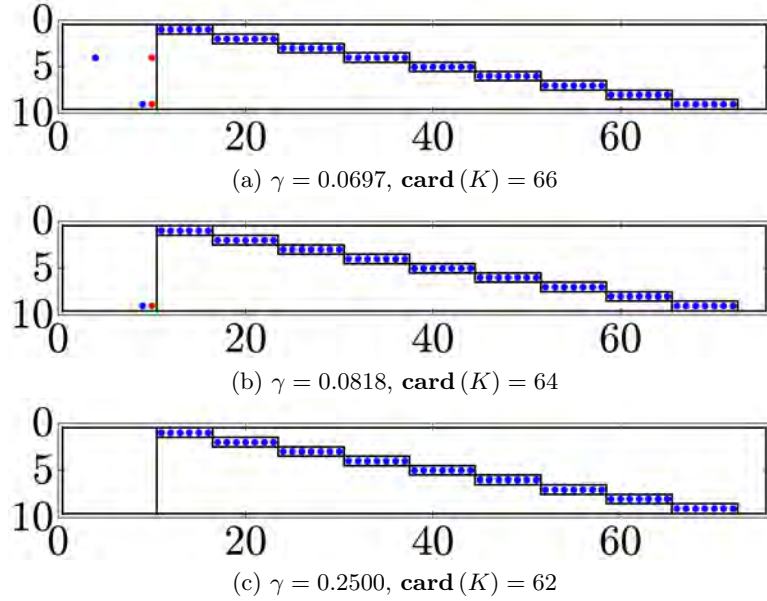


Figure 4.10: Sparsity patterns of K resulting from (4.8).

Compared to the optimal centralized controller, a fully-decentralized controller with structure shown in Fig. 4.10c compromises performance by only 2.34%; see Fig. 4.11. We recall that the fully-decentralized controller with structure shown in Fig. 4.8c degrades performance by 3.02%; cf. Fig. 4.9. Since the block-sparse controller has more degrees of freedom than the elementwise sparse controller, performance improvement does not come as a surprise. We finally note that the jumps in the number of non-zero elements

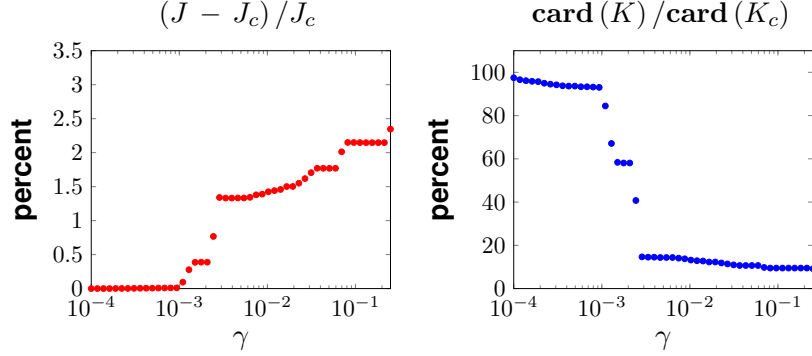


Figure 4.11: Performance vs sparsity comparison of block-sparse K and the optimal centralized controller K_c for 50 logarithmically-spaced points $\gamma = \gamma_\theta = \gamma_r \in [10^{-4}, 0.25]$.

in Fig. 4.11 are caused by elimination of the entire off-diagonal rows of the feedback gain K_r that acts on states different from relative angles.

4.4.3 Comparison of open- and closed-loop systems

We next compare performance of the open-loop system and the closed-loop systems with optimal centralized and fully-decentralized sparse and block-sparse controllers. The structures of these fully-decentralized controllers are shown in Fig. 4.8c and Fig. 4.10c, respectively.

Figure 4.12 compares the spectra of the open- and closed-loop systems. As Fig. 4.12a illustrates, all three controllers (centralized as well as decentralized sparse and block-sparse) move the open-loop spectrum away from the imaginary axis. The dashed lines in Fig. 4.12 identify damping lines. Typically, the mode is considered to have sufficient damping if it is located to the left of the 10% cyan damping line. The numbered black asterisks to the right of the 10% damping line in Fig. 4.12b correspond to the six poorly-damped modes of the open-loop system. Other damping lines show that all of our controllers significantly improve the damping of the system by moving the poorly-damped modes deeper into the left-half of the complex plane. This demonstrates that minimization of the variance amplification (i.e., the closed-loop \mathcal{H}_2 norm) represents an effective means for improving damping in power systems.

Figure 4.13 provides a comparison between the power spectral densities of the four

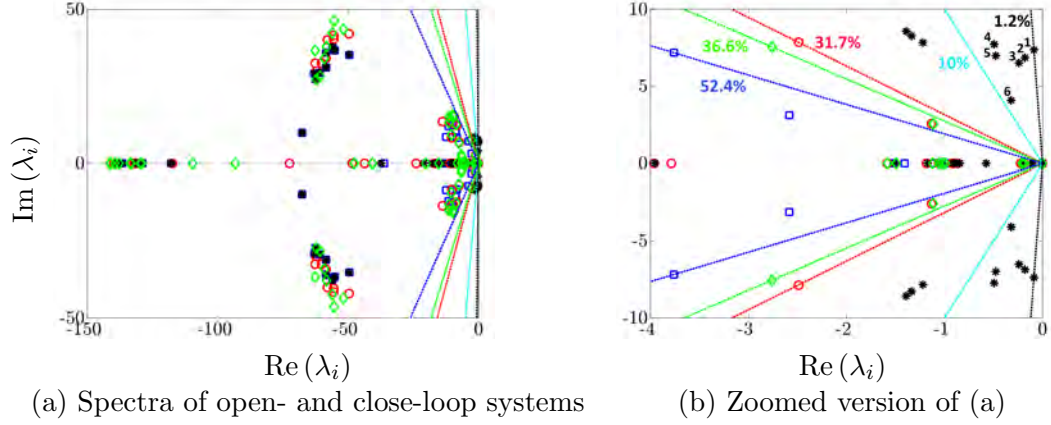


Figure 4.12: The eigenvalues of the open-loop system and the closed-loop systems with sparse/block-sparse/centralized controllers are represented by $*$, \circ , \diamond , and \square , respectively. The damping lines indicate lower bounds for damping ratios and they are represented by dashed lines using the same colors as for the respective eigenvalues. The 10% damping line is identified by cyan color. The numbered black asterisks correspond to the six poorly-damped modes given in Table 4.1.

cases. All three controllers successfully suppress the resonant peaks associated with the poorly-damped modes and significantly improve performance. We also note that the fully-decentralized sparse controllers perform almost as well as the optimal centralized controller for high frequencies; for low frequencies, we observe minor discrepancy that accounts for 2 – 3% of performance degradation in the variance amplification.

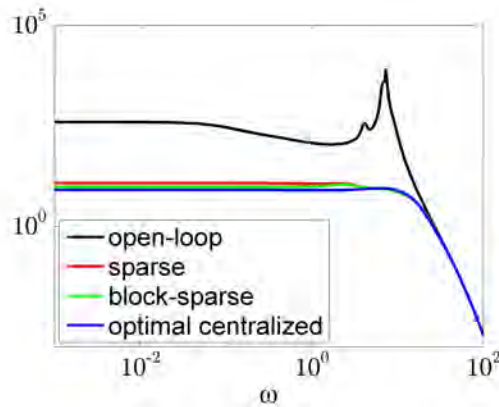


Figure 4.13: Power spectral density comparison.

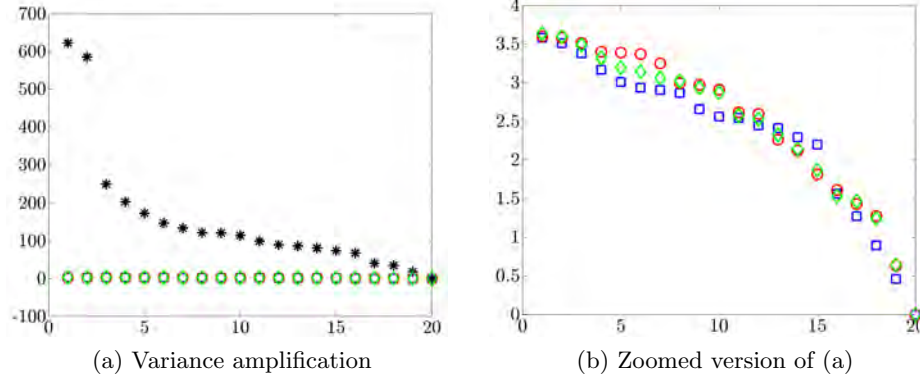


Figure 4.14: Eigenvalues of the output covariance matrix Z_1 . * represents the open-loop system, \circ , \diamond and \square represent the closed-loop systems with sparse, block-sparse, and optimal centralized controllers, respectively.

Figure 4.14 displays the eigenvalues of the output covariance matrix Z_1 for the four cases mentioned above. Relative to the open-loop system, all three feedback strategies significantly reduce the variance amplification. A closer comparison of the closed-loop systems reveals that the diagonal elements of the output covariance matrix are equalized and balanced by both the optimal centralized and the decentralized controllers; see Fig. 4.14b. Similar to the modal observations discussed in [15], the optimal sparse and block-sparse feedback gains not only increase the damping of the eigenvalues associated with the inter-area modes, but also structurally distort these modes by rotating the corresponding eigenvectors.

We use time-domain simulations of the linearized model to verify performance of decentralized block-sparse controller. Figure 4.15 shows the trajectories of rotor angles and frequencies for the open- and closed-loop systems for two sets of initial conditions. These are determined by the eigenvectors of open-loop inter-area modes 2 and 6 in Table 4.1. Clearly, the decentralized block-sparse controller significantly improves performance by suppressing the inter-area oscillations between groups of generators. Furthermore, relative to the open-loop system, the transient response of the closed-loop system features shorter settling time and smaller maximum overshoot.

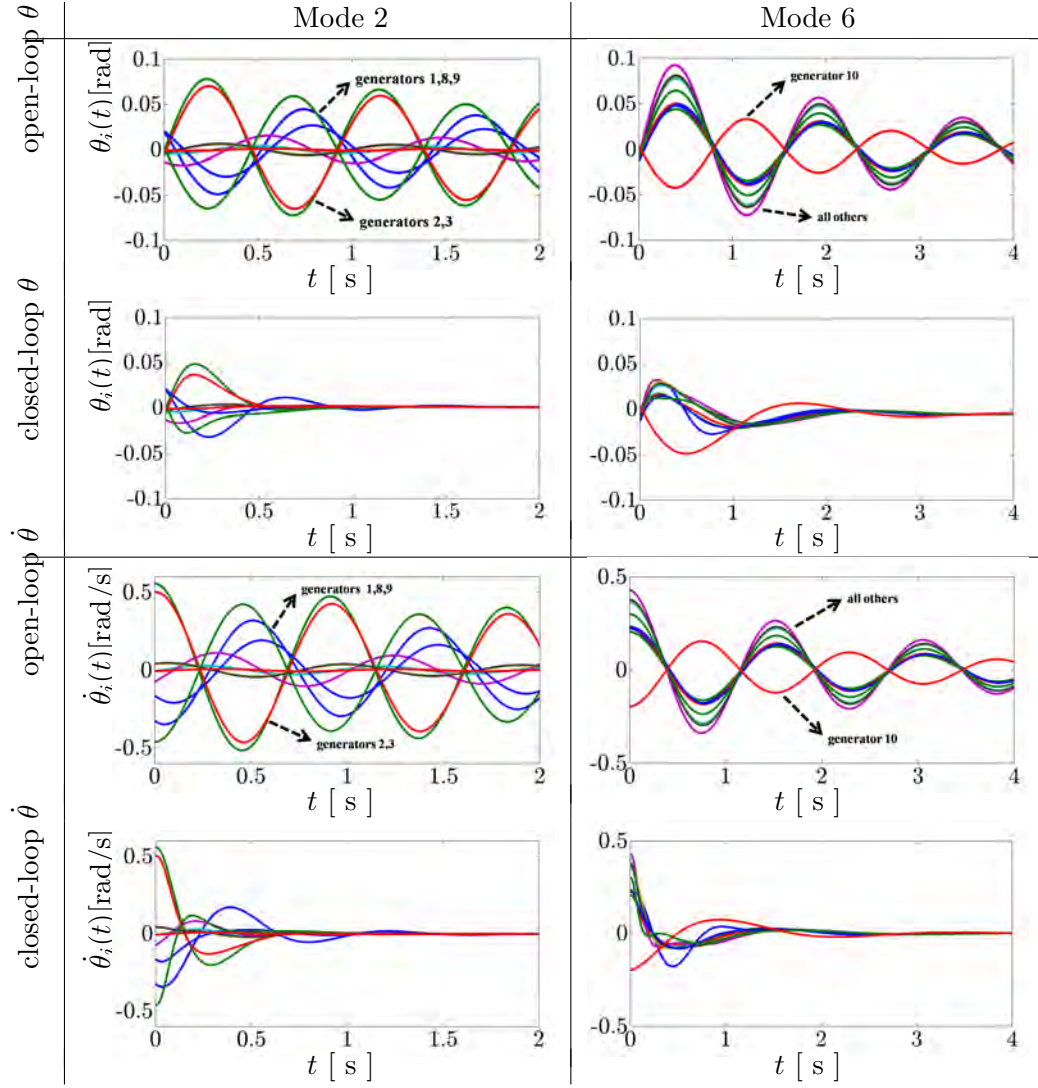


Figure 4.15: Time-domain simulations of the linearized model of the IEEE 39 New England power grid. The rotor angles and frequencies of all generators are shown. The closed-loop results are obtained using the fully-decentralized block-sparse controller. The initial conditions are given by the eigenvectors of the poorly-damped inter-area modes 2 (left) and 6 (right) from Table 4.1.

4.4.4 Robustness analysis

We close this section by examining robustness to the operating point changes of both open- and closed-loop systems. Random load perturbations are used to modify the operating point of the nonlinear system. The loads, that are used for the analysis and control

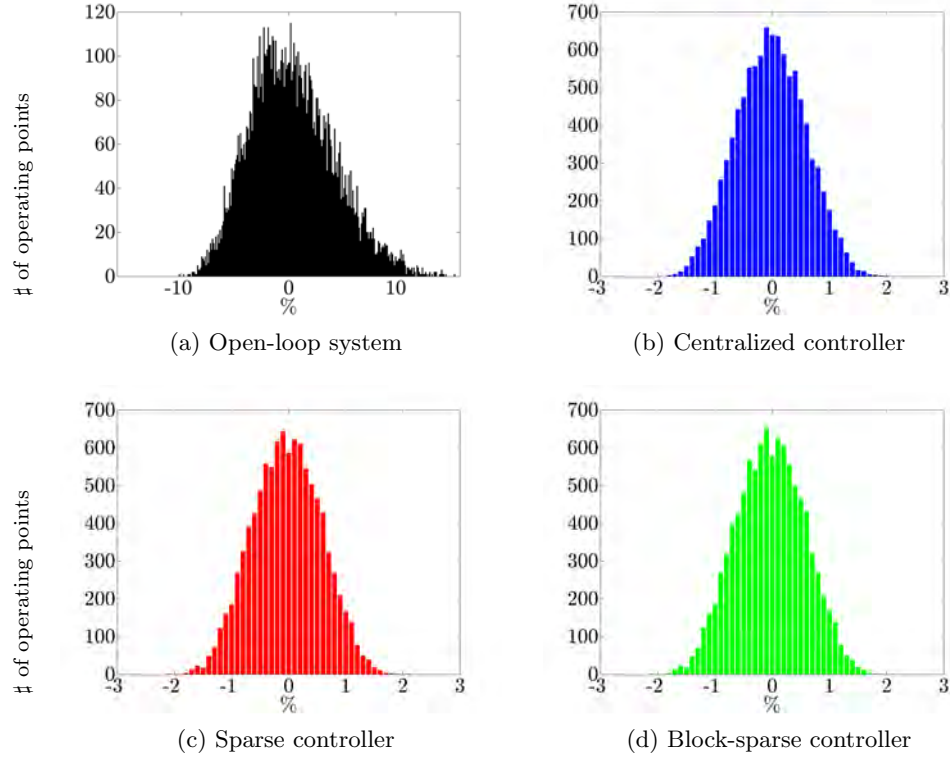


Figure 4.16: Performance histograms of open- and closed-loop linearized systems (with nominal controllers) for 10,000 uniformly distributed operating points.

synthesis, are altered via uniformly distributed perturbations that are within $\pm 20\%$ of the nominal loads. The performance of the *nominal* centralized and decentralized controllers on the *perturbed linearized model* is evaluated by examining the closed-loop \mathcal{H}_2 norm.

Figure 4.16 shows the distribution of performance change for 10,000 operating points around the original equilibria. We observe bell-shaped distributions with symmetric and narrow spread around the nominal performance. In spite of significant changes in the operating points, both centralized and fully-decentralized controllers are within 2% of the nominal performance. In contrast, same perturbations can degrade performance of the open-loop system by as much as 15%. Thus, our decentralized controllers also reduce the sensitivity and improve the robustness with respect to setpoint changes.

To account for delays in communication channels, asynchronous measurements, and

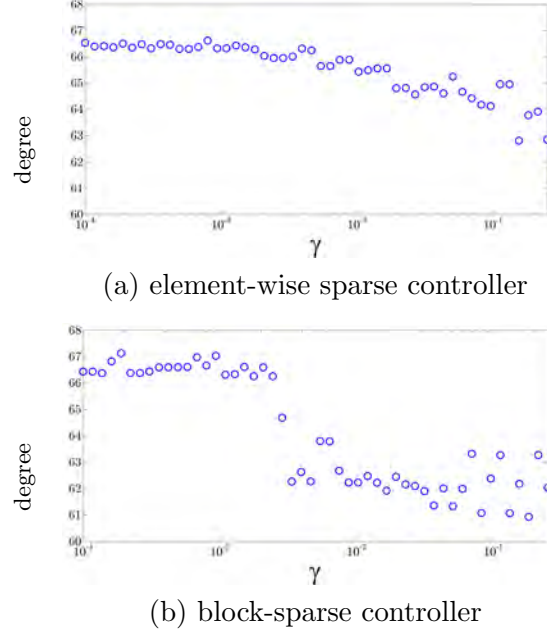


Figure 4.17: Multivariable phase margins as a function of γ .

fast unmodeled dynamics, we utilize multivariable phase margin to quantify the robustness of our sparse optimal controllers. In Fig. 4.17, we investigate how the phase margins of the closed-loop systems change with the sparsity-promoting parameter γ . As our emphasis on sparsity increases, multivariable phase margins degrade gracefully and stay close to a desirable phase margin of 60° .

Our approach thus provides a systematic way for designing optimal sparse controllers with favorable robustness margins and performance guarantees even in a fully-decentralized case.

4.5 Concluding remarks

We have analyzed inter-area oscillations in power systems by studying their power spectral densities and output covariances. Our analysis of the open-loop system identifies poorly-damped modes that cause inter-area oscillations. We have also designed sparse and block-sparse feedback controllers that use relative angle measurements to achieve

a balance between system performance and controller architecture. By placing increasing weight on the sparsity-promoting term we obtain fully-decentralized feedback gains. Performance comparisons of open- and closed-loop systems allowed us to understand the effect of the control design approach both in terms of system performance and with regards to the resulting control architecture. For the IEEE 39 New England model we have successfully tested our analysis and control design algorithms. We have also provided a systematic method for optimal retuning of fully-decentralized excitation controllers that achieves comparable performance to the optimal centralized controller.

Part III

Optimal control in distributed networks

Chapter 5

Design of distributed integral control action in power networks

Recently distributed integral controllers relying on averaging and communication have been proposed as effective means for optimal frequency regulation in power systems, load balancing of network flows, and as natural extensions to static consensus controllers. Typically, only the questions of stability, disturbance rejection, and steady-state resource allocation are addressed in the literature, and the problems of transient performance and optimal communication network design remain open. In this chapter we consider the optimal frequency regulation problem and propose a principled heuristic to identify the topology and gains of the distributed integral control layer. We employ an ℓ_1 -regularized \mathcal{H}_2 -optimal control framework as a means for striking a balance between network performance and communication requirements [118].

The resulting optimal control problem is solved using the alternating direction method of multipliers algorithm. For the IEEE 39 New England benchmark problem, we demonstrate that the identified sparse and distributed integral controller can achieve reasonable performance relative to the optimal centralized controller. Interestingly, the identified control architecture is directed and correlates with the generator rotational inertia and cost coefficients.

5.1 Synchronous frequency and power sharing

In this section, we briefly summarize background material on synchronous frequency and economic load sharing. In the linearized *swing equations* [61]

$$M \dot{\omega} = -L_p \theta - D \omega + \eta + u, \quad (5.1)$$

$(\theta, \omega) \in \mathbb{R}^{2n}$ are the generator rotor angles and frequencies, $u \in \mathbb{R}^n$ is the governor control action, and $\eta \in \mathbb{R}^n$ is a disturbance input accounting for stochastic fluctuations in generation and load, which we model as white noise signals. The diagonal matrices M and D are positive definite with diagonal elements being the generator inertia and damping coefficients, and $L_p = L_p^T \in \mathbb{R}^{n \times n}$ is the network susceptance matrix. We assume that the network is connected so that $L_p \mathbf{1} = \mathbf{0}$, where $\mathbf{1}$ and $\mathbf{0}$ are vectors of unit entries and zeros of appropriate sizes.

Synchronous frequency: If one assumes the existence of a synchronous steady-state with $\dot{\theta}_i = \omega_{\text{sync}} \in \mathbb{R}$ for all $i \in \{1, \dots, n\}$, then by summing all equations in (5.1) in steady state, we obtain the synchronous frequency explicitly as

$$\omega_{\text{sync}} = \frac{\sum_{i=1}^n u_i}{\sum_{i=1}^n D_i} + \frac{\sum_{i=1}^n \eta_i}{\sum_{i=1}^n D_i}. \quad (5.2)$$

The control objective is to design a secondary control strategy so that the frequency deviations converge to zero.

Resource allocation: Aside from driving the frequency deviations to zero it is also desirable to schedule the injections $u_i(t)$ to balance load and generation while minimizing the operational cost [62]:

$$\begin{aligned} & \underset{u}{\text{minimize}} && \sum_{i=1}^n E_i u_i^2 \\ & \text{subject to} && \sum_{i=1}^n (u_i + \eta_i) = 0. \end{aligned} \quad (5.3)$$

Here $E_i > 0$ is the cost coefficient for source $i \in \{1, \dots, n\}$. The optimization problem (5.3) is convex and the essential insight from the optimality conditions is that all units

should produce at *identical marginal costs* of generation:

$$E_i u_i^* = E_j u_j^* \quad \text{for all } i, j \in \{1, \dots, n\}. \quad (5.4)$$

Observe that the budget constraint equation in (5.3) also guarantees a zero frequency deviation in (5.2). A special case of the identical marginal cost requirement is the classical *proportional power sharing* [119] criterion

$$\frac{u_i^*}{\bar{P}_i} = \frac{u_j^*}{\bar{P}_j}, \quad (5.5)$$

where \bar{P}_i is the rating of source i . Clearly, the power sharing objective is a special case of the resource allocation problem (5.3) if one sets each cost coefficient E_i to $1/\bar{P}_i$.

5.2 Distributed integral control

In this section, we first introduce the problem setup and describe a model for frequency control of power systems. We then formulate the design of distributed integral action as a static output-feedback control problem. In the absence of sparsity constraints, we use an augmented Lagrangian method to determine optimal centralized integral controller.

5.2.1 Problem setup

The frequency error can in principle be driven to zero via decentralized integral action of the form

$$\begin{aligned} u &= -K_1 s \\ \dot{s} &= \omega, \end{aligned} \quad (5.6)$$

where s denotes the auxiliary integral states, and K_1 is a diagonal feedback matrix. It is well known, however, that such decentralized integral controllers do not achieve steady-state optimality [67]. Furthermore, they are prone to instabilities that may arise from biased measurement errors [69].

To remedy these shortcomings, we consider the distributed averaging-based integral

controller also used in [66–70]

$$\begin{aligned} u &= -E^{-1}z \\ \dot{z} &= \tilde{K}_1 \omega - L_I z. \end{aligned} \tag{5.7}$$

Here, z is the vector of auxiliary distributed integral states, E and \tilde{K}_1 are diagonal matrices of cost coefficients and positive gains, respectively, L_I is the Laplacian matrix of a connected communication graph in the integral controller. Since $\sum_{i=1}^n \dot{z}_i = \sum_{i=1}^n \tilde{K}_{1,i} \omega_i$, any steady-state solution of (5.7) satisfies $\omega_i = 0$, i.e., the frequency deviations are driven to zero. Because of $L_I z = -L_I E u = 0$, any steady-state solution of (5.7) also satisfies the identical marginal cost criterion (5.4). Hence, the controller (5.7) achieves optimal frequency regulation.

By substituting (5.7) to (5.1) yields the closed-loop system

$$\begin{aligned} \dot{\theta} &= \omega \\ M \dot{\omega} &= -L_p \theta - D \omega - E^{-1} z + \eta \\ \dot{z} &= \tilde{K}_1 \omega - L_I z. \end{aligned} \tag{5.8}$$

Without loss of generality, we assume that integral controllers are installed on all the generators. We also assume that \tilde{K}_1 is a known diagonal matrix and confine our attention to the design of the Laplacian matrix L_I . Equivalently, (5.8) can be written as

$$\begin{bmatrix} \dot{\theta} \\ \dot{\omega} \\ \dot{z} \end{bmatrix} = \underbrace{\begin{bmatrix} 0 & I & 0 \\ -M^{-1}L_p & -M^{-1}D & -(EM)^{-1} \\ 0 & \tilde{K}_1 & -\tilde{K}_2 L_I \end{bmatrix}}_{\hat{A}_{\text{cl}}} \underbrace{\begin{bmatrix} \theta \\ \omega \\ z \end{bmatrix}}_{\hat{x}} + \underbrace{\begin{bmatrix} 0 \\ M^{-1} \\ 0 \end{bmatrix}}_{\hat{B}_1} d$$

where the control action is embedded in the closed-loop system matrix \hat{A}_{cl} . Our objective is to identify topology of L_I and to design the corresponding edge weights in order to optimally enhance performance of the closed-loop network (5.8) in the presence of stochastic disturbances η .

5.2.2 Static output-feedback control problem

The design of L_I can be formulated as a static output-feedback problem for a system with a state-space model

$$\dot{\hat{x}} = \hat{A} \hat{x} + \hat{B}_1 \eta + \hat{B}_2 v, \quad (5.9)$$

where $\hat{x} = \begin{bmatrix} \theta^T & \omega^T & z^T \end{bmatrix}^T$ is the state vector, and the auxiliary control is defined as $v = -G\hat{C}_2\hat{x}$. Here, $G := L_I$ is the control gain to be designed, and the matrices in (5.9) are partitioned conformably with the state \hat{x}

$$\begin{aligned} \hat{A} &= \begin{bmatrix} 0 & I & 0 \\ -M^{-1}L_p & -M^{-1}D & -(EM)^{-1} \\ 0 & \tilde{K}_1 & 0 \end{bmatrix} \\ \hat{B}_1 &= \begin{bmatrix} 0 \\ M^{-1} \\ 0 \end{bmatrix}, \quad \hat{B}_2 = \begin{bmatrix} 0 \\ 0 \\ I \end{bmatrix}, \quad \hat{C}_2 = \begin{bmatrix} 0 & 0 & I \end{bmatrix}. \end{aligned} \quad (5.10)$$

That fact that \hat{C}_2 only contains zero and identity submatrices, enables us to apply the sparsity-promoting optimal control framework developed in [19–21]. We will discuss the details later in Section 5.3.

Since the graph Laplacian of the integral controller satisfies $L_I \mathbf{1} = 0$, we can use similar coordinate transformation on the auxiliary integral states z . It is noteworthy that the average mode \bar{z} is not eliminated from the dynamics, because we can see that absolute value of z is needed to form the integral control action in (5.7), i.e. $-E^{-1}$ does not have Laplacian property. Before introducing the coordinate transformation, we first define the performance output and weight matrices for states and control inputs.

The closed-loop system resulting from (5.9) is given by,

$$\begin{aligned} \dot{\hat{x}} &= (\hat{A} - \hat{B}_2 G \hat{C}_2) \hat{x} + \hat{B}_1 \eta \\ y &= \begin{bmatrix} Q^{1/2} \\ -R^{1/2} G \hat{C}_2 \end{bmatrix} \hat{x}. \end{aligned} \quad (5.11)$$

Here, y is the performance output, $R = R^T \succ 0$ is the control weight, and the state

weight $Q = Q^T \succeq 0$ is selected as

$$Q = \begin{bmatrix} Q_\theta & 0 & 0 \\ 0 & Q_\omega & 0 \\ 0 & 0 & Q_z \end{bmatrix}$$

with $Q_\theta = Q_z = I - (1/n)\mathbf{1}\mathbf{1}^T$ and $Q_\omega = M$. The performance output y in (5.11) accounts for deviations from the averages of θ and z , as well as the kinetic energy and the control effort of the system. The choice of performance indices is inspired by [16] for designing wide-area controller. Hence, $\|y\|_2^2 = x^T Q x$ penalizes frequency deviations and non-identical integral states similar to the distributed averaging-based integral controller (5.7) thereby accelerating the convergence of the integral error state. Together with the frequency penalty Q_ω , the penalty Q_θ on non-identical angle variables aids in the convergence of the dynamics (5.1) as in [15, 16]. Finally, inspired by the quadratic criterion (5.3) a suitable choice for the control weight is $R = E$.

In a power system without a slack bus, the generator rotor angles are only defined in a relative frame of reference, as can be observed in the linearized swing equations (5.1). Thus, all rotor angles θ can be rotated by a uniform amount without changing the dynamics (5.1). Since only differences between the components of $\theta(t) \in \mathbb{R}^n$ enter into (5.8), this rotational symmetry is preserved in the closed-loop system (5.10) as well.

By introducing a coordinate transformation [16, 30]

$$\theta = U\psi + \mathbf{1}\bar{\theta}, \quad (5.12a)$$

we can eliminate the marginally stable average mode $\bar{\theta} = \mathbf{1}^T \theta / n$ from (5.8) and the preserve rotational symmetry. Here, $\psi \in \mathbb{R}^{n-1}$ and the columns of the matrix $U \in \mathbb{R}^{n \times (n-1)}$ form an orthonormal basis of the subspace orthogonal to $\text{span}(\mathbf{1})$. For example, the columns of U can be obtained from the $(n-1)$ eigenvectors of the projector matrix $(I - (1/n)\mathbf{1}\mathbf{1}^T)$. The matrix U has the following properties

$$U^T U = I, \quad U U^T = I - (1/n)\mathbf{1}\mathbf{1}^T, \quad U^T \mathbf{1} = \mathbf{0}.$$

Furthermore, since the Laplacian matrix of the integral controller satisfies $L_I \mathbf{1} = \mathbf{0}$, we can use similar coordinate transformation on the auxiliary integral states z to ensure the Laplacian property of L_I in our control design,

$$z = U \phi + \mathbf{1} \bar{z}, \quad (5.12b)$$

where $\bar{z} = \mathbf{1}^T z / n$ is the average integral state. Note that, in contrast to $\bar{\theta}$, the average of the integral state \bar{z} actually enters into the closed-loop dynamics (5.8).

The structural constraints on θ and z are enforced by the following conditions

$$\begin{aligned} Q_\theta \mathbf{1} &= \mathbf{0}, & L_p \mathbf{1} &= \mathbf{0} \\ Q_z \mathbf{1} &= \mathbf{0}, & L_I \mathbf{1} &= \mathbf{0}. \end{aligned}$$

As an additional benefit, the above choice of Q_z penalizes the z variable relative to the vector $\mathbf{1}$, and thus facilitates the achievement of the identical marginal cost criterion (5.4).

To eliminate the marginally stable average-angle-mode $\bar{\theta}$ and preserve the relative information exchange requirement for the dynamics of z , we combine (5.12a) and (5.12b) to obtain the following coordinate transformation

$$\underbrace{\begin{bmatrix} \theta \\ \omega \\ z \end{bmatrix}}_{\hat{x}} = \underbrace{\begin{bmatrix} U & 0 & 0 & 0 \\ 0 & I & 0 & 0 \\ 0 & 0 & \mathbf{1} & U \end{bmatrix}}_{T_1} \underbrace{\begin{bmatrix} \psi \\ \omega \\ \bar{z} \\ \phi \end{bmatrix}}_x + \begin{bmatrix} \mathbf{1} \\ 0 \\ 0 \\ 0 \end{bmatrix} \bar{\theta}. \quad (5.13)$$

Equivalently, x can be expressed in terms of \hat{x} as

$$\underbrace{\begin{bmatrix} \psi \\ \omega \\ \bar{z} \\ \phi \end{bmatrix}}_x = \underbrace{\begin{bmatrix} U^T & 0 & 0 \\ 0 & I & 0 \\ 0 & 0 & (1/n)\mathbf{1}^T \\ 0 & 0 & U^T \end{bmatrix}}_{T_2} \underbrace{\begin{bmatrix} \theta \\ \omega \\ z \end{bmatrix}}_{\hat{x}}. \quad (5.14)$$

The properties of the matrix U imply that the matrices T_1 and T_2 satisfy $T_2 T_1 = I$ and

$$T_1 T_2 = \begin{bmatrix} I - (1/n)\mathbf{1}\mathbf{1}^T & 0 & 0 \\ 0 & I & 0 \\ 0 & 0 & I \end{bmatrix}.$$

In the new set of coordinates, the closed-loop system (5.7) takes the form

$$\begin{aligned} \dot{x} &= (A - B_2 F C_2)x + B_1 \eta \\ y &= \begin{bmatrix} Q^{1/2} \\ -R^{1/2} F C_2 \end{bmatrix} x \end{aligned} \quad (5.15)$$

where

$$A = T_2 \hat{A} T_1, \quad B_1 = T_2 \hat{B}_1, \quad Q = T_1^T \hat{Q} T_1,$$

and $B_2^T = \begin{bmatrix} 0 & 0 & 0 & U \end{bmatrix}^T$, $C_2 = \begin{bmatrix} 0 & 0 & 0 & I \end{bmatrix}$. The matrices B_2 and C_2 are partitioned conformably with the partition of the state vector x . The feedback matrices G and F (in the \hat{x} and x coordinates, respectively) are related by

$$F = G U \Leftrightarrow G = F U^T.$$

For this static-output feedback problem (5.15), the control objective is to achieve a desirable tradeoff between the \mathcal{H}_2 performance of (5.15) and the sparsity of the feedback gain G . The \mathcal{H}_2 norm from the disturbance η to the output y , which quantifies the steady-state variance (energy) of y of the stochastically forced system (5.15), is defined as

$$J(F) := \begin{cases} \text{trace}(B_1^T P(F) B_1) & F \text{ stabilizing} \\ \infty & \text{otherwise} \end{cases}$$

where the closed-loop observability Gramian P satisfies the Lyapunov equation

$$(A - B_2 F C_2)^T P + P(A - B_2 F C_2) = -(Q + C_2^T F^T R F C_2).$$

While the performance is expressed in terms of the feedback gain matrix F , we will

enhance sparsity of the Laplacian matrix $G = L_I$ in the original coordinates; see Section 5.3.

5.2.3 Optimal design of the centralized integral action

We first focus on the design the centralized integral controller $G = L_I$ that minimizes the \mathcal{H}_2 norm of the closed-loop system, we follow the augmented Lagrangian approach for structured feedback synthesis [120,121]. Since the matrix \hat{C}_2 in (5.15) only contains zero and identity submatrices, we can formulate the static output-feedback problem (5.15) as a structured state-feedback optimal control problem

$$\begin{aligned} \dot{x} &= (A - B_2 K)x + B_1 \eta \\ y &= \begin{bmatrix} Q^{1/2} \\ -R^{1/2} K \end{bmatrix} x \end{aligned} \quad (5.16)$$

where K satisfies the following structural constraint

$$K := \begin{bmatrix} K_\psi & K_\omega & K_{\bar{z}} & K_\phi \end{bmatrix} = \begin{bmatrix} 0 & 0 & 0 & F \end{bmatrix}. \quad (5.17)$$

Finding a solution of the structured optimal control problem (5.16) amounts to solving

$$\begin{aligned} &\underset{K}{\text{minimize}} && J(K) \\ &\text{subject to} && K \in \mathcal{S}, \end{aligned} \quad (5.18)$$

where $J(K)$ is the \mathcal{H}_2 norm of system (5.16) parameterized as a function of K , and \mathcal{S} is a set of stabilizing feedback gains K satisfying the structural constraint (5.17). The algebraic characterization of the structural constraint is given by

$$K \in \mathcal{S} \Leftrightarrow K \circ I_{\mathcal{S}} = K,$$

where \circ is the elementwise matrix multiplication and

$$I_{\mathcal{S}} = \begin{bmatrix} 0 & 0 & 0 & \mathbf{1}\mathbf{1}^T \end{bmatrix}$$

is partitioned conformably with the partition of the state x .

The augmented Lagrangian method developed in [120] solves a sequence of unstructured problems iteratively, and the minimizers of the unstructured problems converge to a minimizer of the optimal control problem (5.18). The resulting centralized $L_I = G = FU^T$ can be used as a warm-start for the sparsity-promoting optimal control problem that is discussed next.

5.3 Sparsity-promoting optimal control

A sparsity-promoting optimal control framework for finding a state feedback that simultaneously optimizes the closed-loop variance and induces a sparse control architecture was developed in [19–21]. In this section, we extend this approach to a static output-feedback optimal control problem.

While we want to minimize the \mathcal{H}_2 norm in terms of the feedback matrix F in the new set of coordinates, we would like to promote sparsity of the Laplacian matrix $G = L_I$ in the physical domain. This procedure is used to identify sparse structure of the integral control layer. This is accomplished by considering the regularized optimal control problem

$$\begin{aligned} & \underset{F, G}{\text{minimize}} && J(F) + \gamma g(G) \\ & \text{subject to} && F U^T - G = 0. \end{aligned} \tag{SP}$$

The regularization term in (SP) is determined by

$$g(G) := \sum_{i,j} W_{ij} |G_{ij}|$$

which is an effective proxy for inducing elementwise sparsity in the feedback gain G [99]. The weights W_{ij} 's are updated iteratively using the solution to (SP) from the previous iteration; see [99] for details. In (SP), γ is positive regularization parameter that characterizes the emphasis on the sparsity level of the feedback matrix G .

The linear constraint in (SP) allows us to exploit structure of the objective functions J and g with the ADMM algorithm. ADMM brings two benefits to the sparsity-promoting control problem: separability of $g(G)$ and differentiability of $J(F)$. The penalty function $g(G)$ is separable with respect to the individual elements of the matrix, however, the closed-loop \mathcal{H}_2 norm can not be decomposed into componentwise

functions of the feedback gain. By separating $g(G)$ and $J(F)$ in the minimization of the augmented Lagrangian \mathcal{L}_ρ , we can determine analytically the solution to the G minimization problem. On the other hand, the square of the closed-loop \mathcal{H}_2 norm $J(F)$ is a differentiable function of F , and this is in contrast to $g(G)$ which is a non-differentiable function.

Next we describe the ADMM algorithm for solving (SP), see [21, 30] for additional details.

Initialization

We follow the augmented Lagrangian approach introduced in Section 5.2.3 to design an optimal $F_0 = GU$ to initialize the iterative procedure.

Form augmented Lagrangian

$$\mathcal{L}_\rho(F, G, \Lambda) = J(F) + \gamma g(G) + \text{trace}(\Lambda^T(FU^T - G)) + \frac{\rho}{2} \|FU^T - G\|_F^2$$

where Λ denotes the matrix of Lagrange multipliers and $\|\cdot\|_F$ is the Frobenius norm of a matrix.

Iterative ADMM algorithm

$$\begin{aligned} F^{m+1} &= \underset{F}{\operatorname{argmin}} \mathcal{L}_\rho(F, G^m, \Lambda^m) \\ G^{m+1} &= \underset{G}{\operatorname{argmin}} \mathcal{L}_\rho(F^{m+1}, G, \Lambda^m) \\ \Lambda^{m+1} &= \Lambda^m + \rho(F^{m+1}U^T - G^{m+1}). \end{aligned}$$

Here, m represents the iteration index. Using the fact that $U^TU = I$, it is readily shown that the F -minimization step amounts to solving the following optimization problem

$$F^{m+1} = \underset{F}{\operatorname{argmin}} \left(J(F) + \frac{\rho}{2} \|F - H^m\|_F^2 \right)$$

where $H^m := (G^m - (1/\rho)\Lambda^m)U$. We apply the KKT necessary conditions [122] for

optimality of $\mathcal{L}_\rho(F, G^m, \Lambda^m)$, and the following equations need to be satisfied

$$\begin{aligned} (A - B_2 F C_2) L + L (A - B_2 F C_2)^T &= -B_1 B_1^T \\ (A - B_2 F C_2)^T P + P (A - B_2 F C_2) &= \\ - (Q + C_2^T F^T R F C_2) 2 (R F C_2 - B_2^T P) L C_2^T + \rho (F - H^m) &= 0. \end{aligned}$$

The resulting set of the matrix-valued equations is solved using the iterative procedure developed in [21].

Similarly, properties of the matrix U can be used to bring the G -minimization problem into the following form

$$G^{m+1} = \underset{G}{\operatorname{argmin}} \left(\gamma g(G) + \frac{\rho}{2} \|G - V^m\|_F^2 \right)$$

where $V^m := F^{m+1} U^T + (1/\rho) \Lambda^m$ and the unique solution is obtained via the soft thresholding operator,

$$G_{ij}^{m+1} = \begin{cases} (1 - a/|V_{ij}^m|) V_{ij}^m & |V_{ij}^m| > a \\ 0 & |V_{ij}^m| \leq a. \end{cases}$$

Here, $a := (\gamma/\rho) W_{ij}$ and, for a given V_{ij}^m , G_{ij}^{m+1} is either set to zero or it is obtained by moving V_{ij}^m towards zero with the amount $(\gamma/\rho) W_{ij}$.

Stopping criterion

$$\|F^{m+1} U^T - G^{m+1}\| \leq \epsilon, \quad \|G^{m+1} - G^m\| \leq \epsilon$$

The ADMM algorithm stops when both primal and dual residuals are smaller than specified thresholds.

Polishing step Finally, we fix the sparsity pattern of G identified using ADMM and solve the optimal control problem with the identified structural constraints. This polishing step improves the \mathcal{H}_2 performance relative to the feedback gain identified by ADMM; see [21] for additional details.

5.4 Case study: IEEE 39 New England model

The IEEE 39 New England Power Grid model consists of 39 buses and 10 detailed two-axis generator models; see Fig. 5.1. All loads are modeled as constant power loads. As previously mentioned, we assume that all the generators are equipped with integral controllers. We extract network susceptance matrix L_p and inertia matrix M of the IEEE 39 New England model from Power System Toolbox [123]. We set the the damping coefficients D_i of each generator to be $0.1M_i$, and the diagonal positive control gain matrix \tilde{K}_1 to be identity matrix. The values of the cost coefficients E_i are chosen to be $E_i = 0.9$ for $i \in \{1, 2, 3, 4, 6, 7, 8, 9, 10\}$, $E_5 = 0.1$, i.e., we assume that generator 5 cost the least to operate while all other generators have the same cost coefficients. The state matrices and performance indices are defined as outlined in Section 5.2.2.

Next, we illustrate that our proposed static output feedback sparsity-promoting optimal control framework is an efficient way to achieve a balance between the system performance and sparsity level of L_I . In Fig 5.2, we show the sparsity pattern of the feedback matrix $G = L_I \in \mathbb{R}^{10 \times 10}$ for different value of γ . The blue dots denote local feedback control gains, and the red dots identify information that needs to be communicated between different generators. For $\gamma = 0.001$, L_I is dense and recovers the communication pattern of the conventional integral controller as shown in Fig. 5.2a. When γ increases from 0.001 to 0.101, the 5th column of L_I becomes sparse while the 5th row becomes the only row with all nonzero elements. This indicates that most generators do not care about generator 5 that has the smallest cost coefficient. At the same time, integral controller on generator 5 has to gather information from all other generators to achieve desired performance of the network.

By further increasing γ to 4.715, the structure of L_I shows that integral state information of generator 1, 3, 6, 9, 10, which have the five largest inertia, is gathered by other integral controllers. Apparently, six other generators need to access information from generator 10, since it has the largest inertia and thus the most reliable frequency measurement in the integral control. Finally, when $\gamma = 10$, only 11 long-range links are required, and integral controller on generator 10 is no longer needed. Since generator 10 is an equivalent aggregated model representing the transmission network of a neighboring area, it has an oversized inertia coefficient and thus also little control agility. Hence,

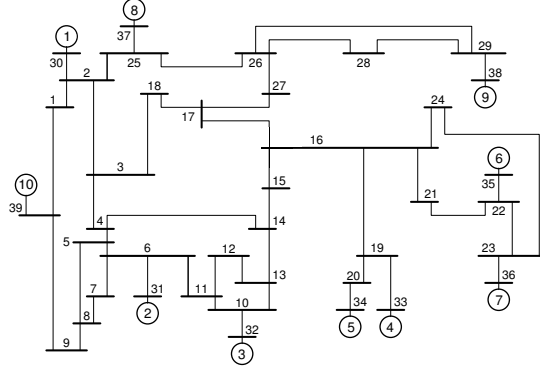
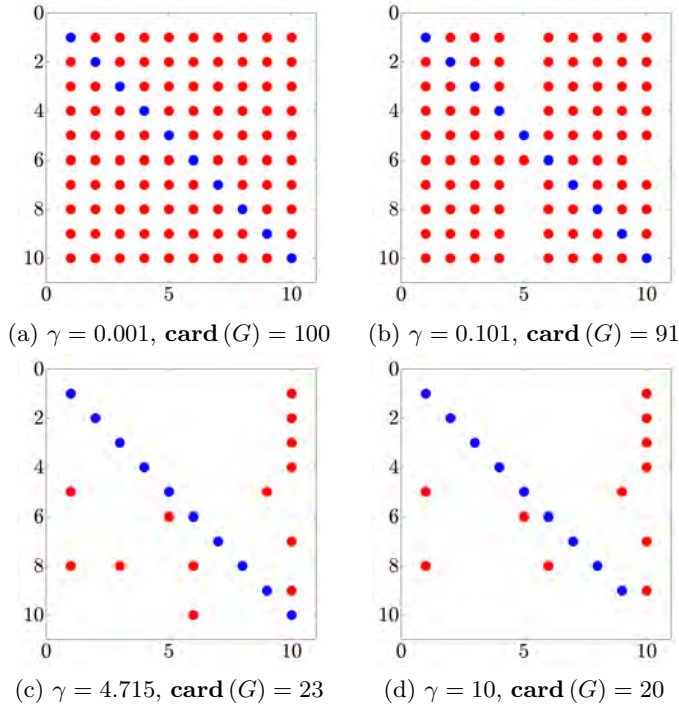


Figure 5.1: The IEEE 39 New England Power Grid.

Figure 5.2: Sparsity pattern of G resulting from (SP).

it is not surprising to drop this virtual controller. Our observation shows that the optimal communication architecture correlates with both inertia and cost coefficients.

In Fig. 5.3, we compare performance degradation and sparsity level for different

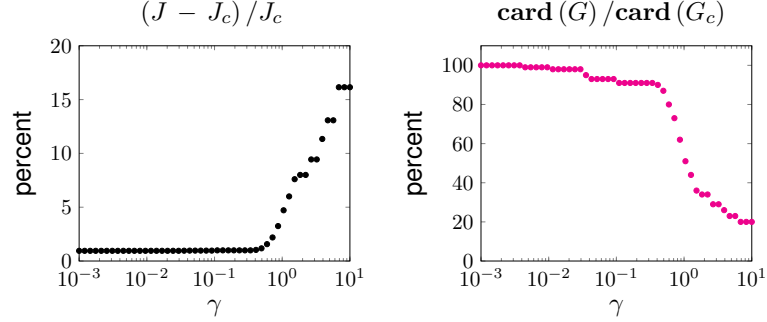


Figure 5.3: Performance vs sparsity comparison of sparse G and the optimal centralized controller G_c for 50 logarithmically-spaced points $\gamma \in [10^{-3}, 10]$.

values of γ . Compared to the optimal centralized integral controller G_c , our sparse G in Fig 5.2d degrades system performance by only 16.15%. Therefore, by constructing only 11 long-range links for the integral controller architecture, reasonable performance is achieved compared to the optimal centralized feedback gain G_c .

5.5 Concluding remarks

In this section, we propose a distributed PI-control strategy for frequency control in power systems. We formulate the topology identification and design of integral controller as a static output-feedback control problem. A coordinate transformation is introduced to enforce the structural constraints on the rotor angles and auxiliary integral states. We find the solution by solving the sparsity-promoting optimal control problem, which balances the tradeoff between system performance and sparsity of the controller. Our development is validated by a benchmark power system example.

Chapter 6

Design of optimal coupling gains for synchronization of nonlinear oscillators

This chapter develops a structured optimal-control framework to design coupling gains for synchronization of weakly nonlinear oscillator circuits connected in resistive networks with arbitrary topologies. The oscillators are modeled as weakly nonlinear Liénard-type circuits, and the coupling gain amounts to the current gain which scales the output current of the oscillator. The structured optimal-control problem allows us to seek a decentralized control strategy (equivalently, a diagonal feedback matrix) that precludes communications between oscillators. To this end, a sparsity-promoting optimal control algorithm is developed to tune the optimal diagonal feedback-gain matrix with minimal performance sacrifice [124]. This involves solving an \mathcal{H}_2 optimal control problem with ℓ_1 regularization by applying the alternating direction method of multipliers (ADMM). Simulation studies with application to voltage regulation in islanded networks composed of power-electronic inverters are provided to validate the approach.

6.1 System of coupled weakly nonlinear oscillator circuits

We begin this section with a description of the oscillator dynamics, and then describe the network interactions.

6.1.1 Nonlinear oscillator model

The oscillator dynamics are governed by

$$\ddot{v} + \varepsilon f(v) \dot{v} + \omega^2 v = \kappa \varepsilon \omega \dot{u}(t), \quad (6.1)$$

where v is the terminal voltage, u is the input current, κ is the *current gain* (interchangeably referred as the *coupling gain*), ε is a positive real constant, and ω is the frequency of the voltage waveform for the unforced ($u = 0$) system in the so-called *quasi-harmonic* limit $\varepsilon \searrow 0$ [96]. All subsequent discussions assume operation in this quasi-harmonic limit since the terminal-voltage dynamics in this limit are approximately sinusoidal [96]. Function $f : \mathbb{R} \rightarrow \mathbb{R}$ satisfies the conditions in Liénard's theorem [84] for existence of a unique and stable limit cycle, in particular,

(A1) $f(v)$ is continuously differentiable $\forall v$.

(A2) $f(v)$ is an even function, i.e., $f(v) = f(-v)$, $\forall v$.

(A3) Function $F(v) := \int_0^v f(z) dz$ has exactly one positive zero at $v = v_0$, is negative for $0 < v < v_0$, is positive and nondecreasing $\forall v > v_0$, and $\lim_{v \rightarrow \infty} F(v) \rightarrow \infty$.

Examples of nonlinear circuits that admit terminal-voltage dynamics of the form (6.1) include the ubiquitous Van der Pol oscillator (see Fig. 6.1 for more details), the dead-zone oscillator [85], a class of operational transconductance amplifiers [92], and dynamic translinear oscillator circuits [91].

To extract the amplitude and phase dynamics from (6.1), we seek a dynamical system representation in polar coordinates. To this end, define the change of variables $v = r \cos(\phi)$, $\omega \int_0^t v dt = r \sin(\phi)$, where r denotes the radius of the oscillator limit cycle, and ϕ represents the instantaneous phase of the resulting oscillations. It is straightforward

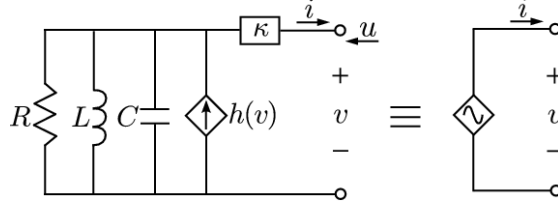


Figure 6.1: The Van der Pol oscillator circuit with a current gain κ admits the dynamics in (6.1). In this case, $\omega = 1/\sqrt{LC}$, $\varepsilon = \sqrt{L/C}$, and $h(v) = \int f(v)dv = \alpha\omega(v - \beta v^3/3)$ where α and β are positive real constants.

to show that with this change of coordinates, we recover the following model:

$$\begin{aligned}\dot{r} &= \varepsilon (h(r \cos \phi) + \kappa \omega u(t)) \cos \phi, \\ \dot{\phi} &= \omega - \left(\frac{\varepsilon}{r} h(r \cos \phi) - \varepsilon \kappa \omega \frac{u(t)}{r} \right) \sin \phi,\end{aligned}\tag{6.2}$$

where $h(z) := \int f(z)dz$. In subsequent developments, we will find it useful to work with the following model:

$$\begin{aligned}\dot{r} &= \varepsilon (h(r \cos(\omega t + \theta)) + \kappa \omega u(t)) \cos(\omega t + \theta), \\ \dot{\theta} &= -\frac{\varepsilon}{r} (h(r \cos(\omega t + \theta)) + \kappa \omega u(t)) \sin(\omega t + \theta).\end{aligned}\tag{6.3}$$

where we define $\theta(t) := \phi(t) - \omega t$, with θ representing the phase offset with respect to the rotating reference frame of frequency ω . Since the system (6.3) is non-autonomous but periodic in t , we leverage averaging methods to obtain an autonomous system which admits similar dynamics [96]. In particular, for small values of ε we can average the periodic vector fields in (6.3) to obtain the so-called *slow flow* equations which are accurate up to $\mathcal{O}(\varepsilon)$ [125].

Let us denote \bar{r} and $\bar{\theta}$ to be the $2\pi/\omega$ -averaged values of the periodic signals r and θ , respectively. In the quasi-harmonic limit, i.e., $\varepsilon \searrow 0$, we apply standard averaging arguments using ε as the *small parameter*, to obtain the averaged dynamics [96, Theorem

10.4] [83, 126]

$$\begin{aligned}
\begin{bmatrix} \dot{\bar{r}} \\ \dot{\bar{\theta}} \end{bmatrix} &= \frac{\varepsilon\omega}{2\pi} \int_0^{2\pi/\omega} \begin{bmatrix} h(\bar{r} \cos(\omega t + \bar{\theta})) \cos(\omega t + \bar{\theta}) \\ -\frac{1}{\bar{r}} h(\bar{r} \cos(\omega t + \bar{\theta})) \sin(\omega t + \bar{\theta}) \end{bmatrix} dt \\
&\quad + \frac{\varepsilon\kappa\omega^2}{2\pi} \int_0^{2\pi/\omega} \begin{bmatrix} u(t) \cos(\omega t + \bar{\theta}) \\ -\frac{1}{\bar{r}} u(t) \sin(\omega t + \bar{\theta}) \end{bmatrix} dt \\
&= \frac{\varepsilon}{2\pi} \begin{bmatrix} -\bar{f}(\bar{r}) + \omega^2 \int_0^{2\pi/\omega} u(t) \cos(\omega t + \bar{\theta}) dt \\ -\kappa\omega^2 \int_0^{2\pi/\omega} \frac{u(t)}{\bar{r}} \sin(\omega t + \bar{\theta}) dt \end{bmatrix}, \tag{6.4}
\end{aligned}$$

where

$$\bar{f}(\bar{r}) := 4 \int_0^{\bar{r}} f(\sigma) \sqrt{1 - \frac{\sigma^2}{\bar{r}^2}} d\sigma. \tag{6.5}$$

6.1.2 Resistive electrical network

We consider a collection of N oscillators with dynamics of the form (6.1) (or equivalently, (6.4)) connected in a resistive electrical network. The oscillators are assumed to be identical in all aspects except for the current gains. The nodes of the resistive electrical network are collected in the set \mathcal{A} , and branches (edges) are collected in the set $\mathcal{E} := \{(j, \ell)\} \subset \mathcal{A} \times \mathcal{A}$. Let $\mathcal{N} := \{1, \dots, N\} \subseteq \mathcal{A}$ denote nodes that the oscillators are connected to, and denote the set of *internal nodes* as $\mathcal{I} := \mathcal{A} \setminus \mathcal{N}$. Shunt loads—also modeled as resistances—are connected to the internal nodes \mathcal{I} . Denote the vectors that collect the nodal current injections and node voltages in the network by $i_{\mathcal{A}}$ and $v_{\mathcal{A}}$, respectively. Note that since the network is resistive, $i_{\mathcal{A}}$ and $v_{\mathcal{A}}$ are real-valued functions of time. The electrical coupling between the oscillators is described by Kirchhoff's and Ohm's laws, which read in matrix-vector form as

$$i_{\mathcal{A}} = G_{\mathcal{A}} v_{\mathcal{A}}, \tag{6.6}$$

with entries of the *conductance matrix* $G_{\mathcal{A}}$ given by

$$[G_{\mathcal{A}}]_{j\ell} := \begin{cases} g_j + \sum_{(j,k) \in \mathcal{E}} g_{jk}, & \text{if } j = \ell, \\ -g_{j\ell}, & \text{if } (j, \ell) \in \mathcal{E}, \\ 0, & \text{otherwise,} \end{cases} \tag{6.7}$$

with $g_j \in \mathbb{R}_{\geq 0}$ denoting the shunt conductance at node j , and $g_{j\ell} = g_{\ell j} \in \mathbb{R}_{\geq 0}$ the conductance of the line (j, ℓ) .

Let $i = [i_1, \dots, i_N]^T$ and $v = [v_1, \dots, v_N]^T$ be the vectors of inverter current injections and terminal voltages, respectively, and let $i_{\mathcal{I}}$ and $v_{\mathcal{I}}$ be the vectors collecting the current injections and nodal voltages for the interior nodes. Note that entries of $i_{\mathcal{I}}$ are zero. With this notation in place, we can rewrite (6.6) as

$$\begin{bmatrix} i \\ 0 \end{bmatrix} = \begin{bmatrix} G_{\mathcal{N}\mathcal{N}} & G_{\mathcal{N}\mathcal{I}} \\ G_{\mathcal{N}\mathcal{I}}^T & G_{\mathcal{I}\mathcal{I}} \end{bmatrix} \begin{bmatrix} v \\ v_{\mathcal{I}} \end{bmatrix}. \quad (6.8)$$

For the resistive networks we consider in this work, $G_{\mathcal{I}\mathcal{I}}$ is always nonsingular due to irreducible diagonal dominance [127]. Therefore, the second set of equations in (6.8) can be uniquely solved for the interior voltages, $v_{\mathcal{I}}$. Then, we obtain the following equations relating the oscillator current injections and terminal voltages:

$$i = l (G_{\mathcal{N}\mathcal{N}} - G_{\mathcal{N}\mathcal{I}} G_{\mathcal{I}\mathcal{I}}^{-1} G_{\mathcal{N}\mathcal{I}}^T) v =: G v. \quad (6.9)$$

We refer to the matrix G in (6.9) as the *Kron-reduced conductance matrix* and this model reduction through a Schur complement of the conductance matrix is known as *Kron reduction* [127]. Notice that the entries of G define the effective electrical conductances between the oscillators in the network, as well as the effective local resistive loads for each oscillator. An illustration of Kron reduction for a network with three oscillators is shown in Fig. 6.2. Under some mild assumptions on the originating network, it follows that the Kron-reduced network is fully connected [127].

With a slight abuse of notation, we denote the effective shunt-conductance load for the j th oscillator by g_j , and the effective conductance of the (j, ℓ) line in the Kron-reduced electrical network by $g_{j\ell}$ in all subsequent discussions. Also, we will find it useful to define $g_{jj} := g_j + \sum_{k=1, k \neq j}^N g_{jk}$.

6.1.3 System dynamical model in polar coordinates

With this notation in place, for the resistive network, the current input for the j th oscillator, $u_j(t)$ is given by:

$$u_j(t) = -i_j(t) = -\sum_{\ell=1}^N g_{j\ell} \bar{r}_\ell \cos(\omega t + \bar{\theta}_\ell). \quad (6.10)$$

Substituting (6.10) in (6.4), and denoting $\bar{\theta}_{j\ell} = \bar{\theta}_j - \bar{\theta}_\ell$, we get the following polar-coordinates representation for the dynamics of the j th oscillator:

$$\frac{d\bar{r}_j}{dt} = -\frac{\varepsilon \bar{f}(\bar{r}_j)}{2\pi} - \frac{\kappa_j \varepsilon \omega}{2} g_{jj} \bar{r}_j + \frac{\kappa_j \varepsilon \omega}{2} \sum_{\ell=1, \ell \neq j}^N g_{j\ell} \bar{r}_\ell \cos(\bar{\theta}_{j\ell}), \quad (6.11a)$$

$$\frac{d\bar{\theta}_j}{dt} = l - \frac{\kappa_j \varepsilon \omega}{2\bar{r}_j} \sum_{\ell=1, \ell \neq j}^N g_{j\ell} \bar{r}_\ell \sin(\bar{\theta}_{j\ell}). \quad (6.11b)$$

6.1.4 State-space representation of linearized system

Our objective is to design an optimal set of coupling gains, $\kappa_1, \dots, \kappa_N$, that ensure the terminal voltages of the nonlinear oscillator dynamics in (6.11) are regulated to a common value. For the class of oscillator models we consider, it is known that there exists a unique and stable limit cycle with radius \bar{r}_{eq} which satisfies $\bar{f}(\bar{r}_{\text{eq}}) = 0$ [84]. With a view towards leveraging control design techniques from linear systems theory, we linearize the system around $(\bar{r}_{\text{eq}} \mathbf{1}_N, \bar{\theta}_{\text{eq}})$ (where $\mathbf{1}_N$ denotes $N \times 1$ vector of all ones);

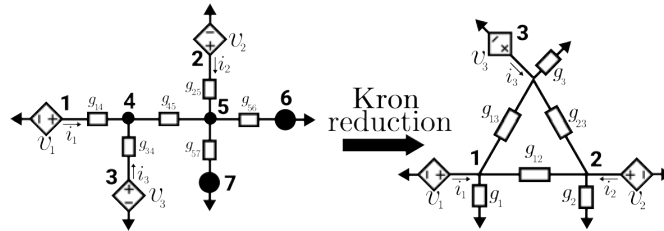


Figure 6.2: Kron reduction illustrated for a network of three oscillators. In this example, $\mathcal{A} = \{1, \dots, 5\}$, $\mathcal{N} = \{1, 2, 3\}$, and $\mathcal{I} = \{4, 5\}$.

$\bar{\theta}_{\text{eq}}$ is the phase-synchronized equilibrium (we comment on it next). The Jacobian of the system around the equilibrium point can be partitioned into blocks as follows:

$$J = \left[\begin{array}{c|c} J_A & J_B \\ \hline J_C & J_D \end{array} \right]. \quad (6.12)$$

The entries of J_A , J_B , J_C , and J_D are specified as:

$$\begin{aligned} [J_A]_{j\ell} &= \begin{cases} -\frac{\varepsilon}{2\pi} f'(\bar{r}_{\text{eq}}) - \kappa_j \frac{\varepsilon\omega}{2} g_{jj} & \text{if } j = \ell \\ \kappa_j \frac{\varepsilon\omega}{2} g_{j\ell} \cos(\bar{\theta}_{\text{eq},j\ell}) & \text{if } j \neq \ell \end{cases} \\ [J_B]_{j\ell} &= -\kappa_j \frac{\varepsilon\omega}{2} g_{j\ell} \bar{r}_{\text{eq}} \sin(\bar{\theta}_{\text{eq},j\ell}) \\ [J_C]_{j\ell} &= \begin{cases} \kappa_j \frac{\varepsilon\omega}{2\bar{r}_{\text{eq}}} \sum_{\ell=1, \ell \neq j}^N g_{j\ell} \sin(\bar{\theta}_{\text{eq},j\ell}) & \text{if } j = \ell \\ -\kappa_j \frac{\varepsilon\omega}{2} g_{j\ell} \sin(\bar{\theta}_{\text{eq},j\ell}) & \text{if } j \neq \ell \end{cases} \\ [J_D]_{j\ell} &= \begin{cases} 0 & \text{if } j = \ell \\ \kappa_j \frac{\varepsilon\omega}{2} g_{j\ell} \cos(\bar{\theta}_{\text{eq},j\ell}) & \text{if } j \neq \ell \end{cases}, \end{aligned}$$

where $f'(\bar{r}_{\text{eq}})$ represents the derivative of $\bar{f}(\cdot)$ evaluated at \bar{r}_{eq} . An inspection of the above Jacobian reveals that the phase-synchronized equilibrium i.e., $\bar{\theta}_{\text{eq},j} = \bar{\theta}_{\text{eq},\ell} \forall j, \ell$, is locally exponentially stable. First, notice that J is block diagonal for this equilibrium and therefore around this equilibrium, the evolution of amplitudes and phases are *decoupled*. Furthermore, while J_D is a real skew-symmetric matrix (which implies that all its eigenvalues are purely imaginary), leveraging LaSalle's invariance principle it can be shown that phase synchronized equilibrium is locally exponentially stable [128, Theorem 4.3]. With these arguments in place, we proceed with the linearized (and decoupled) amplitude dynamics.

For small perturbations about the equilibrium point, we express $\bar{r} = \bar{\mathbf{I}}_N r_{\text{eq}} + \tilde{r}$, where $\tilde{r} := [\tilde{r}_1 \ \tilde{r}_2 \ \cdots \ \tilde{r}_N]^T$. By defining states $x = \tilde{r}$, the linearized system can be written in

the state-space model

$$\begin{aligned}\dot{x} &= l\hat{A}x + u + \hat{B}d \\ &= -\left(\frac{\varepsilon}{2\pi}\bar{f}'(\bar{r}_{\text{eq}})I_N + \frac{\varepsilon\omega}{2}K_d G\right)x + \hat{B}d\end{aligned}\quad (6.13)$$

where I_N is the $N \times N$ identity; $\hat{A} = -\frac{\varepsilon}{2\pi}\bar{f}'(\bar{r}_{\text{eq}})I_N$; the control input, $u = -\frac{\varepsilon\omega}{2}K_d Gx$ (with a slight abuse of notation with regard to (6.1)); and \hat{B} is the input matrix for external disturbances d . Recall that G is the Kron-reduced conductance matrix, and $K_d = \text{diag}\{\kappa_1, \dots, \kappa_N\}$. With regard to control synthesis, K_d takes the connotation of the feedback-gain matrix. In general, \hat{B} can be chosen according to the application; and in this particular case, we make the choice $\hat{B} = G$. With due regard to the optimal control problem to be formulated in Section 6.2, we define the vector of performance outputs, z , as follows:

$$z = \begin{bmatrix} \hat{Q}^{1/2} \\ -\hat{R}^{1/2} K_d G \end{bmatrix} x, \quad (6.14)$$

where \hat{Q} is the state penalty matrix; and \hat{R} is the control input penalty matrix.

A cursory inspection of (6.13)-(6.14) indicates two impediments in applying conventional linear feedback control design approaches: i) the closed-loop system is not in standard feedback control form, (the standard form would be $\dot{x} = (\hat{A} - GK)x + \hat{B}d$); ii) there is a structural constraint on the feedback gain matrix, K , being diagonal (of the form K_d). To reformulate the problem so that conventional linear feedback control design approaches can be used, we first introduce a change of variables, $\psi = Gx$. Note that G is invertible when the network has shunt loads [129]. The state-space model for the system in these new coordinates can be expressed in the following form:

$$\begin{aligned}\dot{\psi} &= (A - GK_d)\psi + Bd \\ \xi &= \begin{bmatrix} Q^{1/2} \\ -R^{1/2} K_d \end{bmatrix} \psi,\end{aligned}\quad (6.15)$$

where

$$\begin{aligned}A &= G\hat{A}G^{-1}, & B &= G\hat{B} \\ Q &= G^{-1}\hat{Q}G^{-1}, & R &= \hat{R}.\end{aligned}$$

Next, we introduce an optimal control design method that will allow us to synthesize a diagonal feedback gain matrix.

6.2 Design of current gains

In this section, we introduce a sparsity-promoting optimal control algorithm developed in [21, 30] to synthesize optimal current gains for the oscillators with the objective of regulating their terminal voltages to a common value.

6.2.1 Linear quadratic control design

We cast the task of synthesizing the current gains as an optimal feedback control design problem. With reference to (6.15), we select the state penalty matrix $\hat{Q} = I_N$ to ensure that the terminal-voltage amplitudes of all circuits coincide. Furthermore, we set the control input penalty matrix $\hat{R} = \rho I_N$, $\rho \in \mathbb{R}^+$. The closed-loop \mathcal{H}_2 norm from input disturbance d to performance output z is defined as

$$J(K) := \begin{cases} \text{trace}(B^T P(K) B) & K \text{ stabilizing} \\ \infty & \text{otherwise,} \end{cases} \quad (6.16)$$

where the closed-loop observability Gramian $P(K)$ satisfies the Lyapunov equation

$$(A - GK)^T P + P(A - GK) = -(Q + K^T R K), \quad (6.17)$$

and K is the feedback-gain matrix. Conventional \mathcal{H}_2 control design methods, such as the Linear Quadratic Regulator (LQR) problem, provide us with an optimal centralized controller. In our problem setting, dense feedback gain matrices require communication links to relay information about oscillator currents. However, we want to ensure that the feedback matrix is diagonal so that each oscillator only requires local current measurements. Next, we introduce the sparsity-promoting optimal control algorithm to incorporate the structure constrain on the feedback matrix K to get a fully diagonal matrix K_d .

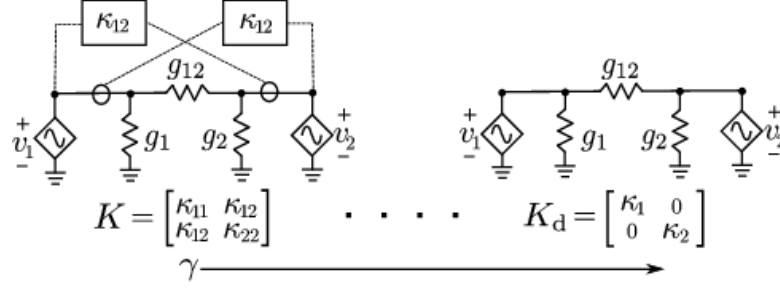


Figure 6.3: Sparsity-promoting optimal current gain design illustrated for a Kron-reduced network and two oscillators. As the sparsity emphasis γ increases, K becomes sparser and we eventually recover a diagonal matrix, K_d , which corresponds to local current gains. Dotted lines indicate communication links that correspond to dense feedback gain matrices.

6.2.2 Sparsity-promoting optimal control

Consider the following optimization problem:

$$\begin{aligned} & \text{minimize} && J(K) + \gamma g(F) \\ & \text{subject to} && K - F = 0, \end{aligned} \tag{6.18}$$

where $J(K)$ is defined in (6.16), $g(F)$ is the sparsity-promoting penalty function, and γ is the emphasis on sparsity. When γ is zero, objective function (6.18) only minimizes $J(K)$, which provides us with the optimal centralized controller. As γ increases, the emphasis on the sparsity penalty function increases, so we obtain sparser feedback-gain matrices, at the expense of system performance. See Fig. 6.3 for an illustration. By decoupling the objective functions J and g and introducing the linear constraint $K - F = 0$ in (6.18), the alternating direction method of multipliers (ADMM) algorithm suggests a solution approach by exploiting the separability of g and differentiability of J ; see [21, 30] for the details of the algorithm. The penalty function $g(F)$ is determined by a weighted ℓ_1 norm [21]:

$$g(F) := \sum_{i,j} W_{ij} |F_{ij}|, \tag{6.19}$$

where $W_{ij} = 1/(|F_{ij}| + \epsilon)$ are positive weights, see [99] for detailed procedure of selecting W_{ij} 's.

The algorithm consists of the following steps: First, we form the augmented Lagrangian; then we use ADMM for the augmented Lagrangian minimization, which includes a K -minimization step, an F -minimization step, and a dual-variable update step. ADMM identifies a specific sparsity pattern and provides a good initial condition for the structured feedback design. Finally, we implement a polishing step, which involves solving a structured \mathcal{H}_2 problem for the fixed controller structure. Readers are referred to [21, 30] for further information.

6.3 Case study

To verify the effectiveness of our algorithm for optimal current-gain design, we test it on a resistive network with the same topology as the IEEE 37-bus benchmark network and a collection of $N = 7$ Van der Pol oscillators (see Fig. 6.6 for the network topology). The dynamics of the oscillators can be described using (6.1) with $f(v) = \alpha\omega(1 - \beta v^2)$, where α and β are positive constants. (See Fig. 6.1 for a detailed circuit schematic). It follows from (6.11) that the averaged voltage-amplitude dynamics of the j th oscillator are:

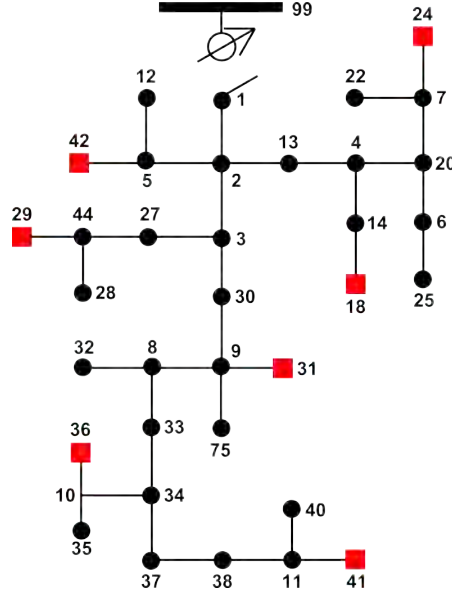


Figure 6.4: Schematic diagram of the electrical network. The topology is adopted from the IEEE 37-bus network.

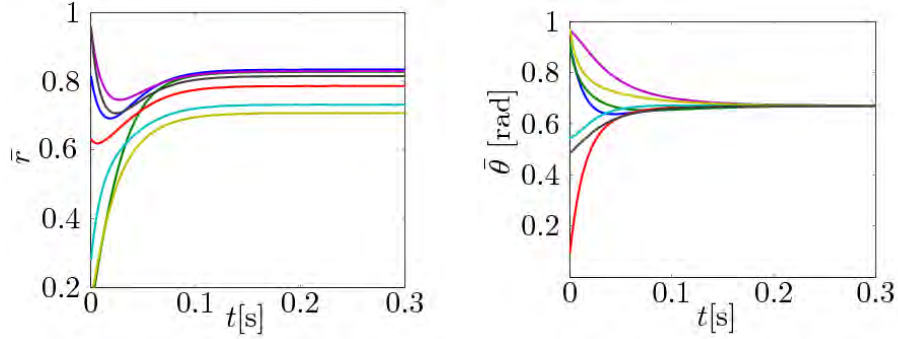


Figure 6.5: Evolution of averaged amplitudes and phases with time for the nonlinear system in (6.11).

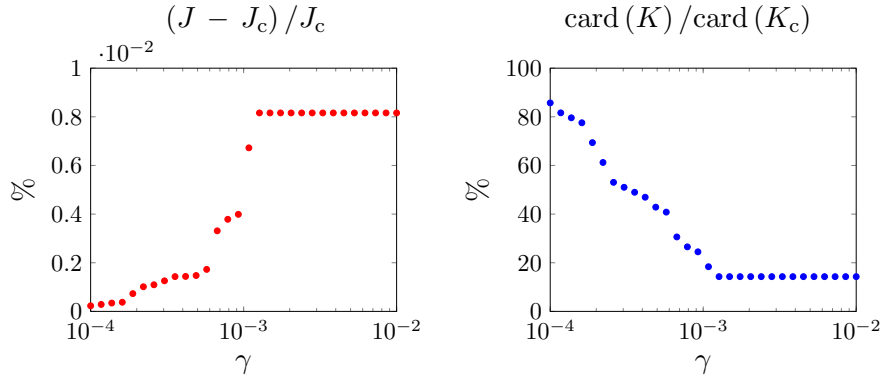


Figure 6.6: Performance versus sparsity comparison of sparse K and the optimal centralized controller K_c .

$$\frac{d}{dt} \bar{r}_j = -\varepsilon \alpha \omega \left(-\frac{1}{2} r_j + \frac{\beta}{8} \bar{r}_j^3 \right) - \frac{\kappa_j \varepsilon \omega}{2} g_{jj} \bar{r}_j + \frac{\kappa_j \varepsilon \omega}{2} \sum_{\ell=1, \ell \neq j}^N g_{j\ell} \bar{r}_\ell \cos(\bar{\theta}_{j\ell}). \quad (6.20)$$

Linearizing (6.20) around the stable equilibrium point of the decoupled oscillator, $\bar{r}_{\text{eq}} = 2/\sqrt{\beta}$ [96], and acknowledging that the phase-synchronized equilibrium is locally exponentially stable, we recover the state-space model of the form (6.13) with $\hat{A} = -\varepsilon \alpha \omega I_N$.

For the simulations that follow, we pick $\alpha = 0.90$, $\beta = 4$, $\omega = 2\pi 60$ rad/s, $\varepsilon = 0.19$; conductances of the lines in the IEEE-37-bus network are sourced from [130].

Fig. 6.5 shows the averaged voltage magnitude and phase trajectories of all seven oscillators when we apply unit current gains (without control design) to the original nonlinear coupled system (6.11). It is evident that the terminal-voltage magnitudes do not synchronize as time evolves but the phases synchronize innately.

6.3.1 Optimal current-gain design

The sparsity-promoting optimal control problem in (6.18) is solved with 30 logarithmically-spaced points for $\gamma \in [10^{-4}, 10^{-2}]$. In Fig. 6.6, we can see that as emphasis on sparsity increases, the number of nonzero elements in the feedback matrix—returned by the cardinality function $\text{card}(\cdot)$ —reduces. For $\gamma = 10^{-2}$, the sparsity-promoting optimal control algorithm returns a diagonal feedback controller, K_d with diagonal entries: $\kappa_1 = 0.0033$, $\kappa_2 = 0.0047$, $\kappa_3 = 0.0026$, $\kappa_4 = 0.0025$, $\kappa_5 = 0.0047$, $\kappa_6 = 0.0038$, $\kappa_7 = 0.0029$. With this fully decentralized controller, we drop 80% of the nonzero elements in the feedback matrix compared to the optimal centralized controller (denoted by K_c with corresponding cost J_c), at the expense of only 0.01% performance loss.

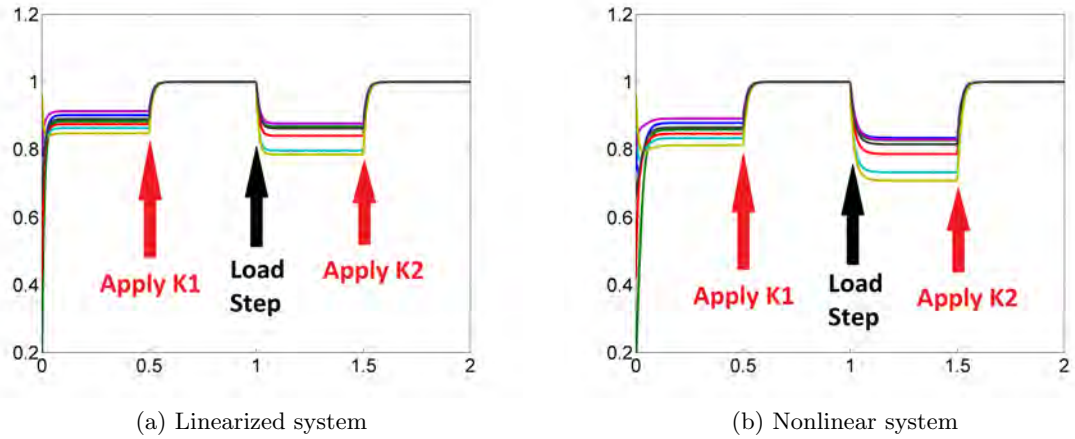


Figure 6.7: Oscillator terminal-voltage magnitudes with designed current gains applied at time $t = 0.1$ s.

6.3.2 Time-domain simulations for original nonlinear and linearized models

To demonstrate the efficacy of our control design method, we simulate both the linear model (6.15) and the original nonlinear model (6.20) for Van der pol oscillators, with the optimal κ 's that are obtained from the sparsity-promoting optimal control algorithm. Fig. 6.7 shows the trajectories of the averaged terminal-voltage magnitudes for each inverter with optimal gains applied at time $t = 0.1$ s, with unit current gains as initial values. From the figure, it is clear that calibrating the current gains leads to synchronization of terminal voltage amplitudes. Furthermore, since the original nonlinear system also achieves amplitude synchronization, it validates our linearized design perspective.

6.4 Concluding remarks

In this chapter, we introduced a systematic way of designing current gains for weakly nonlinear circuits governed by Liénard's equation in a resistive electrical network. The output current of each oscillator is scaled by a current gain; and the objective is to synthesize an optimal set of current gains to ensure voltage regulation in the network. We apply a sparsity-promoting optimal control method to design the current gains. The optimization problem targets simultaneously achieving a desirable system performance and preserving the sparsity pattern, which is the diagonal structure of the feedback matrix. An iterative ADMM algorithm is used to solve the ℓ_1 regularized version of the standard \mathcal{H}_2 optimal control problem. Ongoing research is focused on extending the approach to cover networks with inductive and capacitive elements.

References

- [1] M. Mesbahi and M. Egerstedt. *Graph Theoretic Methods in Multiagent Networks*. Princeton University Press, 2010.
- [2] L. Xiao, S. Boyd, and S.-J. Kim. Distributed average consensus with least-mean-square deviation. *J. Parallel Distrib. Comput.*, 67(1):33–46, 2007.
- [3] A. Ghosh, S. Boyd, and A. Saberi. Minimizing effective resistance of a graph. *SIAM Review*, 50(1):37–66, 2008.
- [4] W. Ren. Synchronization of coupled harmonic oscillators with local interaction. *Automatica*, 44:3195–3200, 2008.
- [5] D. Zelazo and M. Mesbahi. Edge agreement: Graph-theoretic performance bounds and passivity analysis. *IEEE Trans. Automat. Control*, 56(3):544–555, 2011.
- [6] B. Bamieh, M. R. Jovanović, P. Mitra, and S. Patterson. Coherence in large-scale networks: dimension dependent limitations of local feedback. *IEEE Trans. Automat. Control*, 57(9):2235–2249, 2012.
- [7] F. Dörfler and F. Bullo. Synchronization and transient stability in power networks and non-uniform Kuramoto oscillators. *SIAM Journal on Control and Optimization*, 50:1616–1642, 2012.
- [8] A. Mauroy, P. Sacré, and R. J. Sepulchre. Kick synchronization versus diffusive synchronization. In *Proceedings of the 51st IEEE Conference on Decision and Control*, pages 7171–7183, 2012.

- [9] M. Arcak. Synchronization and pattern formation in diffusively coupled systems. In *Proceedings of the 51st IEEE Conference on Decision and Control*, pages 7184–7192, 2012.
- [10] D. Zelazo, S. Schuler, and F. Allgöwer. Performance and design of cycles in consensus networks. *Syst. Control Lett.*, 62(1):85–96, 2013.
- [11] M. Fardad, F. Lin, and M. R. Jovanović. Design of optimal sparse interconnection graphs for synchronization of oscillator networks. *IEEE Trans. Automat. Control*, 59(9):2457–2462, 2014.
- [12] G. E. Dullerud and F. Paganini. *A course in robust control theory*. Springer, 2000.
- [13] M. R. Jovanović and N. K. Dhingra. Controller architectures: tradeoffs between performance and structure. *Eur. J. Control*, 30:76–91, July 2016.
- [14] F. Dörfler, M. R. Jovanović, M. Chertkov, and F. Bullo. Sparse and optimal wide-area damping control in power networks. In *Proceedings of the 2013 American Control Conference*, pages 4295–4300, 2013.
- [15] F. Dörfler, M. R. Jovanović, M. Chertkov, and F. Bullo. Sparsity-promoting optimal wide-area control of power networks. *IEEE Trans. Power Syst.*, 29(5):2281–2291, 2014.
- [16] X. Wu, F. Dörfler, and M. R. Jovanović. Input-output analysis and decentralized optimal control of inter-area oscillations in power systems. *IEEE Trans. Power Syst.*, 31(3):2434–2444, May 2016.
- [17] B. Bamieh, F. Paganini, and M. A. Dahleh. Distributed control of spatially invariant systems. *IEEE Trans. Automat. Control*, 47(7):1091–1107, 2002.
- [18] M. Rotkowitz and S. Lall. A characterization of convex problems in decentralized control. *IEEE Trans. Automat. Control*, 51(2):274–286, 2006.
- [19] M. Fardad, F. Lin, and M. R. Jovanović. Sparsity-promoting optimal control for a class of distributed systems. In *Proceedings of the 2011 American Control Conference*, pages 2050–2055, 2011.

- [20] F. Lin, M. Fardad, and M. R. Jovanović. Sparse feedback synthesis via the alternating direction method of multipliers. In *Proceedings of the 2012 American Control Conference*, pages 4765–4770, 2012.
- [21] F. Lin, M. Fardad, and M. R. Jovanović. Design of optimal sparse feedback gains via the alternating direction method of multipliers. *IEEE Trans. Automat. Control*, 58(9):2426–2431, 2013.
- [22] N. Matni. Communication delay co-design in H_2 distributed control using atomic norm minimization. *IEEE Trans. Control Netw. Syst.*, 2016. accepted; also arXiv:1404.4911.
- [23] N. Matni and V. Chandrasekaran. Regularization for design. *IEEE Trans. Automat. Control*, 2016. accepted; also arXiv:1404.1972.
- [24] S. Boyd, N. Parikh, E. Chu, B. Peleato, and J. Eckstein. Distributed optimization and statistical learning via the alternating direction method of multipliers. *Foundations and Trends in Machine Learning*, 3(1):1–124, 2011.
- [25] Bassam Bamieh and Petros G Voulgaris. A convex characterization of distributed control problems in spatially invariant systems with communication constraints. *Systems & Control Letters*, 54(6):575–583, 2005.
- [26] Michael Rotkowitz and Sanjay Lall. A characterization of convex problems in decentralized control. *IEEE Trans. Automat. Control*, 51(2):274–286, Feb 2006.
- [27] Anders Rantzer. Distributed control of positive systems. In *Proceedings of 50th IEEE Conference on Decision and Control*, pages 6608–6611, Dec 2011.
- [28] N. K. Dhingra, M. Colombino, and M. R. Jovanović. On the convexity of a class of structured optimal control problems for positive systems. In *Proceedings of the 2016 European Control Conference*, pages 825–830, 2016.
- [29] F. Lin, M. Fardad, and M. R. Jovanović. Identification of sparse communication graphs in consensus networks. In *Proceedings of the 50th Annual Allerton Conference on Communication, Control, and Computing*, pages 85–89, Monticello, IL, 2012.

- [30] X. Wu and M. R. Jovanović. Sparsity-promoting optimal control of consensus and synchronization networks. In *Proceedings of the 2014 American Control Conference*, pages 2948–2953, 2014.
- [31] S. Hassan-Moghaddam and M. R. Jovanović. An interior point method for growing connected resistive networks. In *Proceedings of the 2015 American Control Conference*, pages 1223–1228, Chicago, IL, 2015.
- [32] S. Hassan-Moghaddam and M. R. Jovanović. Topology design for stochastically-forced consensus networks. *IEEE Trans. Control Netw. Syst.*, 2016. submitted; also arXiv:1506.03437v3.
- [33] B. Polyak, M Khlebnikov, and P. Shcherbakov. An LMI approach to structured sparse feedback design in linear control systems. In *Proceedings of the 2013 European Control Conference*, pages 833–838, 2013.
- [34] N. K. Dhingra, M. R. Jovanović, and Z. Q. Luo. An ADMM algorithm for optimal sensor and actuator selection. In *Proceedings of the 53rd IEEE Conference on Decision and Control*, pages 4039–4044, 2014.
- [35] N. K. Dhingra and M. R. Jovanović. Convex synthesis of symmetric modifications to linear systems. In *Proceedings of the 2015 American Control Conference*, pages 3583–3588, 2015.
- [36] S. Schuler, P. Li, J. Lam, and F Allgöwer. Design of structured dynamic output-feedback controllers for interconnected systems. *International Journal of Control*, 84(12):2081–2091, 2011.
- [37] Nikolai Matni and Venkat Chandrasekaran. Regularization for design. In *Proceedings of the 53rd IEEE Conference on Decision and Control*, pages 1111–1118, Los Angeles, CA, 2014.
- [38] D. M. Zoltowski, N. K. Dhingra, F. Lin, and M. R. Jovanović. Sparsity-promoting optimal control of spatially-invariant systems. In *Proceedings of the 2014 American Control Conference*, pages 1261–1266, 2014.

- [39] Fernando Alvarado, Chris DeMarco, Ian Dobson, Pete Sauer, Scott Greene, Henrik Engdahl, and Jianfeng Zhang. Avoiding and suppressing oscillations. *PSEERC Project Final Report*, 1999.
- [40] K Prasertwong, N Mithulananthan, and D Thakur. Understanding low-frequency oscillation in power systems. *International Journal of Electrical Engineering Education*, 47(3):248–262, 2010.
- [41] L Rouco. Eigenvalue-based methods for analysis and control of power system oscillations. In *IEE Colloquium on Power System Dynamics Stabilisation*. IET, 1998.
- [42] Graham Rogers. Demystifying power system oscillations. *IEEE Computer Applications in Power*, 9(3):30–35, 1996.
- [43] M. Klein, G. J. Rogers, and P. Kundur. A fundamental study of inter-area oscillations in power systems. *IEEE Trans. Power Syst.*, 6(3):914–921, 1991.
- [44] M. Klein, G. J. Rogers, S. Moorty, and P. Kundur. Analytical investigation of factors influencing power system stabilizers performance. *IEEE Transactions on Energy Conversion*, 7(3):382–390, 1992.
- [45] N. Martins and L. T. G. Lima. Eigenvalue and frequency domain analysis of small-signal electromechanical stability problems. In *IEEE/PES Symposium on Applications of Eigenanalysis and Frequency Domain Methods*, pages 17–33, 1989.
- [46] T. Othman, J. J. Sanchez-Gasca, M. A. Kale, and J. H. Chow. On the design of robust power system stabilizers. In *Proceedings of the 28th IEEE Conference on Decision and Control*, pages 1853–1857, 1989.
- [47] O. P. Malik, G. S. Hope, Y. M. Gorski, V. A. Uskakov, and A. L. Rackevich. Experimental studies on adaptive microprocessor stabilizers for synchronous generators. *IFAC Power System and Power Plant Control*, pages 125–130, 2014.
- [48] C. Zhu, M. Khammash, V. Vittal, and W. Qiu. Robust power system stabilizer design using H_∞ loop shaping approach. *IEEE Trans. Power Syst.*, 18(2):810–818, 2003.

- [49] J. A. Taylor and L. Scardovi. Decentralized control of DC-segmented power systems. In *Proceedings of the 52th Annual Allerton Conference*, pages 1046–1050, 2014.
- [50] J. Xiao, F. Wen, C. Y. Chung, and K. P. Wong. Wide-area protection and its applications—a bibliographical survey. In *IEEE PES Power Systems Conference and Exposition*, pages 1388–1397, 2006.
- [51] K. Seethalekshmi, S. N. Singh, and S. C. Srivastava. Wide-area protection and control: Present status and key challenges. In *Fifteenth National Power Systems Conference*, pages 169–175, 2008.
- [52] A. Heniche and I. Karnwa. Control loops selection to damp inter-area oscillations of electrical networks. *IEEE Trans. Power Syst.*, 17(2):378–384, 2002.
- [53] L. P. Kunjumammed, R. Singh, and B. C. Pal. Robust signal selection for damping of inter-area oscillations. *IET Generation, Transmission & Distribution*, 6(5):404–416, 2012.
- [54] G. E. Boukarim, S. Wang, J. H. Chow, G. N. Taranto, and N. Martins. A comparison of classical, robust, and decentralized control designs for multiple power system stabilizers. *IEEE Trans. Power Syst.*, 15(4):1287–1292, 2000.
- [55] Y. Zhang and A. Bose. Design of wide-area damping controllers for interarea oscillations. *IEEE Trans. Power Syst.*, 23(3):1136–1143, 2008.
- [56] M. Zima, M. Larsson, P. Korba, C. Rehtanz, and G. Andersson. Design aspects for wide-area monitoring and control systems. *Proceedings of the IEEE*, 93(5):980–996, 2005.
- [57] S. Schuler, U. Münz, and F. Allgöwer. Decentralized state feedback control for interconnected systems with application to power systems. *Journal of Process Control*, 24(2):379–388, 2014.
- [58] S. Pirooz, J. A. Taylor, and R. Iravani. Decentralized supplementary control of multiple LCC-HVDC links. *IEEE Trans. Power Syst.*, 2015.

- [59] J. H. Chow and K. W. Cheung. A toolbox for power system dynamics and control engineering education and research. *IEEE Trans. Power Syst.*, 7(4):1559–1564, 1992.
- [60] B. E. Eliasson and D. J. Hill. Damping structure and sensitivity in the NORDEL power system. *IEEE Trans. Power Syst.*, 7(1):97–105, 1992.
- [61] J. Machowski, J. W. Bialek, and J. R. Bumby. *Power System Dynamics*. John Wiley & Sons, 2 edition, 2008.
- [62] A. J. Wood and B. F. Wollenberg. *Power Generation, Operation, and Control*. John Wiley & Sons, 2 edition, 1996.
- [63] Joshua Adam Taylor, Sairaj V Dhople, and Duncan S Callaway. Power systems without fuel. *arXiv preprint arXiv:1506.04799*, 2015.
- [64] S.T. Cady and A.D. Dominguez-Garcia. Distributed generation control of small-footprint power systems. In *North American Power Symposium (NAPS), 2012*. IEEE, 2012.
- [65] Na Li, Lijun Chen, Changhong Zhao, and Steven H Low. Connecting automatic generation control and economic dispatch from an optimization view. In *American Control Conference*, pages 735–740, 2014.
- [66] J. W. Simpson-Porco, F. Dörfler, and F. Bullo. Synchronization and power sharing for droop-controlled inverters in islanded microgrids. *Automatica*, 49(9):2603–2611, 2013.
- [67] F. Dörfler, J. W. Simpson-Porco, and F. Bullo. Breaking the hierarchy: Distributed control and economic optimality in microgrids. *IEEE Transactions on Control of Network Systems*, 3(3):241–253, 2016.
- [68] C. Zhao, E. Mallad, and F. Dörfler. Distributed frequency control for stability and economic dispatch in power networks. In *Proceedings of the 2015 American Control Conference*, pages 2359–2364, Chicago, IL, 2015.

- [69] M. Andreasson, D. V. Dimarogonas, H. Sandberg, and K. H. Johansson. Distributed control of networked dynamical systems: Static feedback, integral action and consensus. *IEEE Transactions on Automatic Control*, 59(7):1750–1764, 2014.
- [70] M. Andreasson, D. V. Dimarogonas, H. Sandberg, and K. H. Johansson. Distributed PI-control with applications to power systems frequency control. In *Proceedings of the 2014 American Control Conference*, pages 3183–3188, 2014.
- [71] S. Bennett. Nicholas minorsky and the automatic steering of ships. *IEEE Control Systems Magazine*, 4(4):10–15, 1984.
- [72] Karl Johan Åström and Tore Hägglund. The future of PID control. *Control Engineering Practice*, 9(11):1163–1175, 2001.
- [73] Mathias Bürger and Claudio De Persis. Dynamic coupling design for nonlinear output agreement and time-varying flow control. *Automatica*, 51:210–222, 2015.
- [74] Jieqiang Wei and AJ van der Schaft. Load balancing of dynamical distribution networks with flow constraints and unknown in/outflows. *Systems & Control Letters*, 62(11):1001–1008, 2013.
- [75] D. Burbano and M. di Bernardo. Consensus and synchronization of complex networks via proportional-integral coupling. In *Circuits and Systems (ISCAS), 2014 IEEE International Symposium on*, pages 1796–1799. IEEE, 2014.
- [76] He Bai, Randy Freeman, Kevin M Lynch, et al. Robust dynamic average consensus of time-varying inputs. In *Decision and Control (CDC), 2010 49th IEEE Conference on*, pages 3104–3109. IEEE, 2010.
- [77] Randy A Freeman, Peng Yang, Kevin M Lynch, et al. Stability and convergence properties of dynamic average consensus estimators. In *IEEE conf. on decision and control*, pages 398–403, 2006.
- [78] Andrej Jokić, Mircea Lazar, and PPJ Van den Bosch. Real-time control of power systems using nodal prices. *International Journal of Electrical Power & Energy Systems*, 31(9):522–530, 2009.

- [79] Lin-Yu Lu. Consensus-based $P - f$ and $Q - \dot{V}$ droop control for multiple parallel-connected inverters in lossy networks. In *IEEE International Symposium on Industrial Electronics*, Taipei, Taiwan, May 2013.
- [80] C. Zhao, E. Mallada, and F. Dörfler. Distributed frequency control for stability and economic dispatch in power networks. In *American Control Conference*, 2015.
- [81] X. Wu, F. Dörfler, and M. R. Jovanović. Analysis and design trade-offs for power network inter-area oscillations. In *Proceedings of the 21st International Symposium on Mathematical Theory of Network and Systems*, pages 657–663, Groningen, The Netherlands, 2014.
- [82] X. Wu, F. Dörfler, and M. R. Jovanović. Decentralized optimal control of inter-area oscillations in bulk power systems. In *Proceedings of the 54th IEEE Conference on Decision and Control*, pages 5532–5537, Osaka, Japan, 2015.
- [83] S Emre Tuna. Synchronization analysis of coupled lienard-type oscillators by averaging. *Automatica*, 48(8):1885–1891, 2012.
- [84] Steven H. Strogatz. *Nonlinear Dynamics and Chaos: With Applications to Physics, Biology, Chemistry, and Engineering*. Studies in nonlinearity. Westview Press, 1 edition, Jan. 2001.
- [85] B. B. Johnson, S. V. Dhople, A. O. Hamadeh, and P. T. Krein. Synchronization of parallel single-phase inverters with virtual oscillator control. *IEEE Trans. Power Electron.*, 29(11):6124–6138, Nov. 2014.
- [86] L. A. B. Tôrres, J. P. Hespanha, and J. Moehlis. Power supplies dynamical synchronization without communication. In *Proceedings of the Power & Energy Society 2012 General Meeting*, July 2012.
- [87] Krešimir Josić and Slaven Peleš. Synchronization in networks of general, weakly nonlinear oscillators. *Journal of Physics A: Mathematical and General*, 37(49):11801, 2004.
- [88] Florian Dörfler and Francesco Bullo. Synchronization in complex networks of phase oscillators: A survey. *Automatica*, 50(6):1539–1564, 2014.

- [89] A. Mauroy, P. Sacré, and R. J. Sepulchre. Kick synchronization versus diffusive synchronization. In *IEEE Conference on Decision and Control*, pages 7171–7183, 2012.
- [90] T. Koga and M. Shinagawa. An extension of the lienard theorem and its application [nonlinear circuits]. In *Circuits and Systems, 1991., IEEE International Symposium on*, pages 1244–1247 vol.2, Jun 1991.
- [91] Wouter A Serdijn, Jan Mulder, Albert C van der Woerd, and Arthur HM van Roermund. A wide-tunable translinear second-order oscillator. *Solid-State Circuits, IEEE Journal of*, 33(2):195–201, 1998.
- [92] Kofi Odame. *Exploiting Device Nonlinearity in Analog Circuit Design*. PhD thesis, Georgia Institute of Technology, 2008.
- [93] Pietro De Lellis, Mario di Bernardo, and Franco Garofalo. Synchronization of complex networks through local adaptive coupling. *Chaos: An Interdisciplinary Journal of Nonlinear Science*, 18(3), 2008.
- [94] S Emre Tuna. LQR-based coupling gain for synchronization of linear systems. *arXiv preprint arXiv:0801.3390*, 2008.
- [95] A. Hamadeh, G.-B. Stan, and J. Goncalves. Constructive synchronization of networked feedback systems. In *IEEE Conference on Decision and Control*, pages 6710–6715, December 2010.
- [96] H. K. Khalil. *Nonlinear Systems*. Prentice Hall, 3 edition, 2002.
- [97] X. Wu and M. R. Jovanović. Sparsity-promoting optimal control of systems with symmetries, consensus and synchronization networks. *Syst. Control Lett.*, 2016. submitted.
- [98] Prabha Kundur, Neal J Balu, and Mark G Lauby. *Power system stability and control*, volume 7. McGraw-hill New York, 1994.
- [99] E. J. Candès, M. B. Wakin, and S. P. Boyd. Enhancing sparsity by reweighted ℓ_1 minimization. *J. Fourier Anal. Appl*, 14:877–905, 2008.

- [100] M. Yuan and Y. Lin. Model selection and estimation in regression with grouped variables. *Journal of the Royal Statistical Society: Series B (Statistical Methodology)*, 68(1):49–67, 2006.
- [101] A. Beck and M. Teboulle. A fast iterative shrinkage-thresholding algorithm for linear inverse problems. *SIAM Journal on Imaging Sciences*, 2(1):183–202, 2009.
- [102] J. Barzilai and J. M. Borwein. Two-point step size gradient methods. *IMA Journal of Numerical Analysis*, 8(1):141–148, 1988.
- [103] N. K. Dhingra, X. Wu, and M. R. Jovanović. Sparsity-promoting optimal control of systems with invariances and symmetries. In *Proceedings of the 10th IFAC Symposium on Nonlinear Control Systems*, pages 648–653, Monterey, CA, 2016.
- [104] N. K. Dhingra and M. R. Jovanović. A method of multipliers algorithm for sparsity-promoting optimal control. In *Proceedings of the 2016 American Control Conference*, pages 1942–1947, Boston, MA, 2016.
- [105] N. K. Dhingra and M. R. Jovanović. The proximal augmented Lagrangian method for nonsmooth composite optimization. *IEEE Trans. Automat. Control*, 2016. submitted; also arXiv:1610.04514.
- [106] M. Fardad, F. Lin, and M. R. Jovanović. On optimal link creation for facilitation of consensus in social networks. In *Proceedings of the 2014 American Control Conference*, pages 3802–3807, Portland, OR, 2014.
- [107] V. Jonsson, A. Rantzer, and R. M. Murray. A scalable formulation for engineering combination therapies for evolutionary dynamics of disease. *Proceedings of the 2014 American Control Conference*, 2014.
- [108] V. Jonsson, N. Matni, and R. M. Murray. Reverse engineering combination therapies for evolutionary dynamics of disease: An H_∞ approach. In *Proceedings of the 52nd IEEE Conference on Decision and Control*, pages 2060–2065, 2013.
- [109] G. E. Dullerud and F. Paganini. *A course in robust control theory: a convex approach*, volume 36. Springer Science & Business Media, 2013.

- [110] J. Swift and P. C. Hohenberg. Hydrodynamic fluctuations at the convective instability. *Physical Review A*, 15(1):319, 1977.
- [111] J. A. C. Weideman and S. C. Reddy. A MATLAB differentiation matrix suite. *ACM Transactions on Mathematical Software*, 26(4):465–519, December 2000.
- [112] M. Grant and S. Boyd. CVX: Matlab software for disciplined convex programming, version 2.0 beta. <http://cvxr.com/cvx>, September 2013.
- [113] J. H. Chow and P. Kokotović. Time scale modeling of sparse dynamic networks. *IEEE Trans. Automat. Control*, 30(8):714–722, 1985.
- [114] D. Romeres, F. Dörfler, and F. Bullo. Novel results on slow coherency in consensus and power networks. In *Proceedings of the 12th European Control Conference*, pages 742–747, 2013.
- [115] L. N. Trefethen and M. Embree. *Spectra and pseudospectra: the behavior of non-normal matrices and operators*. Princeton University Press, 2005.
- [116] M. R. Jovanović and B. Bamieh. Componentwise energy amplification in channel flows. *J. Fluid Mech.*, 534:145–183, 2005.
- [117] B. K. Lieu, M. R. Jovanović, and S. Kumar. Worst-case amplification of disturbances in inertialess Couette flow of viscoelastic fluids. *J. Fluid Mech.*, 723:232–263, May 2013.
- [118] X. Wu, F. Dörfler, and M. R. Jovanović. Topology identification and design of distributed integral action in power networks. In *Proceedings of the 2016 American Control Conference*, pages 5921–5926, Boston, MA, 2016.
- [119] J. M Guerrero, M. Chandorkar, T.-L. Lee, and P. C. Loh. Advanced control architectures for intelligent microgrids, part i: decentralized and hierarchical control. *IEEE Transactions on Industrial Electronics*, 60(4):1254–1262, 2013.
- [120] F. Lin, M. Fardad, and M. R. Jovanović. Augmented Lagrangian approach to design of structured optimal state feedback gains. *IEEE Trans. Automat. Control*, 56(12):2923–2929, December 2011.

- [121] M. Fardad, F. Lin, and M. R. Jovanović. On the optimal design of structured feedback gains for interconnected systems. In *Proceedings of the 48th IEEE Conference on Decision and Control*, pages 978–983, Shanghai, China, 2009.
- [122] D. P. Bertsekas. *Nonlinear programming*. Athena Scientific, 1999.
- [123] J. H. Chow and K. W. Cheung. A toolbox for power system dynamics and control engineering education and research. *IEEE Transactions on Power Systems*, 7(4):1559–1564, 1992.
- [124] V. Purba, X. Wu, M. Sinha, S. V. Dhople, and M. R. Jovanović. Design of optimal coupling gains for synchronization of nonlinear oscillators. In *Proceedings of the 54th IEEE Conference on Decision and Control*, pages 1310–1315, Osaka, Japan, 2015.
- [125] R. H. Rand. Lecture notes on nonlinear vibrations. 2012.
- [126] M. Sinha, F. Dörfler, B. B. Johnson, and S. V. Dhople. Uncovering droop control laws embedded within the nonlinear dynamics of van der pol oscillators. *IEEE Trans. Control of Networked Sys.*, 2014. In review.
- [127] F. Dörfler and F. Bullo. Kron reduction of graphs with applications to electrical networks. *IEEE Transactions on Circuits and Systems I: Regular Papers*, 60(1):150–163, Jan. 2013.
- [128] F. Dörfler and F. Bullo. Exploring synchronization in complex oscillator networks. In *Proceedings of the 51th IEEE Conference on Decision and Control*, pages 7157–7170, 2012.
- [129] S. V. Dhople, B. B. Johnson, F. Dörfler, and A. O. Hamadeh. Synchronization of nonlinear circuits in dynamic electrical networks with general topologies. *Circuits and Systems I: Regular Papers, IEEE Transactions on*, 61(9):2677–2690, 2014.
- [130] L. Ling and S. V. Dhople. Spatiotemporal model reduction of inverter-based islanded microgrids. *IEEE Transactions on Energy Conversion*, 29(4):823–832, Dec 2014.